Czech Technical University in Prague

Faculty of Electrical Engineering

Doctoral Thesis

June 2016 *Peter Pikna*

Czech Technical University in Prague

Faculty of Electrical Engineering
Department of Electrotechnology

PASSIVATION OF THIN FILM SILICON SOLAR CELLS

Doctoral Thesis

Peter Pikna

Prague, June 2016

Ph.D. Programme: Electrical Engineering and Information Technology
Branch of study: Electrotechnology and Materials

Supervisor: ***prof. Ing. Vítězslav Benda, CSc.***
Supervisor-Specialist: ***RNDr. Antonín Fejfar, CSc.***

Declaration of Originality

I hereby declare that this thesis is my own original work except assistance of my supervisors and colleagues that have been duly acknowledged (see Acknowledgement) and I have clearly referenced all sources used in this work (see Bibliography).

June 2016 Peter Pikna

Abstract (English)

Passivation of electronic defects is a necessary step in production of solar cells based on polycrystalline silicon thin film on glass. Standard passivation method is plasma hydrogenation, which however, represents the second most expensive production step. We used solid phase crystallized (SPC) silicon samples to explore an alternative cheaper passivation approach using annealing in water vapour. Open-circuit voltage V_{OC} measured by Suns-V_{OC} method was the key parameter to determine success of the treatment.

Annealing of SPC Si thin film solar cells in water vapour was explored in the temperature range from 145°C to 650°C under steam pressure from atmospheric pressure to 1.0 MPa at the exposure times of 5-225 minutes. For this purpose a special passivation chamber enabling an independent control of a sample temperature and steam pressure was designed and built. We achieved the best V_{OC} of 360 mV (from the starting 220 mV) demonstrating the annealing in water vapour as a possible low cost alternative passivation method.

Some SPC poly-Si solar cells were annealed in hydrogen gas, a mixture of steam and hydrogen gas, or a mixture of steam and oxygen. These experiments uncovered that neither hydrogen gas nor the mixtures are able to passivate silicon as effectively as water vapour. While the plasma hydrogenation represents a saturation of silicon dangling bonds by hydrogen radicals, annealing in water vapour is an oxidation of silicon and hydrogen acts just as a catalyst. On the basis of the realized experiments and a review of scientific literature, principles of the water vapour passivation were described, explained and presented as a model of steam passivation.

Still, the plasma hydrogenation can achieve better V_{OC} for the same samples. We achieved the best V_{OC} of 497 mV for the same SPC samples. This value resulted from optimization of the plasma hydrogenation parameters at the Helmholtz-Zentrum Berlin during which we suggested to use 1) the higher hydrogen pressure of 300-1,000 Pa in comparison with a commonly used 100 Pa, 2) the longer exposure time of 15-20 minutes, and mainly 3) to keep the usually omitted bias voltage V_{bias} constant during the whole passivation process up to the plasma termination. Since all experiments in the hydrogen plasma were realized as a closed system without a hydrogen flux with very satisfying results, the generally accepted necessity to run the plasma hydrogenation process with a continuous hydrogen flux was called into question.

The development of the crystalline silicon on glass solar cells led to replacement of SPC by liquid phase crystallized (LPC) for which V_{OC} over 600 mV can be achieved. We tested the effect of passivation for LPC poly-Si samples crystallized either by a laser or an electron beam (with the SiO_x diffusion barrier deposited either by plasma enhanced chemical vapour deposition or by physical vapour deposition). In these experiments hydrogen plasma increased the V_{OC} from the typical value of 535 mV to 570 mV for most of the parameter values.

Some SPC Si samples treated in the hydrogen plasma were analyzed by both Suns-V_{OC} method and also optical pump transient terahertz probe spectroscopy which represents optical method for measurement of photogenerated carrier transport at ultrafast time scales. While each of these methods characterizes the solar cell in a different state, a clear correlation between V_{OC} and the lifetime of charge carriers was observed. Terahertz spectroscopy analyzes the sample before the photogenerated charge carriers can be redistributed by a space charge region and therefore V_{OC} is not built up yet. In contrary to this, Suns-V_{OC} method characterizes the cell at a quasi-steady state, when V_{OC} is already built up.

Abstrakt (Czech)

Pasivace elektricky aktivních defektů je nezbytný krok při výrobě polykrystalických křemíkových tenkovrstvých solárních článků na skle. Běžně používaná plazmová hydrogenace je druhým nejdražším krokem výroby. Ve snaze najít levnější alternativu jsme polykrystalické křemíkové solární články připravené krystalizací z pevné fáze (solid phase crystallization SPC) žíhali ve vodní páře. Pro stanovení účinnosti pasivace křemíku ve vodní páře nám sloužilo zejména napětí naprázdno V_{OC} solárního článku měřené Suns-V_{OC} metodou.

Žíhání SPC Si solárních článků bylo prováděno při teplotách 145°C až 650°C a tlaku vodní páry v rozmezí od atmosférického tlaku po 1.0 MPa s dobou působení 5 až 225 minut. Pro potřeby experimentů ve vodní páře byla navržena a postavena pasivační komůrka umožňující nezávislou regulaci teploty vzorku a tlaku vodní páry. Žíhání SPC Si solárních článků s nejlepším výsledek pasivace V_{OC} = 360 mV (před pasivací 220 mV) prokázalo jednoznačný pasivační účinek vodní páry na křemík a tudíž i její potenciál stát se levnější alternativou pro pasivaci.

Některé SPC poly-Si solární články byly žíhány ve vodíku nebo ve směsi vodíku a vodní páry, případně směsi vodní páry a kyslíku. Podle těchto experimentů měla nejsilnější pasivační účinek na křemík právě vodní pára. Při bližším zkoumání pasivačního procesu bylo zjištěno, že na rozdíl od plazmové hydrogenace, kde nastává navázání vodíkových radikálů na nenasycené vazby křemíku, dochází při žíhání ve vodní páře k navazování kyslíku a vodík tady funguje jen jako katalyzátor pasivačního procesu. Na základě provedených experimentů a prozkoumání odborné literatury byly popsány a vysvětleny principy pasivace křemíku ve vodní páře.

Nicméně plazmová hydrogenace představuje i nadále efektivnější způsob pasivace křemíku. Nejvyšší dosažená hodnota V_{OC} = 497 mV je výsledek optimalizace pasivačního procesu ve vodíkovém plazmatu v Helmholtz-Zentrum Berlin, během které jsme doporučili použít a) vyšší tlak vodíku (300-1000 Pa) ve srovnání s běžně používaným tlakem 100 Pa, 2) delší dobu pasivace (15-20 minut) a především 3) udržování běžně opomíjeného napětí mezi elektrodou a vzorkem V_{bias} na konstantní hodnotě po celou dobu pasivace až do vypnutí plazmatu. Vzhledem k uspokojivým výsledkům pasivace ve vodíkovém plazmatu prováděné jako uzavřený systém (bez průtoku vodíku) vyvstává otázka, zda má běžně deklarovaná nutnost provádět pasivaci za stálého průtoku vodíku skutečné opodstatnění.

Vývoj tenkovrstvých křemíkových solárních článků na skle na bázi krystalického křemíku vedl k nahrazení SPC Si křemíkem krystalizovaným z kapalné fáze (liquid phase crystallized LPC) s potenciálem převyšujícím V_{OC} = 600 mV. Tyto LPC Si solární články krystalizované buď laserovým, nebo elektronovým svazkem (s SiO_x difuzní bariérou připravenou buď metodou plazmou podpořená chemická depozice z plynné fáze, nebo fyzikální depozicí z plynné fáze) jsme žíhali ve vodíkovém plazmatu a nejlepší dosažený výsledek byl 570 mV oproti V_{OC} hodnotě před pasivací 535 mV.

Některé vzorky SPC křemíku byly po žíhání ve vodíkovém plazmatu analyzovány jak Suns-V_{OC} metodou, tak optickou tranzientní terahertzovou spektroskopií, což je metoda pro měření transportu fotogenerovaných nosičů náboje v ultra krátkých časových škálách. Zatímco terahertzová pulzní měření zkoumají vzorek ještě před přeuspořádáním fotogenerovaných nosičů náboje oblastí prostorového náboje (V_{OC} ještě není vytvořené), Suns-V_{OC} metoda charakterizuje solární článek v kvazistacionárním stavu, tedy ve stavu, kdy je V_{OC} už vytvořené. I navzdory tomu, že každá z měřících metod analyzuje solární článek v jiném režimu, srovnání V_{OC} a doby života volných nosičů náboje prokázalo jejich korelaci.

Content

Aims of the Doctoral Thesis

1) Passivation of thin film polycrystalline silicon solar cells in hydrogen plasma and in water vapour at various processing conditions to achieve maximum passivation effect.
2) In-situ analysis of the water vapour passivation process.
3) Analysis of the passivated solar cells by available methods to explain and describe mechanisms of the water vapour passivation process.
4) Comparison of the passivation in hydrogen plasma and in water vapour.

Introduction

A human population on the Earth increases permanently and a demand for electric energy is only one of many problems connected with this trend. Nevertheless, one can conclude after a detailed consideration that most of mankind's sorrows is somehow connected with energy deficiency. Here are a few examples – drinking water could be easily prepared from salt sea water if enough energy was available [1], enough food for everybody could be ensured, and natural resources would be easier to access. However, all the above mentioned issues can be solved with a powerful and well abundant energy source only if there is a good will that is often missed and it cannot be replaced by anything.

In my opinion, human responsibility for environment is the other side of the same coin representing an acquisition of electric energy. However, this statement expects use of ethics when decisions are made and it can be very unpopular. While there are some doubts about a connection between human activity (pollution caused mainly by industrial production) and greenhouse effect, there is still a question of responsibility for further generations. All traditional energy resources (petroleum, coal, natural gas, uranium) are limited, there is no question about this. The question could be how much of them remain. If we are aware of this fact, a logical step seems to use a part of the traditional resources that still remain to find other ways to gain energy.

In general, each source of electric energy somehow impacts the surrounding environment, there is no exception also in the case of renewable energy resources. Hydro energy has a negative impact on fishes and other beings living there, wind energy produces noise and it is a threat to wild life nearby. Solar energy occupies agricultural lands, dangerous and toxic chemicals are used at silicon production and solar cell manufacturing. Geothermal energy can produce dangerous and greenhouse gases. Biomass energy produces harmful toxins released to the atmosphere where amount of air emissions depends on the feedstock of the plant and huge areas gained by deforestation are needed to produce enough energy. These areas could be used to grow fruits, vegetables and feed. The question "What energy source does not have any negative impact on the environment?" does not make sense, there is no such a source. More appropriate question is "What energy source harms the environment as little as possible?".

Since traditional energy resources are limited and their negative effect on the environment is much stronger than of the renewable ones, it seems that the last mentioned is the better choice and perhaps the only one that mankind has nowadays. It would not be smart to prefer some of the renewable energy sources and to refuse the others. Searching for new energy resources to cover energy demand of our planet is a process, a brainstorming of mankind happening right now. Each renewable energy source can find its specific application and only time will choose the one or their appropriate combination that is able to ensure a sustainable development.

On this place, let me thank to Prof. Quaschning for his inspiring book ''Regenerative Energiesysteme'' [2].

The content of the thesis is divided into chapters according to the topic:

Chapter 1 focuses on a solar cell description and basic principles of its operation.

Chapter 2 is devoted to silicon structure and the corresponding optical properties.

Chapter 3 reports on state-of-the-art of silicon passivation in hydrogen plasma and water vapour.

Chapter 4 describes some of measuring methods used in this thesis Suns-V_{OC} method, a sun simulator, EQE.

Chapter 5 aims to present the state-of-the-art of solid phase crystallized (SPC) and liquid phase crystallized (LPC) thin film silicon solar cells, their structure, achieved results and perspectives.

Chapter 6 researches optimum processing conditions of the water vapour passivation for SPC Si.

Chapter 7 investigates a passivation effect of hydrogen plasma on SPC and LPC poly-Si solar cells.

Chapter 8 reports on a possible synergetic passivation effect of water vapour and hydrogen plasma.

Chapter 9 compares plasma hydrogenation and water vapour passivation.

Chapter 10 presents optical pump transient terahertz probe spectroscopy as a useful tool for a contactless investigation of ultrafast processes in SPC Si solar cells.

Chapter 11 brings a conclusion with the most important results and observations.

Chapter 12 summarizes contributions of the thesis in the fields of silicon passivation and characterization.

Chapter 13 presents further possible research steps in the field of silicon passivation processes and material characterization.

1 Solar Cell

Description of a PN-junction is presented in the first part of the chapter. In the second part, the most important solar cell parameters, one and two diode models are discussed and finally standard testing conditions are here shortly mentioned.

1.1 PN-junction

In general, a solar cell is a semiconductor device that produces electric current when exposed to light [3]. A PN-junction is a typical example of such a device, see Fig. 1.1. It is a connection of two semiconductors where one (P-type semiconductor) contains a predominant concentration of available positively charged free carriers (hole = missing electron) and negatively charged free carriers (electrons) represent the main source of electrical conductivity in the N-type semiconductor.

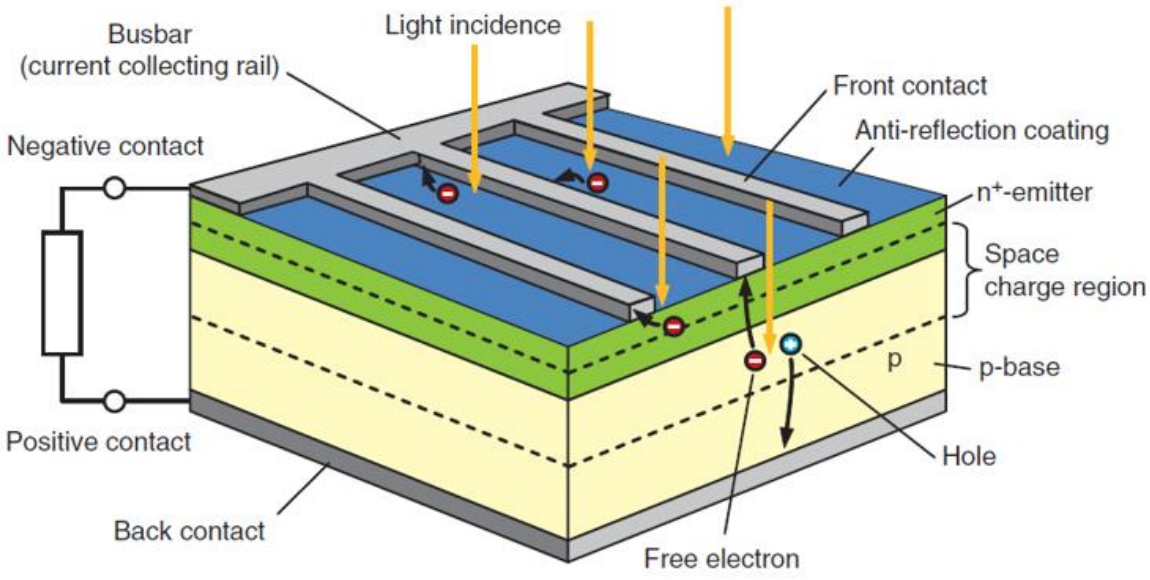

Fig. 1.1. PN-junction used as a solar cell [4].

A potential barrier is built on the interface of these two semiconductors when they are connected and an electric filed is spread across a depletion (called also a space charge) region. A width of this region depends basically on the doping density of P-type (acceptor concentration N_A) and N-type (donor concentration N_D) parts, see Fig. 1.2 and on an applied voltage (forward or reverse regime), see Fig. 1.4.

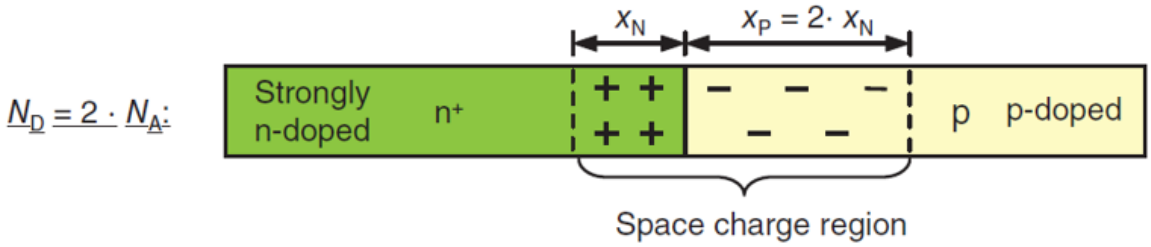

Fig. 1.2. Width of the space charge region [4].

The depletion region with a built-in electric field plays a key role in the transformation process of light into electricity. Each recombined free charge carrier (electron or hole) is a loss. Desirable steps of photovoltaic transformation in a solar cell are:

a) light absorption in the depletion region (or in surrounding regions no further than the diffusion length of minority charge carriers) and generation of electron-hole pairs,
b) redistribution of the free electrons (into N-type) and holes (into P-type) in the electric field (drift) of the depletion region,
c) collection of the free charge carriers by electrodes and current flow through an external wiring with a load.

If N- and P-type parts of the solar cell are connected by an external wiring, current flows through it. If the circuit is open, electrons concentrate in the N-type part and holes in the P-type part of the PN-junction beyond the space charge region and they recombine according to their lifetime given by the electrical quality of the semiconductor, i.e. electrical activity of structural defects and impurities.

There are many ways how a free charge carrier can be lost in the photovoltaic transformation process, e.g. radiative or band-to-band recombination (energy lost to photon), trap-assisted or Shockley-Read-Hall recombination (energy lost to lattice in form of phonon), and Auger recombination (energy lost to another carrier), see Fig. 1.3. Only free electrons and holes that survive all the above mentioned steps of the photovoltaic transformation and participate in the resulting current flowing through the external wiring are included into the final solar cell efficiency.

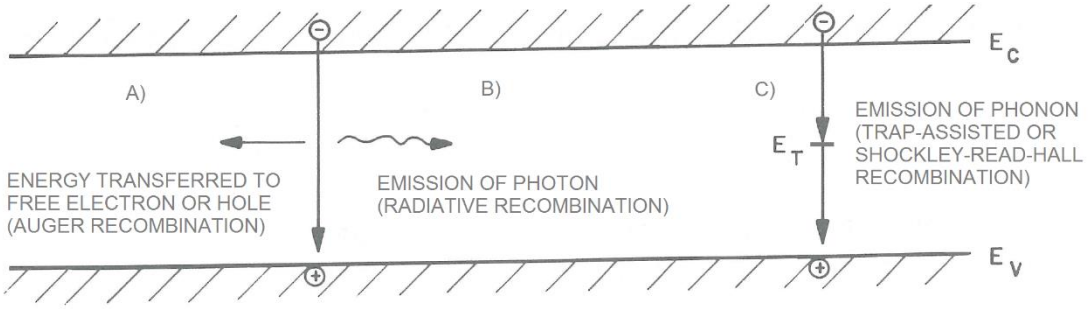

Fig. 1.3. Recombination processes in a semiconductor: a) Auger recombination, b) radiative recombination, c) Shockley-Read-Hall recombination. Taken with modifications from [5].

The most important feature of a PN-junction is its rectifying ability. It means amount of electric current that can flow through the junction is significantly dependent on direction of the current flow – whether the current should flow from P-type into N-type semiconductor or vice versa. When external voltage is connected to the PN-junction in dark with a plus pole on the side of P-type silicon and a minus pole on the side of N-type silicon, the current flowing through the PN-junction is significantly higher than in opposite arrangement, see Fig. 1.4. A current-voltage (I-V) characteristic of the PN-junction in dark is present in quadrants I. and III.

Mechanisms taking place in the PN-junction under a forward voltage (plus pole on P-type and minus pole on N-type doped Si) and the corresponding current are presented in Fig. 1.4.a) and b), quadrant I. is discussed. Threshold voltage V_t is an important parameter because only a negligibly small current can flow through the junction under this voltage, Fig. 1.4.a) and the current increases significantly at the voltage over V_t up to the diode destruction, Fig. 1.4.b).

I-V curve of the reversely polarized PN-junction is presented in Fig. 1.4.c) and d) and it consists of two regions. The first one, see Fig. 1.4.c), where the reverse voltage is smaller than the breakdown voltage V_{br}, corresponding reverse saturation current I_0 is negligibly small and almost constant. Nevertheless, I_0 is a very important parameter and it will appear in many following equations characterizing a solar cell operation. The second region of the quadrant III., where the reverse voltage is higher than V_{br}, the reverse current significantly increases up to the diode destruction, Fig. 1.4.d).

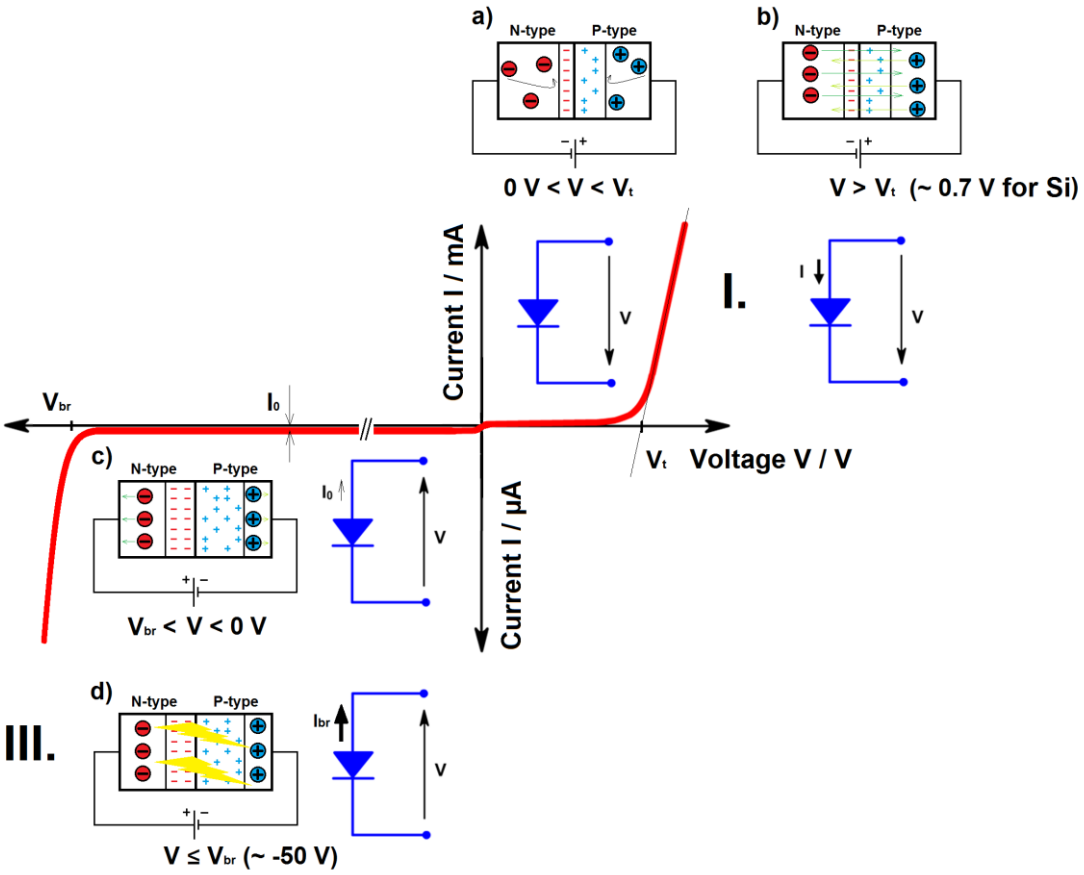

Fig. 1.4. Current-voltage characteristic of a PN-junction in dark: a) schematic diagram of a PN-junction at a forward voltage smaller than the threshold voltage V_t b) schematic diagram of a PN-junction at a forward voltage over V_t c) schematic diagram of a PN-junction with an extended depletion region at a reverse voltage higher than V_{br} d) schematic diagram of a PN-junction at a reverse voltage smaller than V_{br} resulting into electric breakdown.

1.2 Basic Principles of a Solar Cell Operation

Current-voltage characteristic of a PN-junction operating in dark can be described by the equation

$$I = I_0 \left[exp\left(\frac{qV}{mkT}\right) - 1 \right] = S.J_0 \left[exp\left(\frac{qV}{mkT}\right) - 1 \right] \qquad \text{(Eq. 1.1)}$$

where: I ….. current flowing through the diode,
I_0 …. reverse saturation current of the diode in dark,
J_0 … reverse saturation current density of the diode in dark,
V …. voltage,
m … ideality factor of the diode,
k …. Boltzmann's constant,
T …. absolute temperature,
S …. area of the PN-junction.

$$J_0 = qn_i^2 \left(\frac{\sqrt{D_n}}{N_A \sqrt{\tau_n}} + \frac{\sqrt{D_p}}{N_D \sqrt{\tau_p}} \right) \quad . \quad \text{(Eq. 1.2)}$$

Current-voltage characteristic of a PN-junction operating in dark (blue curve) shifts down under different light intensities (red curves), see Fig. 1.5. Quadrant I. – forward region, where a small voltage change has a strong current response. Quadrant III. – a photodiode operation region of almost constant reverse current linearly proportional to light intensity. Quadrant IV. – a solar cell operation region with a typical knee in the current-voltage characteristic.

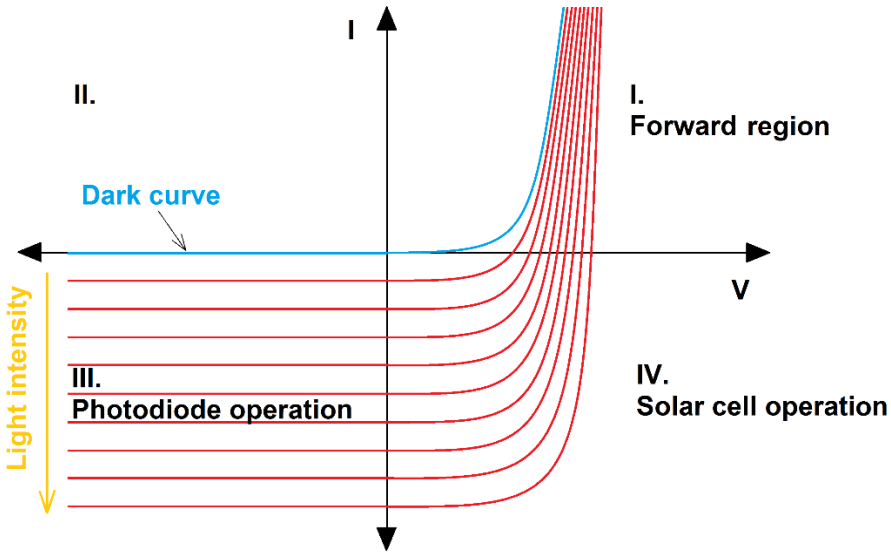

Fig. 1.5. Current-voltage characteristic of a PN-junction at different light intensities.

Current-voltage characteristic of an illuminated PN-junction is shifted down by an increasing light intensity, size of the shift is linearly proportional to the light intensity. An illuminated diode operating in the Quadrant IV. is no more a power consumer, it becomes a power generator and its I-V curve is commonly presented in an inverted form with respect to voltage-axis, see Fig. 1.6.

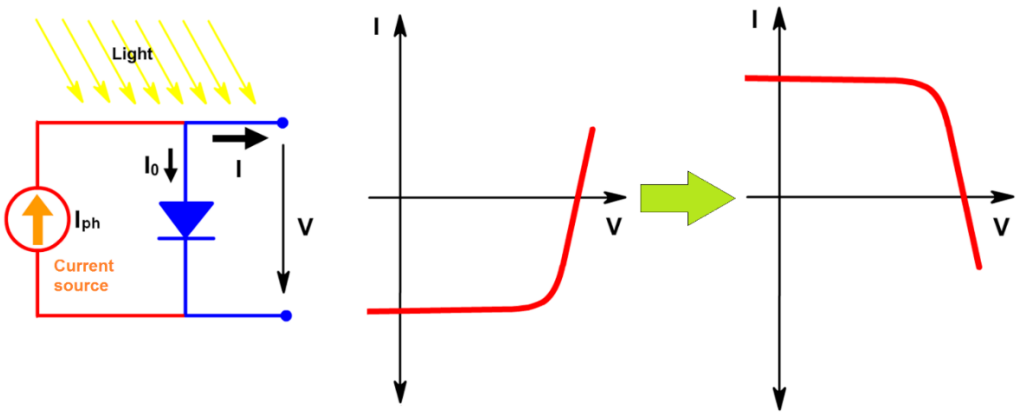

Fig. 1.6. Current-voltage characteristic of a solar cell presented as a power generator: a) schematic diagram of an illuminated solar cell, b) I-V curve of the solar cell shifted down due to an incident light, c) inverted I-V curve of the solar cell to emphasize its power generating character.

1.2.1 One Diode Model and Two Diode Model

An illuminated solar cell can be described by the following equation that corresponds to a ***one diode model*** presented in Fig. 1.7.

$$I = I_{ph} - I_0 \left\{ exp\left[\frac{q(V+R_s I)}{mkT}\right] - 1 \right\} - \frac{V+R_s I}{R_{sh}} \qquad \text{(Eq. 1.3)}$$

where: I ….. current flowing out of the solar cell,
I_{ph} … photogenerated current generated by a solar cell linearly proportional to the light intensity,
I_0 …. reverse dark saturation current flowing through the PN-junction, this model expects predominant recombination in silicon bulk and at surfaces,
V_{oc} .. open-circuit voltage measured at open circuit, when no current flows out of the cell,
V …. voltage of the solar cell,
R_{sh} .. shunt resistance of the PN-junction representing mainly quality of the diode's depletion region, R_{sh} should be as big as possible corresponding to a low concentration of defects and imperfections,
R_s … series resistance of the solar cell's bulk region without electric field and whole resistance arising from wiring and all contacts standing in the path of the current, R_s should be as small as possible,
m … ideality factor dependent on an injection level of charge carriers; it is close to 1 at a low injection level $\Delta n << N$ and close to 2 at a high injection level $\Delta n >> N$.

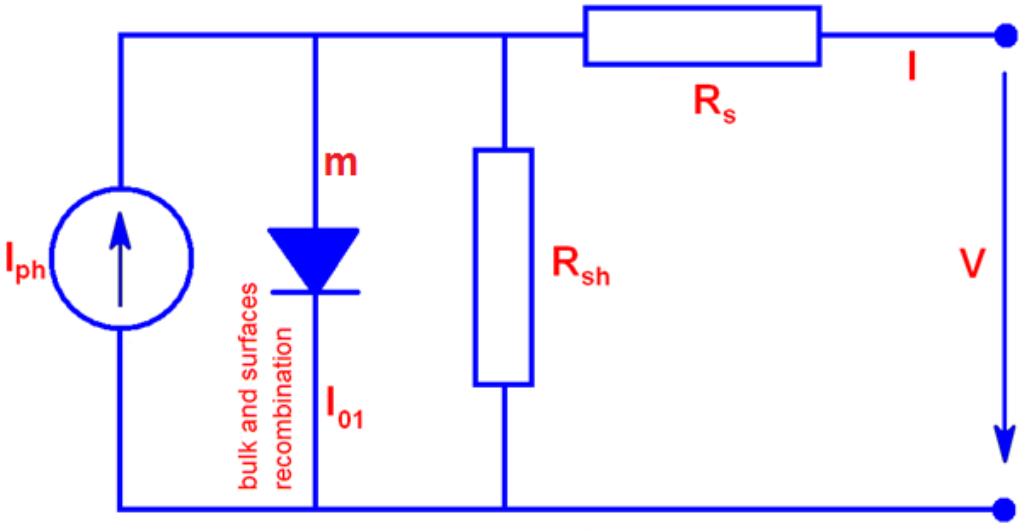

Fig. 1.7. One diode model of a solar cell, where surface and bulk recombination predominate.

One diode model assuming a constant ideality factor m = 1 implies a low injection level of charge carriers and recombination takes place mainly in the bulk and at the surfaces. However, when the injection level is high, the voltage across the cell becomes low and recombination at the depletion region of the PN-junction cannot be neglected, then n ≥ 2 and the one diode model is no more valid. A ***two diode model***, Fig. 1.8, expecting a predominant recombination in the depletion region gives more accurate results in this case. Nevertheless, suitability of a particular solar cell model depends on many factors, e.g. a solar cell structure and operation conditions. Equation describing the solar cell according to the ***two diode model*** is

$$I = I_{ph} - I_{01}\left\{exp\left[\frac{q(V + R_s I)}{m_1 kT}\right] - 1\right\} - I_{02}\left\{exp\left[\frac{q(V + R_s I)}{m_2 kT}\right] - 1\right\} - \frac{V + R_s I}{R_{sh}}$$

(Eq. 1.4)

where: I_{01} …reverse dark saturation current flowing through the diode 1, this model expects predominant recombination in silicon bulk and at the surfaces,
I_{02} …reverse dark saturation current flowing through the diode 2, this model takes into account recombination in the depletion region of the junction.

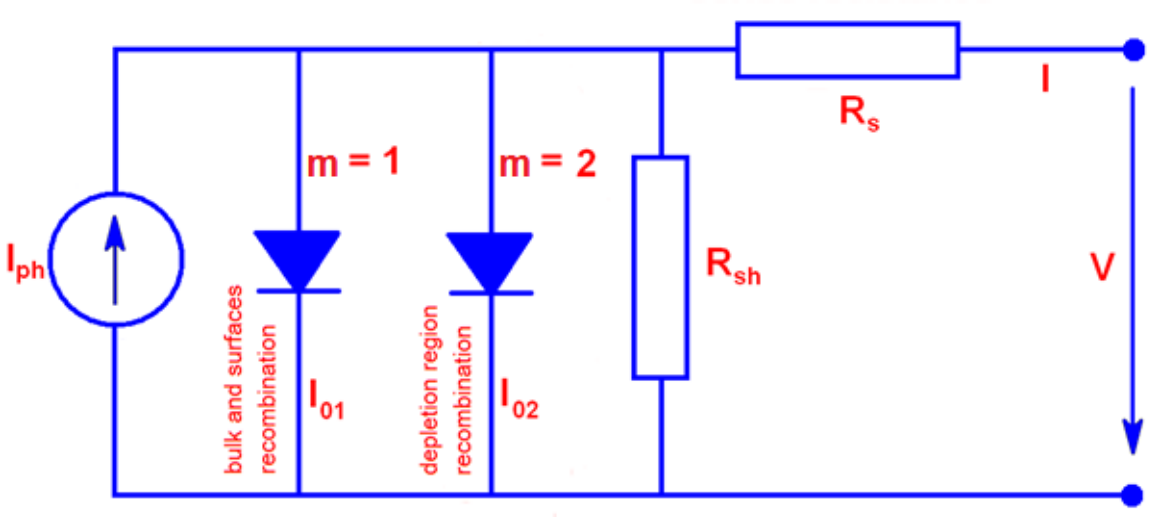

Fig. 1.8. Two diode model of a solar cell, where recombination predominates at the depletion region of the PN-junction.

It should be remarked that both equations Eq. 1.3 and 1.4 express the current I flowing out of the solar cell through the wiring that closes the external circuit of the solar cell. This current would be equal to photogenerated current I_{ph}, if all other equation parts with minus sign (-) could be neglected. In other words, when the recombination in the bulk, at the surfaces and in the depletion region is not significant, shunt resistance achieves desirably high values and series resistance is small enough, operation of the solar cell becomes similar to the ideal case and $I \approx I_{ph}$.

1.2.2 Standard Testing Conditions

Current-voltage characteristic is the most important characterization of a solar cell. It should be measured at the ***standard testing conditions*** (STC): a) temperature of 25 °C, b) light intensity of 1,000 W/m^2, c) light spectrum AM 1.5 (air mass) – spectrum of the Sun light that passes through the Earth atmosphere (in other words air mass) under the angle of around 42°. Definition of AM 1.5 and the corresponding spectrum are presented in Fig. 1.9 and 1.10, respectively. It should be mentioned that Sun spectrum depends also on altitude above sea level. Solar cell parameters are strongly dependent on the testing conditions. Therefore, it is necessary to keep them constant to enable comparison of different solar cells.

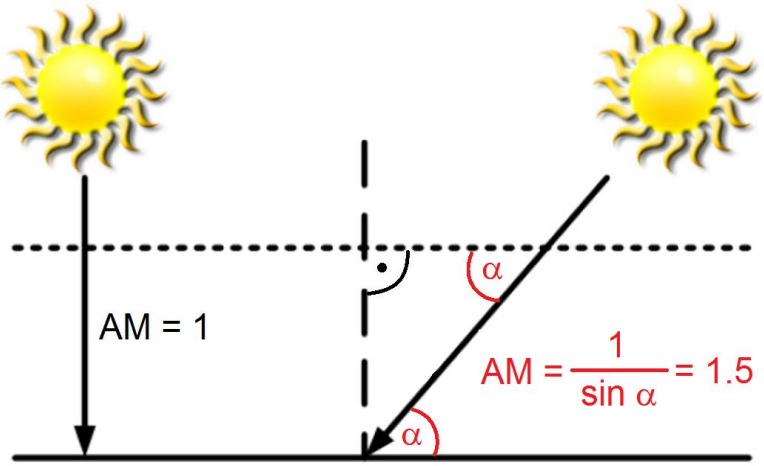

Fig. 1.9. Definition of a light source spectrum AM 1.5 (air mass) as one of 3 standard testing conditions.

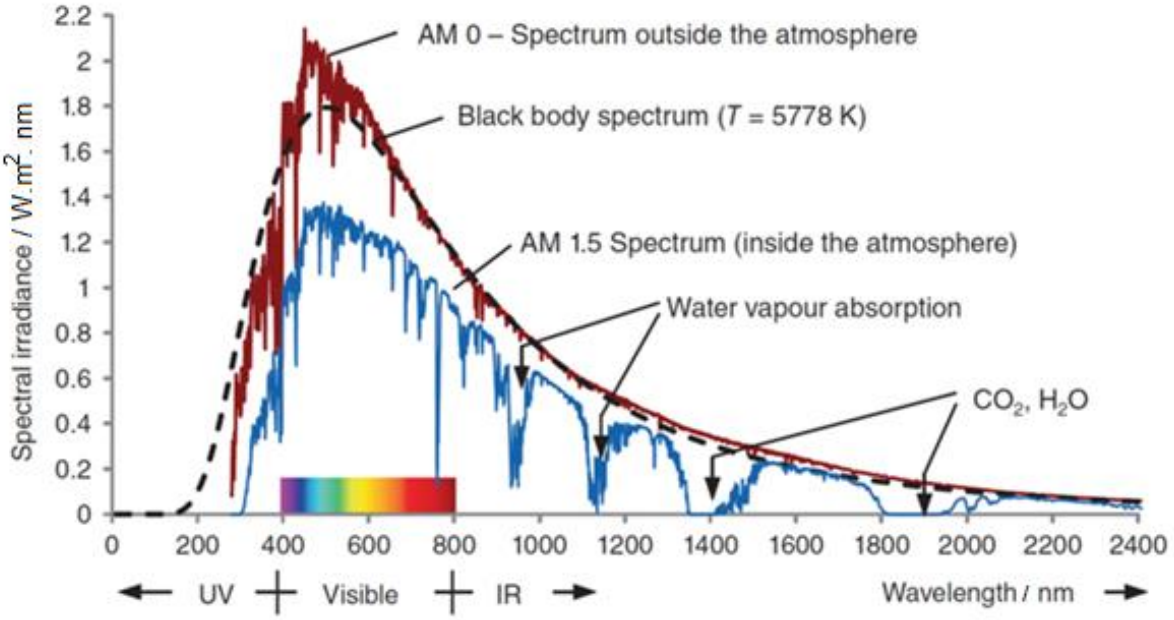

Fig. 1.10. Spectrum of the Sun light corresponding to AM (air mass) 0 and 1.5, and of a black body [4].

1.2.3 Basic Solar Cell Parameters

Current-voltage characteristic can be measured as output current and voltage of a solar cell, when an external series resistance so called load R_L is connected to the solar cell. Modulation of this R_L enables to determine I and the corresponding V starting commonly at the point of open-circuit voltage V_{OC}, where R_L is infinite (disconnection of the circuit), to the point of short-circuit I_{SC}, where R_L is zero (only theoretical case), Fig. 1.11. Example of a current-voltage characteristic with respect to the modulated R_L is shown in Fig. 1.12.

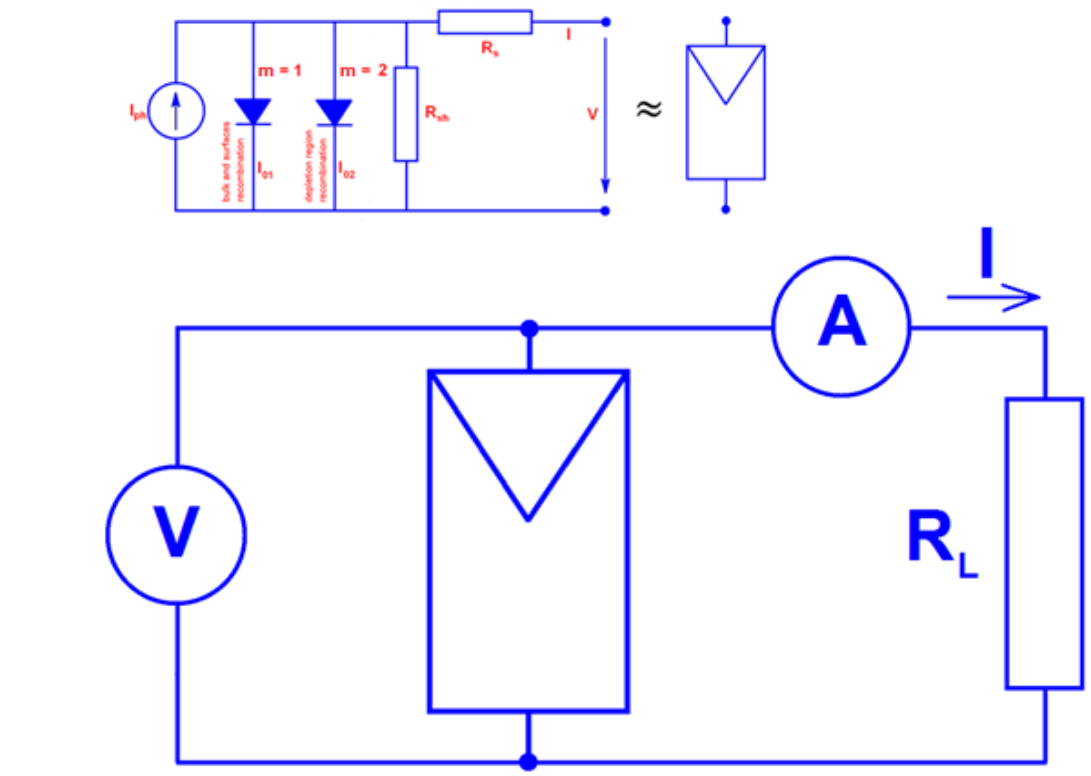

Fig. 1.11. Equivalent circuit for a current-voltage characteristic measurement.

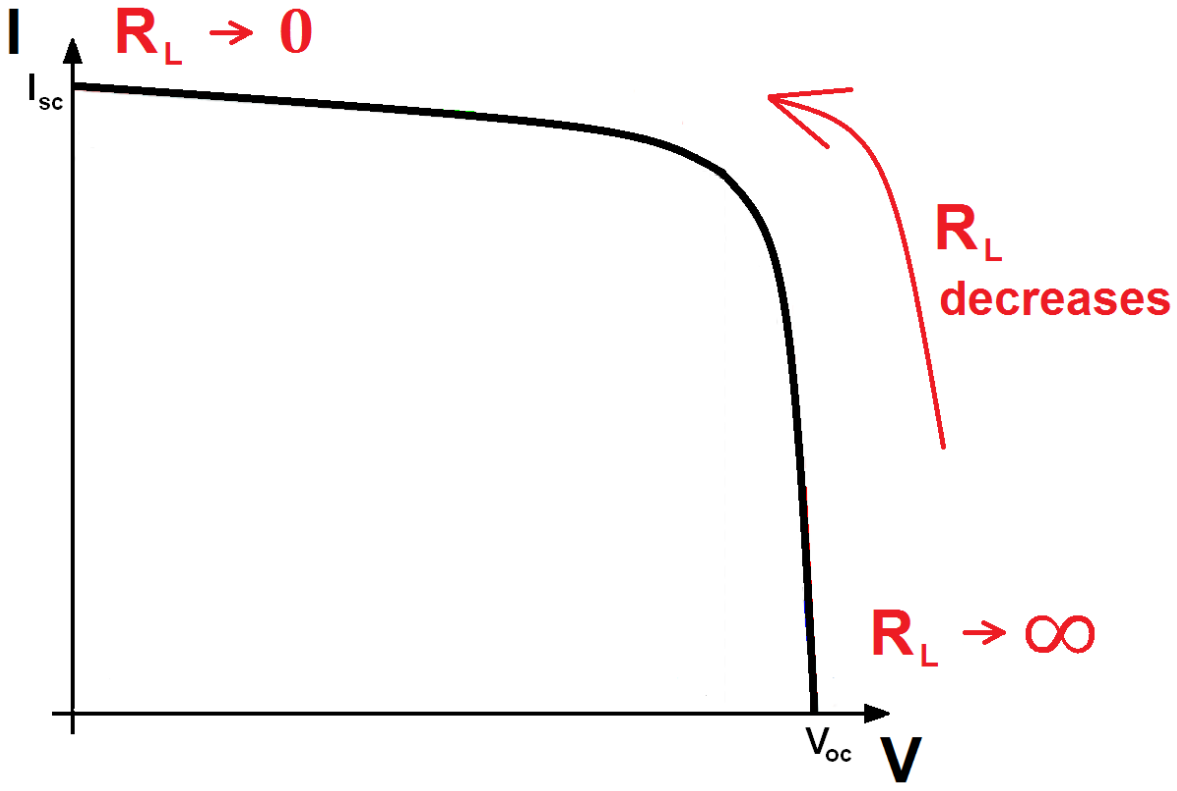

Fig. 1.12. Current-voltage characteristic of a solar cell with respect to a modulated load R_L.

Basic solar cell parameters that can be obtained from a current-voltage characteristic are presented in Fig. 1.13:

a) open-circuit voltage V_{OC} (at disconnected circuit),
b) short-circuit current I_{SC} (at negligibly small R_L in comparison with R_s of the solar cell),
c) series resistance R_s determined as a slope of the tangent line to the solar cell's I-V curve at $V = V_{OC}$; the slope is negative, but R_s has to be positive,
d) shunt resistance R_{sh} determined as a slope of the tangent line to the solar cell's I-V curve at $V = 0$; the slope is negative, but R_{sh} has to be positive,
e) maximum power point P_{MPP} corresponds to the maximum electric power coming out from the solar cell (optimum load is needed),
f) fill factor FF is defined as a comparison of the power in P_{MPP} and the power that would come out the solar cell, if R_s were zero and R_{sh} infinite,
g) efficiency η gives information about how much power is transformed from light power into electric power calculated as a ratio of the power coming out the solar cell to the power of the light.

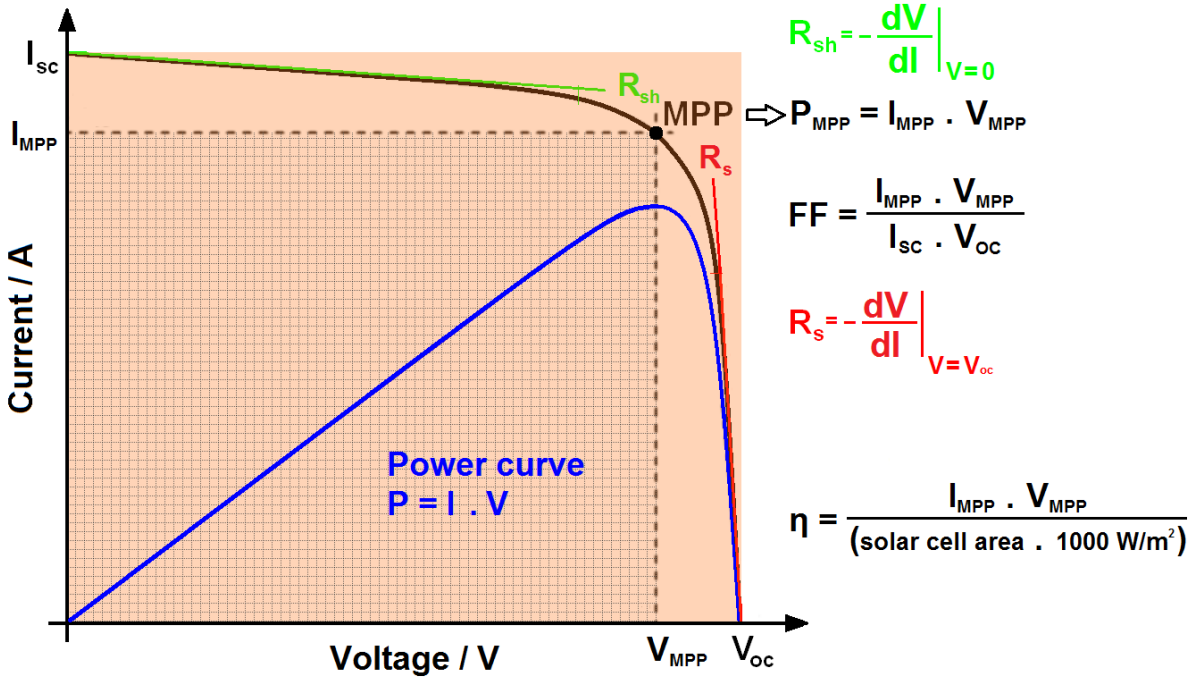

Fig. 1.13. Basic parameters of a solar cell's current-voltage characteristic.

Light is a power input for a solar cell and its intensity strongly impacts solar cell parameters, e.g. in ideal theoretical case ($R_s \rightarrow 0\ \Omega$, $R_{sh} \rightarrow \infty\ \Omega$), there is a linear dependence of short-circuit current I_{SC} and a logarithmic dependence of open-circuit voltage V_{OC} on the light intensity, see Fig. 1.14.

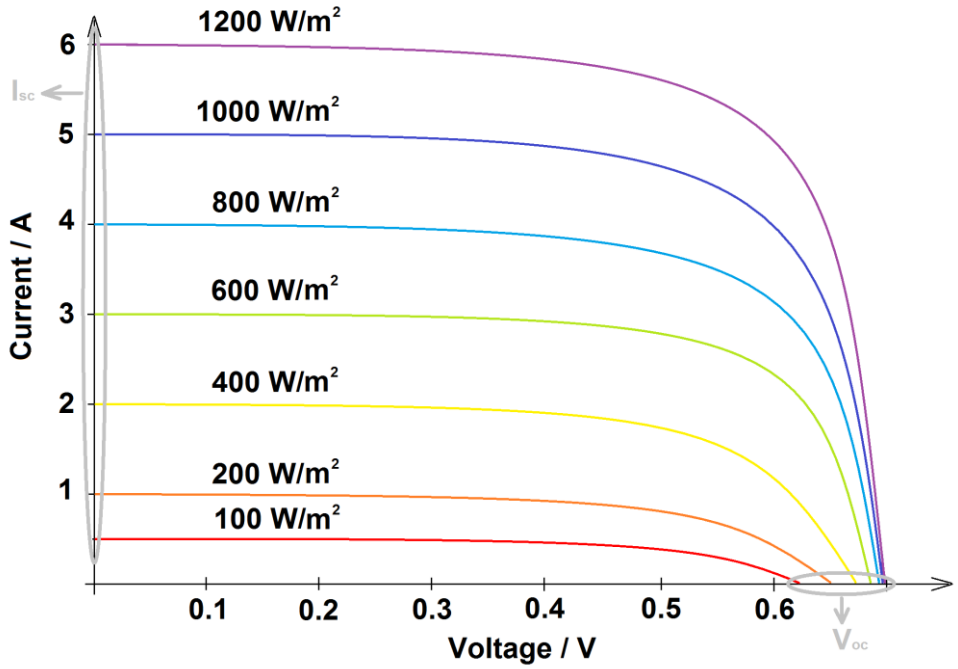

Fig. 1.14. Dependence of a solar cell's current-voltage characteristic on light intensity.

Besides light intensity, there is a strong impact of temperature on the current-voltage characteristic. V_{OC} significantly decreases and I_{SC} slightly increases with increasing temperature, see Fig. 1.15. As a result, electric power generated by the solar cell decreases with an elevated temperature.

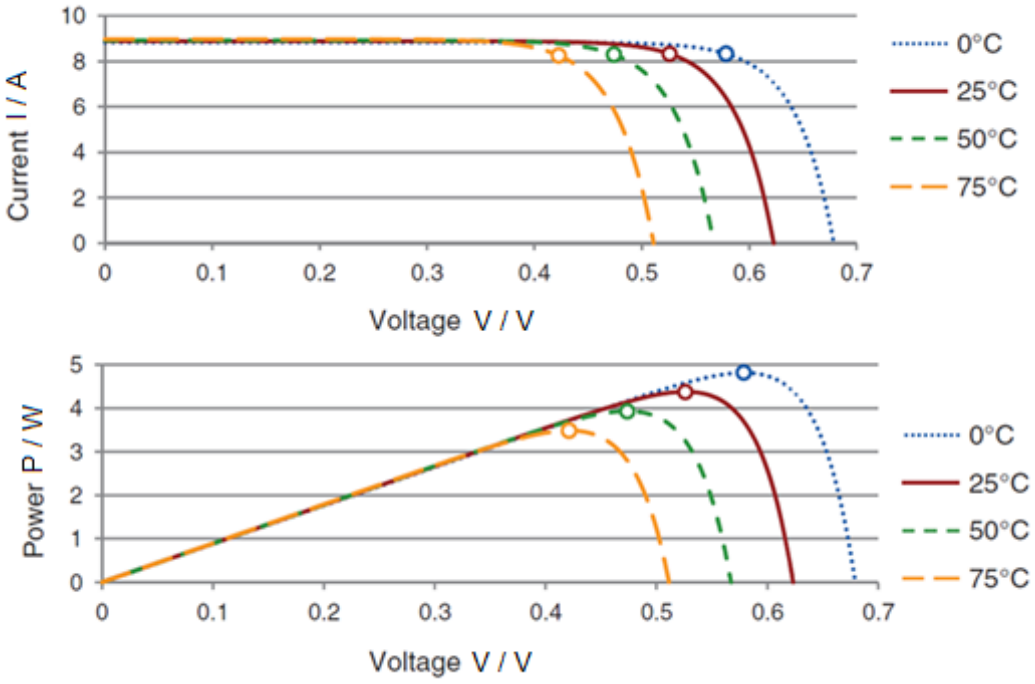

Fig. 1.15. Effect of an elevated temperature on a solar cell's current-voltage characteristic [4].

While R_s should achieve values as small as possible (typically ≈ Ω), R_{sh} (typically ≈ MΩ) should be significantly higher than R_s. Simulations of a solar cell's current-voltage characteristics at different R_s and R_{sh} are presented in Fig. 1.16.a) and b), respectively.

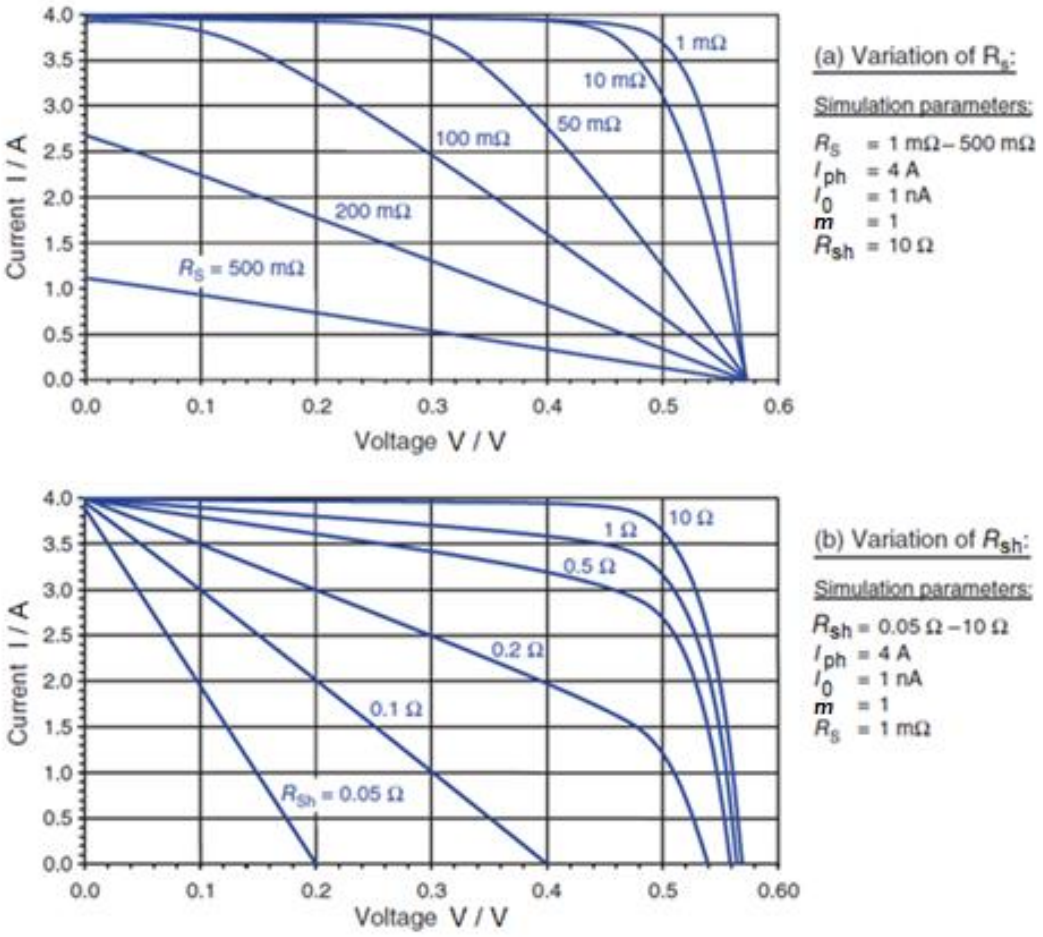

Fig. 1.16. Dependence of a solar cell's current-voltage characteristic on: a) series resistance and b) shunt resistance [4].

2 Silicon Structure and Optical Properties

Optical and structural properties of thin film and wafer-based silicon solar cells are discussed in this chapter. They deserve appropriate attention at solar cells designing and manufacturing.

2.1 Silicon Structure

Thickness and structure of thin silicon films are the most important differences in comparison with wafer-based solar cells. While thickness of the last mentioned solar cell type is around 180 μm, thickness of thin film solar cells is in range of a few μm.

Arrangement of silicon atoms in an ideal silicon crystal is regular in all 3 dimensions through-out the whole structure. There are no structural defects or impurities. Nevertheless, there is still a surface of the crystal that represents a planar imperfection.

Monocrystalline silicon (mono-Si) does not represent an ideal crystal, but it is very close to this case, Fig. 2.1.a). Multicrystalline silicon (multi-Si) consists of grains with a size of mm and cm whose crystallographic orientation is random, Fig. 2.1.b). Polycrystalline silicon (poly-Si) is a type of crystalline silicon with an even lower level of structural order, where a size of grains is around μm, Fig. 2.1.c). Microcrystalline silicon (micro-Si), shown in Fig. 2.1.d), includes grains of crystalline phase as well as amorphous silicon (a-Si:H). Amorphous silicon is a structure with randomly arranged silicon atoms, Fig. 2.1.e). There are many other silicon types with different arrangement of silicon atoms in bulk and their names and definitions are not always strictly specified. Nevertheless, the above mentioned silicon abbreviations are going to be used in this thesis except cases, where it is directly specified.

Different structure affects silicon properties, e.g. while a band gap E_g of mono-Si, multi-Si, poly-Si and micro-Si is 1.12 eV, E_g of a-Si:H is around 1.8 eV. There is a high concentration of free dangling bonds in amorphous silicon that are very reactive and need to be saturated. Hydrogen atom is due to its small dimensions and just one valence electron the appropriate particle to saturate these free bonds. The a-Si:H band gap becomes wider with increasing hydrogen content. A sufficient amount of hydrogen in the silicon structure is needed to observe the above described enlargement of the band gap. Typical concentration of hydrogen in a-Si:H is around 10 % [6], but it can vary in a broad range.

Different crystalline silicon (c-Si) types (mono-, multi-, and poly-Si) are distinguished from each other by different grain size and consequently also by concentration of grain boundaries that represent structural imperfections. Dislocations are other structural imperfections often present in silicon. In general, concentration of structural defects is significantly higher in thin films than in wafer-based solar cells.

In our case, defects are understood as crystallographic imperfections in semiconductor lattice. They can be classified from a dimensional point of view into four groups:

a) point defects (vacancy, interstitial, Frenkel and extrinsic defects),
b) line defects (straight dislocations and dislocation loops),
c) area defects (surface, stacking faults, twins and grain boundaries), and
d) volume defects (precipitates and voids).

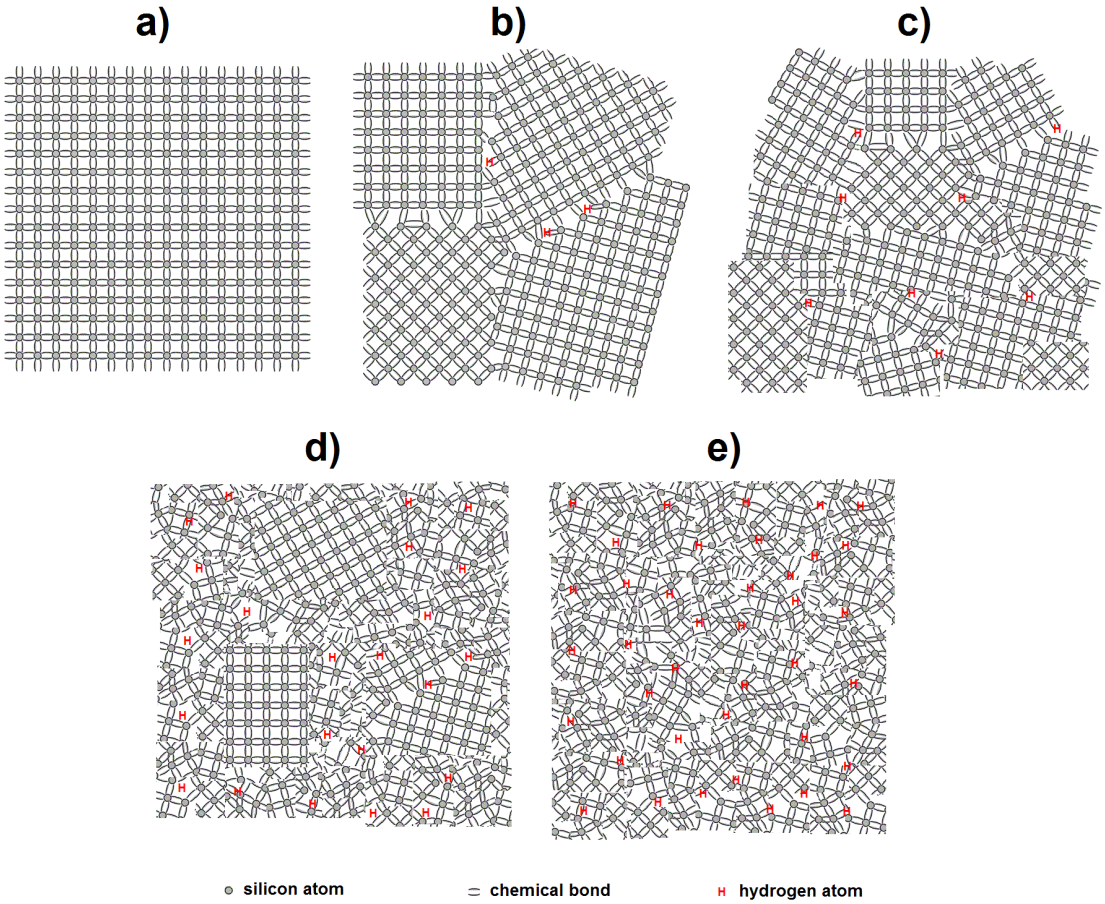

Fig. 2.1. Arrangement of silicon atoms in: a) monocrystalline silicon (mono-Si), b) multicrystalline silicon (multi-Si), c) polycrystalline silicon (poly-Si), d) microcrystalline silicon (micro-Si), e) amorphous silicon (a-Si:H).

These defects are often so called decorated by impurities (undesirable atoms of a different element). Structural defects represent more favourable places for impurities than a defects-free crystal. A decoration of grain boundaries is a typical example. The reason why defects and impurities attract such attention is their negative impact on transformation of absorbed light into electricity. When defects or impurities are electrically active they act as recombination centres. They form an electronic level in the band gap of the semiconductor (a deep or shallow level or a whole defect band in some cases) and decrease efficiency of the photovoltaic transformation this way.

Structure of polycrystalline silicon thin film solar cells investigated in this work is shown in Fig. 2.2. The map was measured by electron backscatter diffraction (EBSD) under observation angle of 60° at the Helmholtz-Zentrum Berlin, Germany. Poor quality of poly-Si is commonly explained by a high concentration of grain boundaries, in other words small grain size ≈ 2 μm [7]–[9]. More recent studies [10]–[14] offer a high concentration of intra-grain defects, mainly dislocations, as a more likely reason of such a low polycrystalline silicon quality connected with open-circuit voltage V_{OC} below 250 mV for as-crystallized poly-Si thin film solar cells [15], [16].

A cross-section of a polycrystalline silicon thin film solar cell on glass displayed by a scanning electron microscope is presented in Fig. 2.3. The glass substrate is dipped in a solution of glass beads that stick to the glass. The texture of the subsequently deposited poly-Si thin film adopts the shape of the glass substrate with beads. More details to the preparation of solid phase crystallized Si thin film solar cells used for experiments in the frame of this work are presented in Chapter 5.

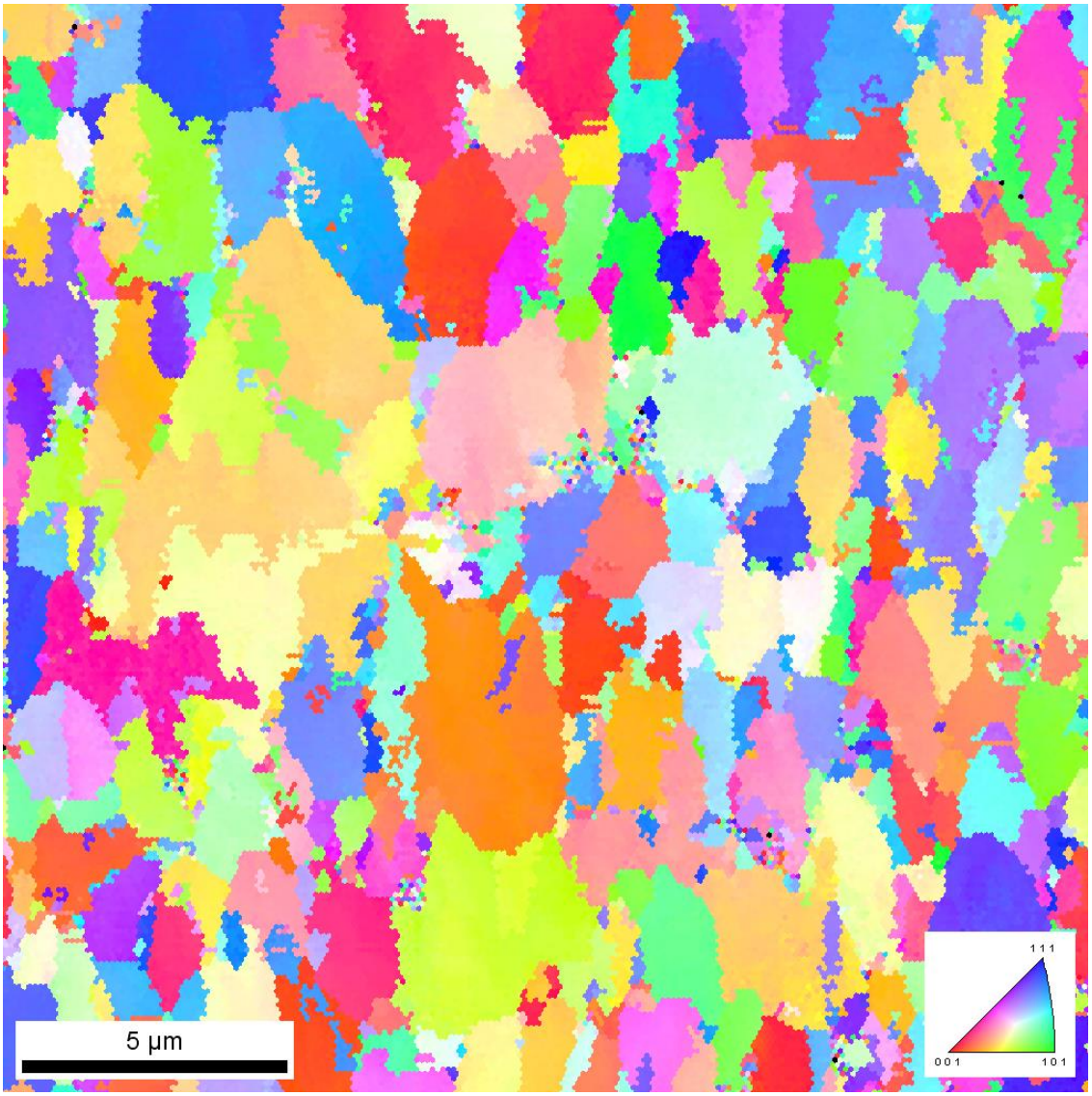

Fig. 2.2. A polycrystalline silicon thin film solar cell scanned by electron backscatter diffraction (EBSD), different colours correspond to particular crystallographic orientation of silicon grains, measured at the Helmholtz-Zentrum Berlin, Germany.

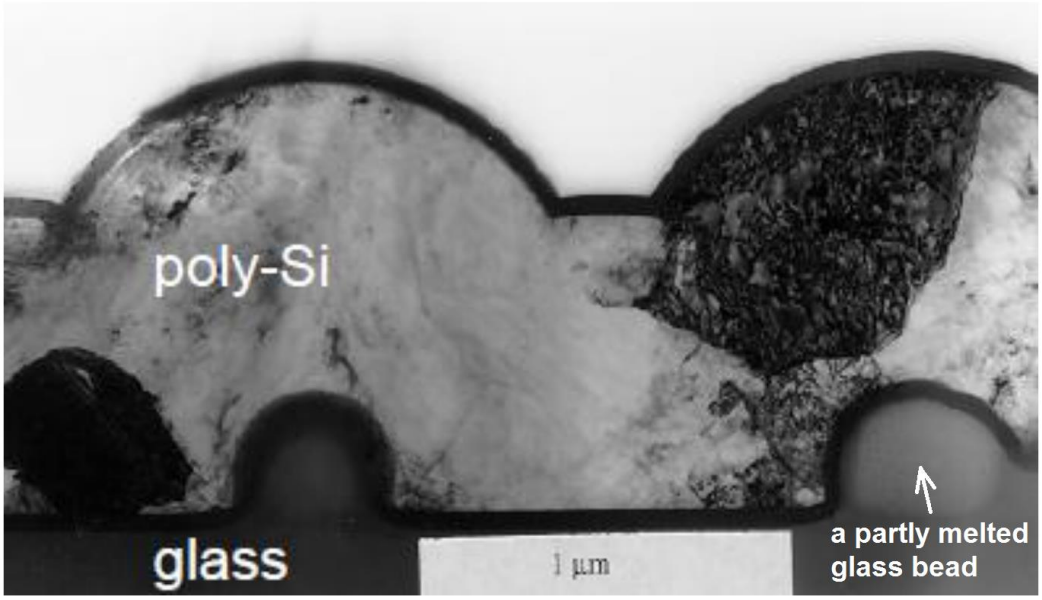

Fig. 2.3. A cross-section of a polycrystalline silicon thin film solar cell on a glass substrate with glass beads [16].

2.2 Optical Properties of Silicon

There are two key drawbacks about polycrystalline silicon thin film solar cells that need to be taken into account during designing and manufacturing process:

a) structural defects (grain boundaries and dislocations) that need to be passivated to prevent low quality of silicon connected with a poor solar cell open-circuit voltage V_{OC}, for more details see Chapter 3.
b) poor light absorption due to a small absorption coefficient of polycrystalline silicon in visible wavelength range and due to a small thickness of Si layer of around 2 μm together resulting in a small photogenerated current I_{ph} and consequently a small short-circuit current I_{SC}.

Absorption coefficient of crystalline silicon and poly-Si is significantly smaller in comparison with that of a-Si:H for most of visible light wavelengths and there are semiconductors with more suitable optical parameters than silicon, Fig. 2.4. Nevertheless, silicon is a non-toxic material and it is produced from sand that is abundantly present on the Earth. Its electrical properties can be modified in a large range from a very low electric conductivity (SiO_2) to conductivities close to metallic materials (by doping), and there is also a long-time technological experience with silicon based electronic mass production. All these aspects predetermine silicon to be the mainstream material of the photovoltaic mass production.

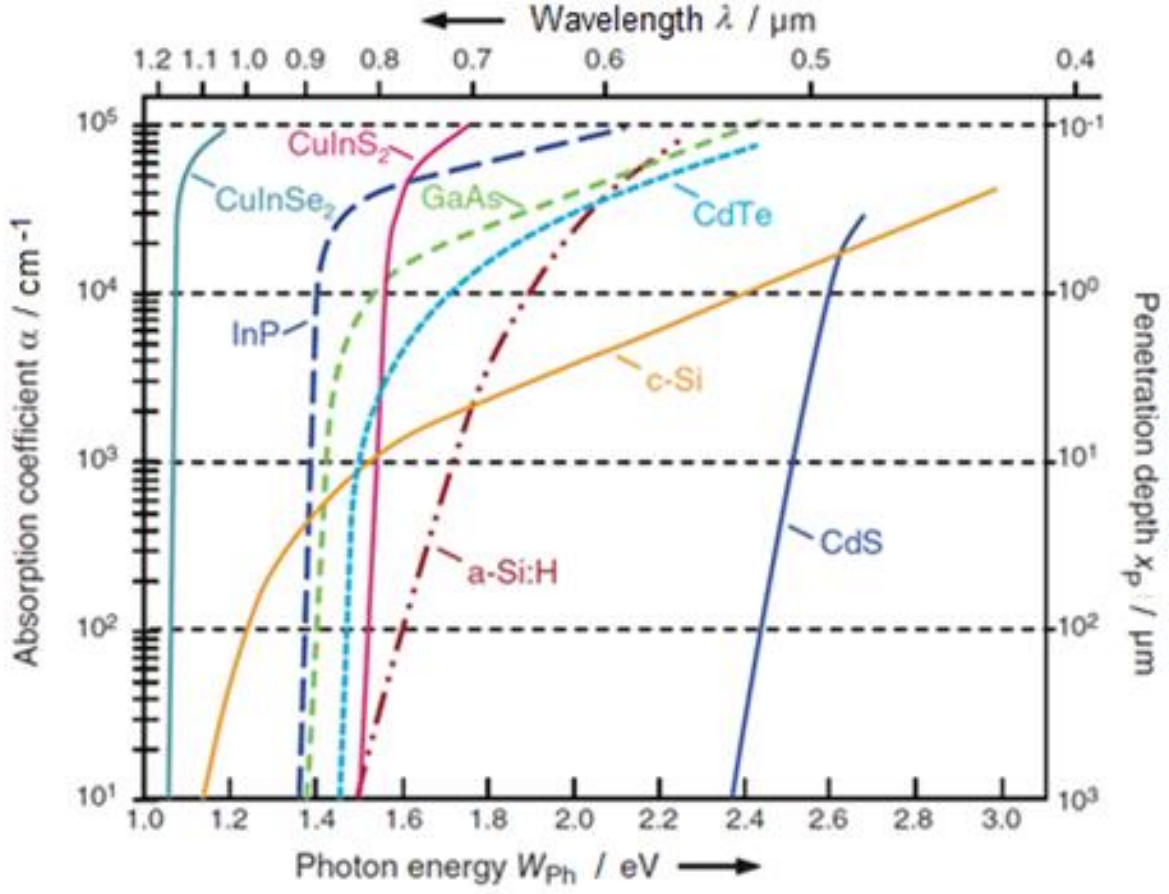

Fig. 2.4. Absorption coefficient and penetration depth as a function of photon energy and wavelength for semiconductors [4].

Low absorption coefficient of c-Si is compensated by a bigger thickness of mono-Si and multi-Si wafer-based solar cells achieving around 200 μm. Nevertheless, even

this Si thickness is not enough to effectively absorb all available Sun light wavelengths. To increase amount of light coming into a solar cell a surface texturing (e.g. pyramids prepared by etching in KOH) and antireflection coating (e.g. SiN layer) are often used. Probability of light absorption in silicon can be significantly improved by a back reflector (e.g. Al, Ag). Importance of an effective light trapping system is even more important in the case of thin film Si solar cells.

An optimum location of a PN-junction under the front surface of a c-Si solar cell can be determined on the base of the Sun spectrum at AM 1.5, see Fig. 2.5, spectral sensitivity of a c-Si solar cell, see Fig. 2.6, and dependence of absorption depth on wavelength for c-Si, see Fig. 2.7 and 2.8.

Only around a half of the Sun light spectrum AM 1.5 is usable for a crystalline silicon solar cell, Fig. 2.5. Photons of short light wavelengths with too much energy are absorbed in silicon, but a significant part of this energy is lost as a ***thermalisation***. In contrast to this, longer wavelengths have too low energy to enable excitation of an electron from a valence band into a conductive band and these photons are lost due to a ***transmission***.

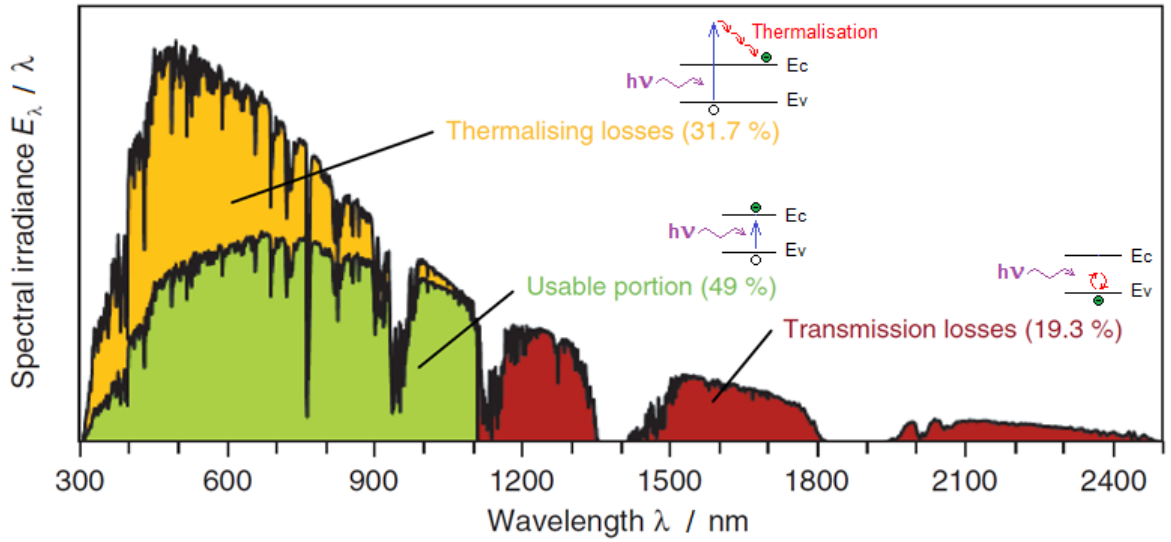

Fig. 2.5. The Sun spectrum AM 1.5 with marked thermalisation and transmission losses, with modifications from [4].

There is also a spectral sensitivity of a c-Si solar cell that needs to be taken into account. ***Spectral sensitivity*** is the ratio of the current generated by the solar cell to the power incident on the solar cell, while ***quantum efficiency*** gives the number of electrons output by the solar cell compared to the number of photons incident on the device, see Chapter 4.3. An ideal spectral sensitivity, a response for a standard c-Si solar cell and for a high efficiency PERL solar cell (with inverted pyramids, a **p**assivated **e**mitter and **r**ear **l**ocally diffused solar cell) are shown in Fig. 2.6. The reasons of a higher spectral sensitivity for a high efficiency cell are a pyramidal structure decreasing reflection of short visible light wavelengths and a back reflector increasing absorption probability of short infrared wavelengths in silicon. Crystalline silicon solar cells are sensitive mainly to long visible and short infrared wavelengths at around 800-900 nm. These wavelengths are absorbed in the depth of around 20 μm, see Fig. 2.7.

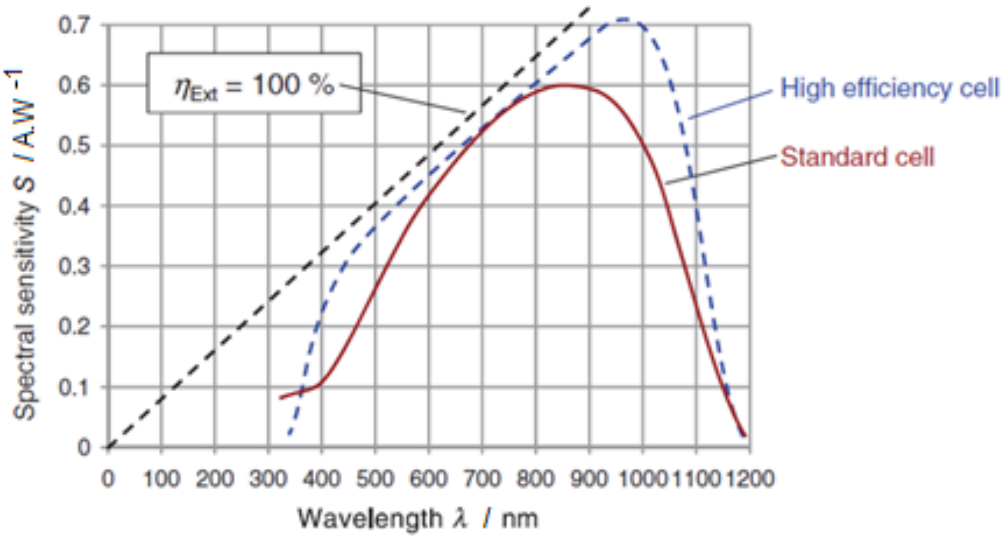

Fig. 2.6. Spectral sensitivity of a standard and high efficiency (e.g. PERL) silicon solar cell as a function of wavelengths [4].

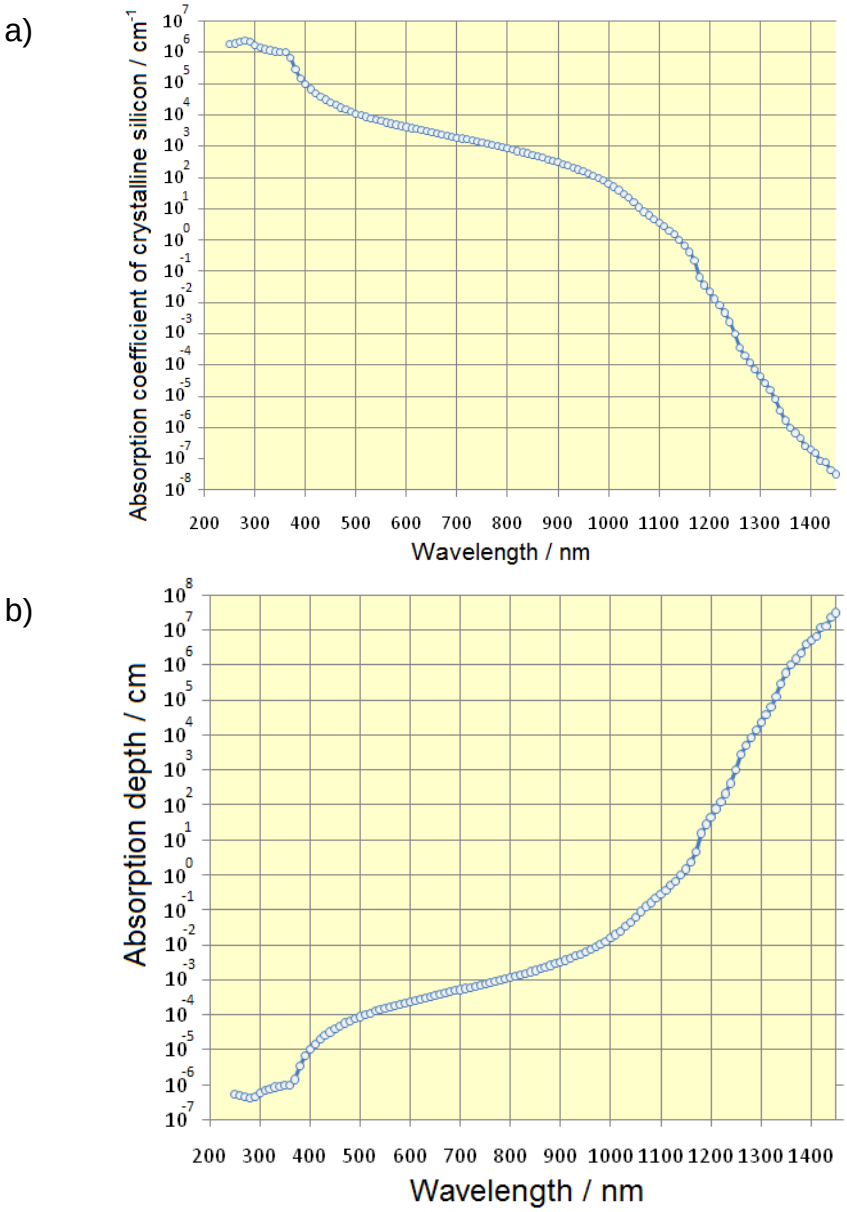

Fig. 2.7. Absorption coefficient a) and absorption depth b) for crystalline silicon [17].

In general, light intensity in a semiconductor decreases exponentially with increasing penetration depth. This phenomenon is characterized by ***absorption coefficient α*** of materials and it depends on wavelength of the absorbed light. Decreasing light intensity with increasing distance x from the surface in material is defined as

$$\theta(x) = \theta_0 . exp(-\alpha . x) \qquad \text{(Eq. 2.1)}$$

where θ_0 is an initial light intensity, θ(x) is a light intensity at depth x and x_L is an absorption depth

$$\alpha = \frac{1}{x_L} \qquad \text{(Eq. 2.2)}$$

Light intensity $\theta(x_L)$ of a particular wavelength at absorption depth x_L is defined by the following equation

$$\theta(x_L) = \theta_0 . exp\left(-\frac{x}{x_L}\right) \qquad \text{(Eq. 2.3)}$$

According to the Eq. 2.3, light intensity gradually decreases from the initial value θ_0 at the surface to $\theta(x_L)$ at absorption depth. Light intensity at x_L is approximately 37 % from the initial intensity due to exponential character of the function, see Fig. 2.8.

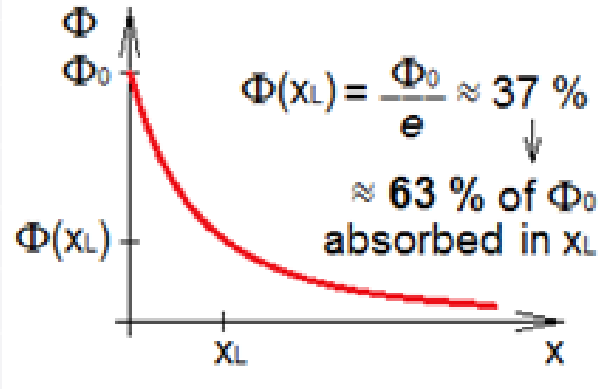

Fig. 2.8. Dependence of light intensity θ(x) on distance x from the surface in material.

Absorption coefficient and absorption depth as a function of light wavelength are specific for particular materials and strongly connected with the material structure. For instance, absorption of visible light wavelengths is significantly higher for amorphous silicon a-Si:H than for crystalline silicon, see Fig. 2.4. The reason is that while amorphous silicon is the semiconductor with a direct band gap diagram, crystalline silicon is one with an indirect diagram.

Semiconductors with a direct band gap (e.g. GaAs, CdTe, $CuInSe_2$) have a global minimum of a semiconductor's conduction band located directly above a position of a global maximum of its valence band, so the electron that absorbs a photon of appropriately high energy can jump directly over the band gap and no interaction with phonon (a vibrating energy quantum of lattice) to change electron's momentum is required, see Fig. 2.9 a). In contrary to this, photon absorption in a semiconductor with an indirect band gap (S, Ge) is possible only with the assistance of a phonon, see Fig. 2.9 b). As a consequence, absorption in this case is less probable than for a semiconductor with a direct band gap.

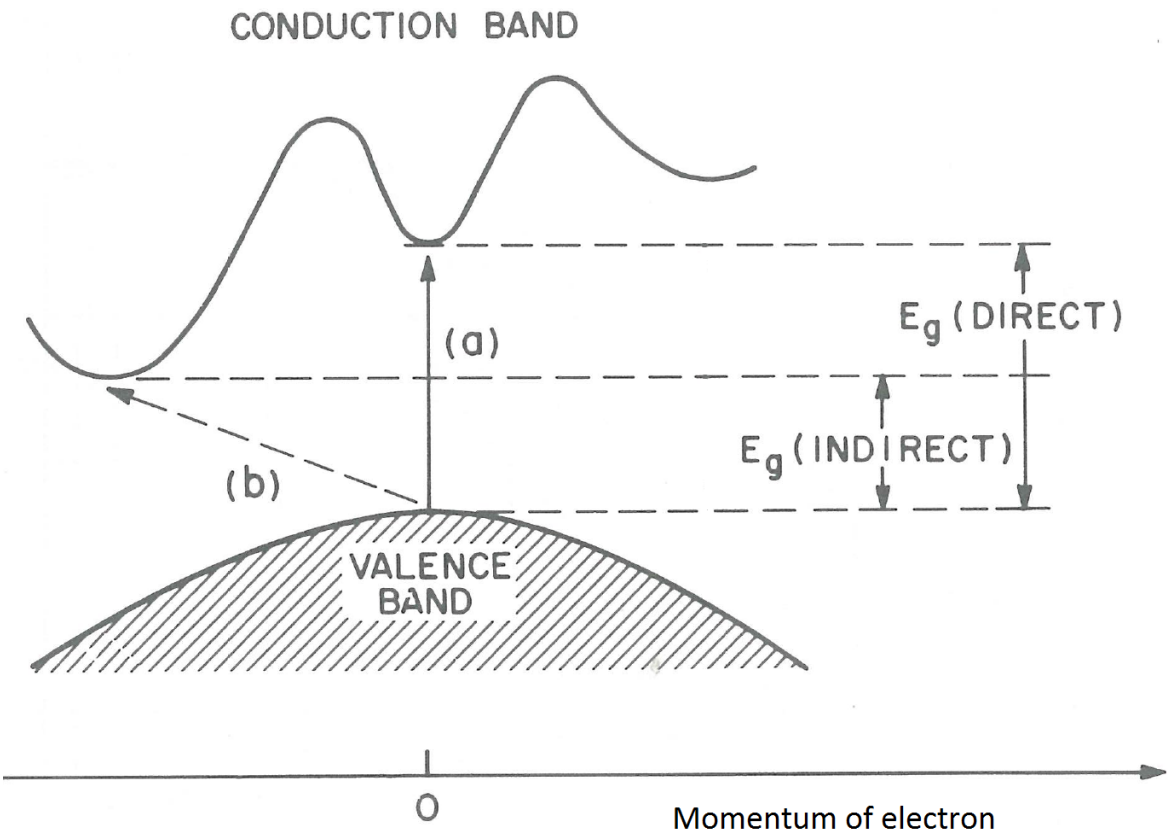

Fig. 2.9. Semiconductor with a) a direct (e.g. GaAs, CdTe, $CuInSe_2$) and b) indirect (e.g. Si, Ge) band gap diagram [5].

Thickness of the thin film polycrystalline silicon solar cells investigated in this thesis is around 1.5 μm corresponding to the absorbed wavelengths from 400 nm to 600 nm. Although most light passes through the cell, the absorbed light suffices to achieve open-circuit voltage of 492 mV (in our case 497 mV, see Chapter 7) and short-circuit current of 29.5 mA/cm^2 in the case of the best solid phase crystallized polycrystalline Si solar cell [16]. These results were achieved also due to the PIN structure of the tested SPC poly-Si cells ensuring electric field across the whole solar cell. In general, distance of the PN-junction from the surface in wafer based solar cells is very important to effectively transport photogenerated charge carriers into the part of the junction where they represent major charge carrier (electron into N-type, hole into P-type) before they recombine. The requirement of a fast charge redistribution is even more important in the case of thin film polycrystalline silicon solar cells with a higher defect density (grain boundaries 10^{16} cm^{-3} and dislocations 10^{10} cm^{-2} [18]).

Diffusion length L of free charge carriers is another important solar cell parameter defined as a distance between the position of its generation and recombination passed by diffusion (no electric field), it is defined by

$$L = \sqrt{D.\tau} \qquad \text{(Eq. 2.4)}$$

where D is diffusion coefficient and τ is a lifetime of charge carriers. Diffusion coefficient of a free charge carrier depends on its mobility μ:

$$D = \frac{kT}{q}\mu \qquad \text{(Eq. 2.5)}$$

Long diffusion length of minority charge carriers is important to achieve high density of generated current. The reason is that there is a significant part of charge carriers photogenerated beyond the depletion region (where no electric field is present) and they can move only by diffusion to reach the region. However, only electrons (minority charge carriers in P-type Si) and holes (minority charge carriers in N-type Si) that diffused into the depletion region and subsequently were transported by the electric field of the space charge region into the part where they become majority charge carriers, only they participate in the generated current, therefore a long diffusion length of minority charge carriers is so important, see Fig. 2.10.

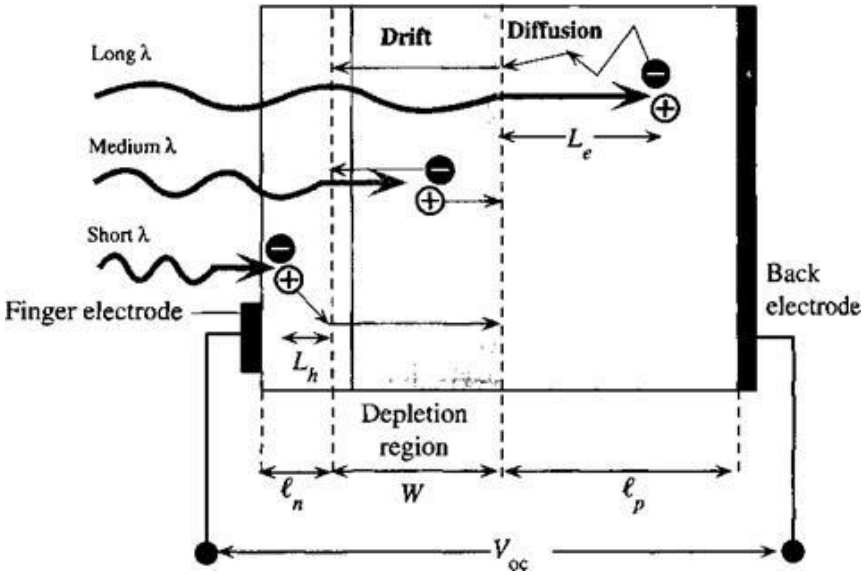

Fig. 2.10. Absorption of different light wavelengths in a solar cell and redistribution of the photogenerated charge carriers [19].

While diffusion length of electrons in P-type low doped mono-Si is 100-300 μm, it is only around μm in poly-Si [20]. Lower quality of poly-Si is partly compensated by the PIN-junction, where the depletion region with the built-in electric field is spread across almost the whole solar cell volume. The electric field accelerates photogenerated charge carriers and their recombination probability is significantly reduced this way. A comparison of silicon wafer-based (PN-junction) and thin film (PIN-junction) solar cells is shown in Fig. 2.11.a) and b).

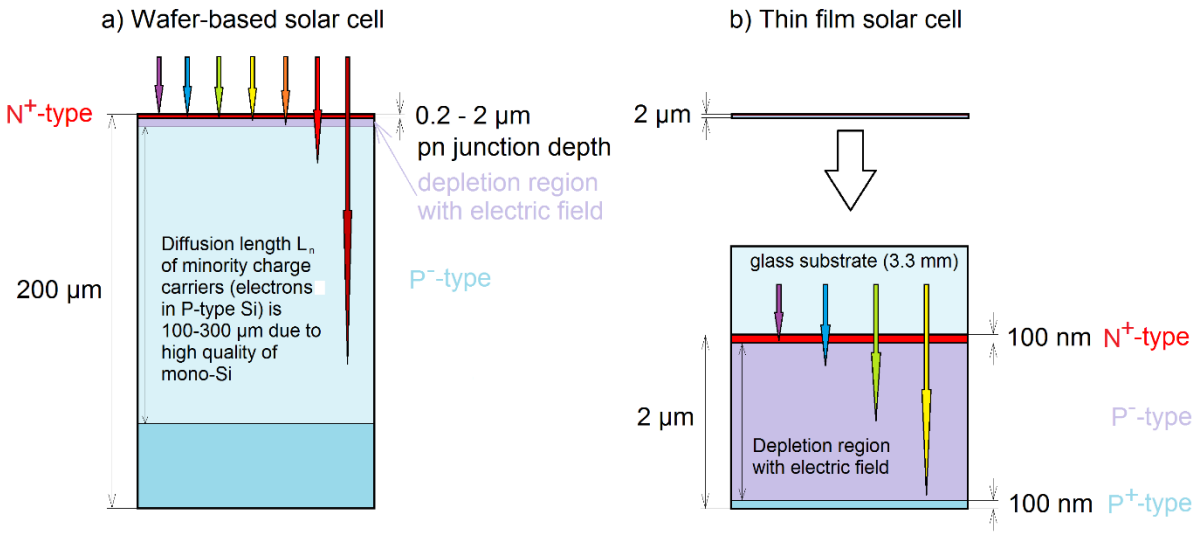

Fig. 2.11. Absorption of particular light wavelengths in: a) a wafer-based and b) a thin film crystalline silicon solar cell.

3 Passivation of Thin Film Silicon Solar Cells

Passivation can be understood as a material protection. In this context it is often spoken about a surface passivation of metals, e.g. aluminium or zinc, where a thin layer of metal oxide covers the metal surface and protects it against further oxidation.

Similar type of a surface passivation can be observed also in the case of silicon. When it is exposed to an oxidizing ambient, a thin layer of SiO_2 covers the silicon surface and prevents further oxidation. Electrical quality of this layer and SiO_2/Si interface is very important in the case of microelectronic and photovoltaic production. Passivation of semiconductors can be understood also as a deactivation of defects acting like recombination centres present

a) at its surface or
b) inside material (bulk).

3.1 Silicon Surface Passivation

In general, surface is a planar defect and its impact on processes in thin films is due to the surface-bulk ratio even stronger than in the case of wafer-based solar cells. Passivation of the silicon surface is commonly performed by ***preparation of a SiO_2 layer*** (thickness around 100 nm). This manufacturing step is well-known and often used in semiconductor industry [21].

Nevertheless, electrical quality of the surface SiO_2 layer and the Si/SiO_2 interface can significantly impact final device parameters and so additional technological steps, e.g. ***annealing in water vapour***, are often needed to achieve a sufficient electrical quality level [22]. Annealing of silicon in water vapour at the temperature of 850°C or higher is commonly used for a surface passivation by creation of thermally grown SiO_2 [23]. Low level of defects at the SiO_2/Si interface and in the SiO_2 layer is the key requirement of a successful surface passivation used for instance in microelectronic and photovoltaic industry [22], [24]–[28].

3.1.1 Preparation of a Surface Passivation SiO_2 Layer

Silicon surface SiO_2 layer can be prepared as:

a) a dry oxidation in an oxidizing ambient at high temperature (1,000-1,200°C) or
b) a wet oxidation in water vapour at lower temperatures of around 800°C [29].

Annealing of silicon in the water vapour can be used as an alternative to a dry silicon surface oxidation to prepare a SiO_2 layer of a high electrical quality, i.e. higher lifetime of charge carriers, lower surface recombination velocity. Dry silicon surface oxidation requires relatively high temperature, typically over 1,000°C causing a significant deterioration of bulk lifetime. In contrast to this, a wet silicon oxidation realized at lower temperatures impacts bulk lifetime only slightly and it still offers a passivated SiO_2/Si interface of desired electrical quality [29].

3.1.2 Improvement of Si/SiO_2 Interface by a Passivation

Electrical quality of the Si/SiO_2 interface prepared as dry or wet oxidation can be further improved by annealing in water vapour at lower temperature of around 300°C [30]. The main aim of this treatment is to suppress recombination activity of silicon dangling bonds in the SiO_2 layer and at the Si/SiO_2 interface. This process is very close

to the passivation investigated in this thesis because no additional SiO_2 is intentionally grown. The difference is that in our case deactivation of the recombination centres is required not only at the silicon surface, but also in silicon bulk.

There are already water vapour systems available commercially operating at atmospheric pressure and temperature of around 400°C [31].

Improvement of the Si/SiO_2 interface by the water vapour annealing is discussed more in detail in Chapter 3.4.

3.2 Silicon Bulk Passivation

Passivation of silicon bulk can be performed in a hydrogen plasma [32] or a water vapour [33]. Passivating particles (hydrogen radicals, -OH, -O-) diffuse into silicon and saturate free silicon dangling bonds at grain boundaries and intra-grain structural imperfections acting as undesirable recombination centres. In this case, no SiO_2 layer is intentionally grown on the silicon surface.

Necessity of the effective passivation arises from the demand of a sufficient silicon quality, i.e. low concentration of structural imperfections and impurities. An example of multicrystalline silicon structure with defects and impurities is presented in Fig. 3.1. In general, structural and electrical quality of thin film silicon solar cells is significantly lower than of mono-Si and multi-Si wafer-based solar cells. The main reason comes from the preparation procedure of thin film Si solar cells on glass, i.e. crystallization from a solid phase. It brings a higher concentration of dislocations inside grains and of grain boundaries due to a small grain size of around μm. These defects are often so called decorated by impurities.

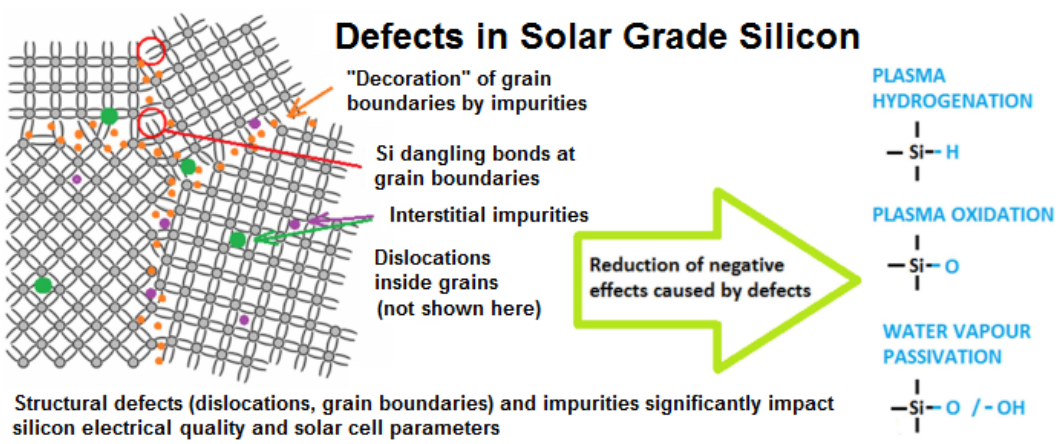

Fig. 3.1. Passivation of recombination centres (dislocations, grain boundaries with Si dangling bonds and impurities) in multicrystalline silicon by plasma hydrogenation, plasma oxidation and water vapour passivation.

3.3 Plasma Hydrogenation

Plasma hydrogenation can be used as a passivation procedure for silicon [8], [9], [32], [34]. There are more ways how hydrogen plasma can be ignited, e.g. direct current glow discharge, capacitively coupled plasma, inductively coupled plasma. While the plasma ignition mechanisms can be different, the basic idea is always same, to prepare hydrogen radicals of a sufficient concentration. Radicals are very reactive and moveable particles [35]–[38], and if silicon is exposed to their presence, they stick to the silicon surface, cover it and build a hydrogen reservoir from which H radicals can diffuse into silicon bulk. H_2 molecules interact with the silicon surface only negligibly [39].

Connection between hydrogenation parameters and resulting passivation effect on silicon has already been thoroughly investigated. Nevertheless, this task includes both plasma chemistry and semiconductor physics, what makes the research in this field very complex. Gorka [32] investigated the passivation effect of the hydrogen plasma on solid phase crystallized silicon and brought very valuable results. One of them is a correlation of the plasma break down voltage V_{brk} with open-circuit voltage V_{OC} of the passivated solar cell, maximum V_{OC} was achieved at minimum V_{brk}. Break down voltage is a minimum voltage to ignite plasma at corresponding hydrogen pressure and distance between electrodes. The same conclusion was confirmed for 3 temperatures (400°C, 500°C, 600°C). As the best passivation parameters were chosen the hydrogen pressure of 100 Pa with the corresponding electrode gap of 20 mm, the temperature of 600°C, and the exposure time of 10 minutes.

Passivation effect of the hydrogen plasma on silicon was investigated mainly in connection with different defect types like silicon dangling bonds at grain boundaries and dislocations inside grains whose recombination activity needs to be suppressed to achieve a sufficient photovoltaic efficiency [16], [40]. Moreover, grain boundaries act as H sinks [41].

Hydrogenation experiments [9], [11], [14], [42]–[45] and simulations [7], [10] revealed that grain boundaries have a predominant impact on silicon lifetime only in the case of a satisfactory intra-grain silicon electrical quality. Otherwise, defects inside grains play a key role in recombination processes.

Hydrogen plasma is able not only to passivate defects, but it can also create them. Typical temperature used for the plasma hydrogenation is about 600°C to support hydrogen diffusion into silicon bulk and through the whole solar cell [46]. However, it appears that the cooling phase of the process can significantly impact the resulting passivation effect. Plasma has to be terminated at appropriate temperature because too high plasma termination temperature (e.g. 600°C) leads to hydrogen out-diffusion from silicon and too low temperature (e.g. 200°C) causes silicon surface plasma damage due to a bombardment by atomic hydrogen [34].

There are also platelet defects that should be mentioned besides the commonly discussed recombination centres creating deep levels in the silicon band gap, i.e. already mentioned dangling bonds at grain boundaries decorated by impurities and intra-grain dislocations. Platelet defects were studied in a context of direct versus remote plasma passivation [47]. In the case of the direct hydrogenation plasma system, passivated samples are located between electrodes of the plasma system and they are exposed to direct bombardment of hydrogen ions [48], [49]. This surface plasma damage causes creation of so called hydrogen platelets in sub-surface regions [41]. According to some studies, these defects are microcracks in silicon lattice localized between two neighbouring planes of silicon atoms filled with hydrogen molecules [50]. These defects also act like recombination centres.

Since solid phase crystallized silicon did not achieve a required electrical quality, silicon crystallized from a liquid phase became a new generation of thin film polycrystalline silicon on glass [46], [51], [52]. Its grains are in range of mm and of significantly better quality. Nevertheless, the better silicon electrical quality before the passivation, the smaller relative improvement of silicon after the plasma hydrogenation. For this reason, there is only a slight, but still observable passivation impact of the hydrogen plasma on liquid phase crystallized silicon.

To observe more easily a passivation impact of hydrogen plasma and/or water vapour on silicon, SPC poly-Si solar cells were used for most of experiments in this thesis.

3.4 Water Vapour Passivation

Efficiency of the photovoltaic effect in solar cells depends on silicon electrical quality in the bulk and at the surfaces. Silicon dangling bonds at grain boundaries and intra-grain defects create energetic levels in the silicon band gap that act as recombination centres [34]. In this thesis, passivation means deactivation of these electrically active defects. Preparation of a surface SiO_2 layer is not our aim, rather incorporation of desired passivating particles into the silicon and bonding them with the dangling bonds of silicon and other defects. These passivating particles can be for instance hydrogen atoms produced during a commonly used plasma hydrogenation process [32]. Nevertheless, water vapour has a similar passivation potential according to the previous investigations [33], [53] and lower processing costs make this approach very attractive.

Passivation effect of water vapour on silicon has been investigated in many previous studies. Most of them can be divided into two basic groups according to the location, where the passivation of silicon has been investigated i.e. at the silicon surface or in silicon bulk.

The first group represents studies focusing mainly on passivation of a silicon surface and Si/SiO_2 interface. Silicon dioxide layer was in the most cases prepared by the thermal evaporation of powdered SiO or by the sputtering method. Passivation effect of the water vapour on silicon surface was determined by the following parameters:

Tab. 3.1. Investigated parameters to determine a success of the ***silicon surface*** water vapour passivation process.

Investigated parameter	**Research works**
Density of trap states at Si/SiO_2 interface	[30], [54]–[63]
Density of fixed oxide charges	[30], [54]–[57], [59], [60], [63]
Density of silicon dangling bonds	[64], [65]
Wave number, peak and FWHM of the antisymmetric stretching mode for Si-O-Si bonding	[30], [54], [55], [57], [64]–[66]
Si-O-Si bonding angle and its distribution	[55], [67]
Strain relaxation at the SiO_2/Si interface	[67]
Surface recombination velocity	[57], [60], [64]–[66], [68]
Lifetime of charge carriers	[57], [60], [65], [66], [68]
Diffusion length of charge carriers	[66]
Solar cell parameters	[66]
Specific parameters of the tested transistors	[56], [58], [59], [69]

Optimum passivation effect of the water vapour on the silicon surface and Si/SiO_2 interface was achieved by applying the following processing parameters:

a) steam pressure – mostly over the atmospheric pressure from 5×10^5 Pa to 54×10^5 Pa,
b) silicon temperature – mostly in the range from 250 to 350°C,
c) exposure time – mostly from 1 to 3 hours.

The second group of the research works was focused mainly on the passivation of silicon bulk, where no SiO_2 layer was intentionally grown on the silicon surface. The following table summarizes the parameters that were investigated to determine a success of the passivation treatment in the water vapour:

Tab. 3.2. Investigated parameters to determine a success of the ***silicon bulk*** water vapour passivation process.

Investigated parameter	**Research works**
Density of defect states	[33], [53], [61], [70]–[75]
Density of silicon dangling bonds	[70], [75], [76]
Activation energy of defect reduction reaction	[70], [75], [76]
Dark electrical conductivity	[70]–[73], [75], [77]–[79]
Electrical photoconductivity	[71], [72], [76]–[79]
Optical absorption spectra	[71], [72], [77]
Potential barrier height at grain boundaries	[53], [70], [73], [75]
Lifetime of charge carriers	[80]–[83]
Diffusion length of charge carriers	[66]
Carrier mobility	[56], [61], [63], [74], [84]
Hall mobility	[33], [53], [78]
Band-to-band transition	[82]
Tensile stress in Si film	[53]
Solar cell parameters	[77], [82], [85]
Quantum efficiency	[85]
Specific parameters of tested transistors	[61], [74], [84]
Hydrogen concentration/occurrence	[33], [53], [71], [72], [76], [78], [79], [81]
Oxygen concentration/occurrence	[76], [78]

Optimum passivation effect of the water vapour on the silicon bulk was achieved by applying the following processing parameters:

a) steam pressure – mostly from atmospheric pressure up to 30 x 10^5 Pa,
b) silicon temperature – mostly in the range from 200 to 350°C,
c) exposure time – mostly from 1 to 3 hours.

While the passivation of the silicon surface in the water vapour was investigated on different silicon types (mainly monocrystalline silicon wafers, but also polycrystalline and amorphous silicon thin films), passivation of the silicon bulk was tested in most cases with usage of polycrystalline silicon thin films.

According to the research in scientific literature presented above, passivation effect of the water vapour on the silicon surface and bulk cannot be separated. This conclusion is demonstrated by very similar treatment conditions for both mentioned research groups focused either on silicon surface or on silicon bulk passivation. This thesis could be rather a part of the second group, but the boundary separating these two research aims vanishes in some cases. Since applied passivation conditions presented above are very similar, one can assume that passivation of the silicon surface and the bulk are two simultaneous processes. The main difference between these two research groups was only a different object of their investigations, the silicon surface or the bulk.

While some scientists hold the opinion that silicon dangling bonds are terminated by –O, $–O_2$, –OH or –H coming from H_2O molecules [53], [54], [69], [70], [79], there are also other research groups supporting the opinion that hydrogen plays just a catalytic role in the water vapour passivation process and only oxygen saturates the recombination centres [81], [84]. Some of them assume a hydrolysis reaction between the SiO_2 thin film and H_2O molecules [30], [66], [67]. They believe that two weak Si-O bonds with a low bonding angle in SiO_2 are broken by H_2O molecules resulting in two Si-OH bonds. However, these two Si-OH are just an intermediate stage because they

react with each other and two more stable Si-O bonds with a larger bonding angle are formed at parallel release of H_2O molecule. This concept can be summarized as:

$$Si-O-Si + H_2O \Rightarrow 2\,Si-O-H \Rightarrow Si-O-Si + H_2O \quad \text{. (Eq. 3.1)}$$

There are also investigations comparing a passivation effect of hydrogen plasma, oxygen plasma and water vapour on silicon. While the hydrogen plasma both passivates and also generates defects, the oxygen plasma passivates only some defects, only the water vapour is able to passivate all defects without generation of new ones [33], [62].

According to some research works, photoluminescence of silicon nanoparticles and thin films can be observed after their annealing in the water vapour [86], [87]. After silicon clusters were co-deposited with the water vapour onto a cold target, spectral analysis revealed a Si/SiO core-shell structure of the nanoparticles and luminescence at blue wavelength was observed [88].

Bright and stable photoluminescence was achieved by annealing of porous silicon in the water vapour at the temperature of 400-500°C. It is assumed that Si-H bonds on the surface of porous silicon cores formed during the etching in HF acid are replaced by a high quality SiO_2 passivation layer [89].

Stabilization of porous silicon photonic structures from near-ultraviolet to near-infrared was observed after the high pressure water vapour annealing [87], [90]–[93].

While a passivation effect of the water vapour on silicon has already been investigated widely, there are still questions about the process that need to be answered, e.g. What is the key parameter of the process to maximize the passivation effect? Is there some synergetic effect of the water vapour and hydrogen or oxygen plasma?, and many others.

This thesis brings new approaches in an effort to understand the passivation process more deeply. Firstly, a steam pressure chamber built in the frame of this thesis should be mentioned. It enables an independent regulation of a sample temperature and the temperature of steam offering uncommon combinations of testing conditions. Usually these two processing parameters are connected according to the phase diagram of water. Then the temperature range investigated in this thesis is much broader (150-650°C) and the tested exposure time longer (from 5 minutes to almost 4 hours) than at the above presented experiments, see Tab. 3.1 and 3.2. Moreover, success of the passivation process was determined by Suns-V_{OC} method, see Chapter 4. Besides water vapour a few other media (hydrogen, oxygen, and their mixtures with steam) were also tested. On the basis of the realized experiments, a model of the water vapour passivation process was prepared. It confirms the key role of oxygen at saturation of silicon dangling bonds and no less important catalytic role of hydrogen in the process.

4 Measuring Methods

A description of measuring methods is given in this chapter. These methods were used to analyse the passivated samples. Electrical properties of the poly-Si thin film solar cells were measured by Suns-V_{OC} method and a sun simulator. Optical properties were analysed by a method of external quantum efficiency (EQE).

4.1 Suns-V_{OC} Method

Suns-V_{OC} method offers a measurement of a pseudo-current-voltage characteristic based on detection of a solar cell's open-circuit voltage at different light intensities [15]. The main idea of the method arises from the knowledge that the current generated in the illuminated solar cell is linearly proportional to the light intensity. An appropriately long light flash (longer than the lifetime of charge carriers) is used to operate the cell in a quasi-steady state. The balance between photogenerated and recombined charge carriers at every moment of the flash enables the measurement of the cell's V_{OC} at different light intensities. During the flash, light intensity is measured by an external photodiode placed close to the analysed solar cell. Photogenerated voltage of the cell is measured by an oscilloscope. Nevertheless, the value of solar cell's short-circuit current at the light intensity of 1,000 W/m^2 is needed as an input data to correctly recalculate the measured light intensity into photogenerated current.

A typical Suns-V_{OC} measurement is presented in Fig. 4.1 [15], where light intensity (red curve) and the corresponding solar cell's open-circuit voltage (green curve) are measured during the light flash. A xenon flash lamp is commonly used as a light source. The most important part of the characteristic is a linear decrease of the voltage from the point corresponding to the light intensity of 1,000 W/m^2 to the end of the flash (linear part of the green curve). To convert the measured dependence of open-circuit voltage on the light intensity into a current-voltage characteristic presented in a common way, the voltage is put on x-axis and the corresponding light intensity on y-axis recalculated into electric current or current density on the basis of solar cell's short-circuit current I_{SC}, see Fig. 4.2 [15].

The main advantage of the Suns-V_{OC} method is that solar cells with high series resistance or without metallization can be measured because only the photovoltage of the cell is detected. The measurement is fast, so temperature fluctuations impacting results are negligible.

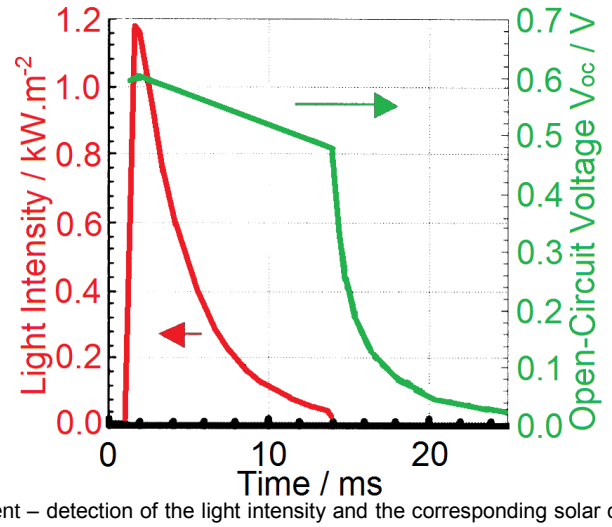

Fig. 4.1. Suns-V_{OC} measurement – detection of the light intensity and the corresponding solar cell's open-circuit voltage during the light flash [15].

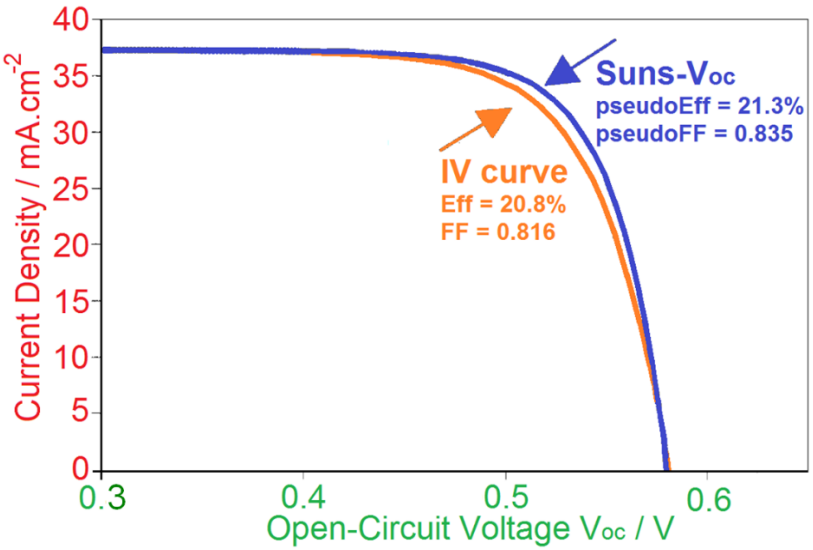

Fig. 4.2. Comparison of a current-voltage characteristic measured in a common way and a pseudo-current-voltage characteristic measured by the Suns-V_{OC} method, with modifications from [15].

As the weakness of the Suns-V_{OC} method it should be mentioned that the value of short-circuit current at 1,000 W/m^2 has to be provided by another method.

Suns-V_{OC} measurement gives a pseudo-current-voltage characteristic with pseudo-efficiency and pseudo-FF. All these data present a potential of the solar cell with a perfect metallization, where series resistance can be neglected.

Since there is a connection between the charge carrier lifetime τ and open-circuit voltage V_{OC} of the solar cell through the dark saturation current density J_o, this method is often used to determine electrical quality of silicon [52], [94]:

$$V_{OC} = \frac{mkT}{q} ln\left(\frac{J_{ph}}{J_o} + 1\right) \quad . \qquad \text{(Eq. 4.1)}$$

The dark saturation current density J_o, see Eq. 1.2, depends on charge carrier lifetime through recombination processes caused mainly by crystallographic imperfections (grain boundaries, dislocations …) and impurities. Effective lifetime of a solar cell τ_{eff} is given by bulk lifetime τ_{bulk} and surface lifetime$\tau_{surface}$:

$$\frac{1}{\tau_{eff}} = \frac{1}{\tau_{bulk}} + \frac{1}{\tau_{surface}} \quad . \qquad \text{(Eq. 4.2)}$$

Bulk lifetime τ_{bulk} depends on recombination mechanisms

$$\frac{1}{\tau_{bulk}} = \frac{1}{\tau_{rad}} + \frac{1}{\tau_{Auger}} + \frac{1}{\tau_{SRH}} \qquad \text{(Eq. 4.3)}$$

where τ_{rad} represents the radiative recombination lifetime (electron jumps from conductive band to valence band), τ_{Auger} is Auger recombination lifetime (mainly at high charge carrier concentrations) and τ_{SRH} stands for Shockley-Read-Hall recombination lifetime (recombination due to defects creating deep levels in the band gap), see Chapter 1.1.

Surface lifetime $\tau_{surface}$ depends on the surface recombination velocities S_1 and S_2 of the surfaces 1 and 2, the cell width W (the distance between the surfaces), and

the diffusion coefficient D of minority charge carriers. The precise mathematical definition is relatively complicated, therefore only approximate solutions for special cases [95] are presented here:

a) the surfaces are identical, $S_1 = S_2 = S$,

$$\tau_{surface} = \frac{W}{2S} + \frac{1}{D}\left(\frac{W}{\pi}\right)^2 \quad , \qquad \text{(Eq. 4.4)}$$

b) one surface is perfectly passivated, $S_2 = 0$,

$$\tau_{surface} = \frac{W}{S_1} + \frac{4}{D}\left(\frac{W}{\pi}\right)^2 \quad , \qquad \text{(Eq. 4.5)}$$

c) both surfaces are perfectly passivated, $S_1 = S_2 = 0$,

$$\tau_{surface} = \infty \quad , \qquad \text{(Eq. 4.6)}$$

d) both surfaces have a high recombination, S_1 and S_2 are large,

$$\tau_{surface} = \frac{1}{D}\left(\frac{W}{\pi}\right)^2 \quad , \qquad \text{(Eq. 4.7)}$$

e) one surface has a high recombination the other one has a low recombination, $S_1 = 0$ and $S_2 = \infty$,

$$\tau_{surface} = \frac{4}{D}\left(\frac{W}{\pi}\right)^2 \quad . \qquad \text{(Eq. 4.8)}$$

4.2 Sun Simulator

Basic diagnostic of a solar cell can be given by a sun simulator. There are two most important requirements that a sun simulator should meet:

a) spectrum as close as possible to the Sun's spectrum and
b) homogeneous light intensity on an illuminated surface.

Since a spectrum of a xenon lamp resembles the spectrum of the Sun, xenon lamps are often used as light sources in sun simulators in both flash and continuous regimes. Flash systems have the advantage of a fast measurement and consequently also a negligible impact by temperature fluctuations.

Current-voltage characteristics of solar cells and panels are measured at the light intensity of 1,000 W/m^2 according to the standard testing conditions. Nevertheless, knowledge of solar panel parameters at different light intensities, e.g. 800 W/m^2, can be useful in some cases, typically for a customer who would like to place the panels at the regions with lower Sun light intensities.

Example of a sun simulator is presented in Fig. 4.3. It includes a light source of the appropriate spectrum, a current-voltage source, an ammeter, a voltmeter, a cooled stage for samples, and a thermometer.

Besides xenon lamps also halogen lamps are sometimes used, see Fig. 4.4. A dichroic filter is used in the case of an ELH halogen lamp to suppress infrared wavelengths. The ELH is an American Standards Institute (ANSI) code that describes this type of lamp.

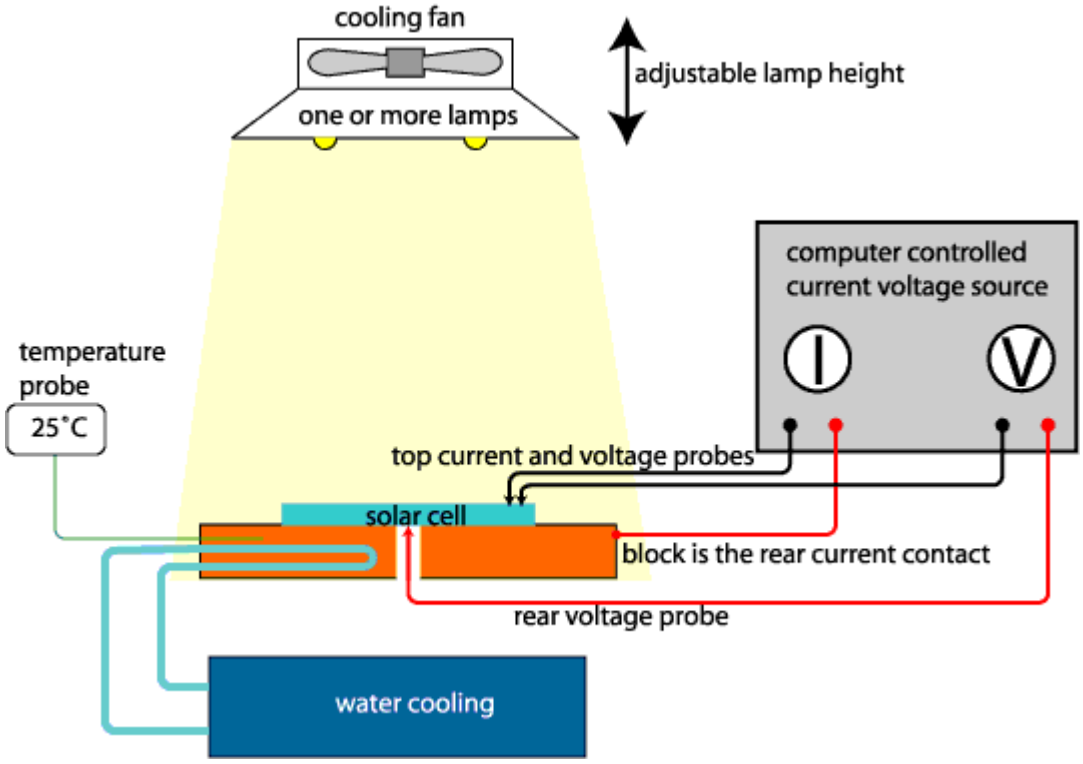

Fig. 4.3. Scheme of a sun simulator [96].

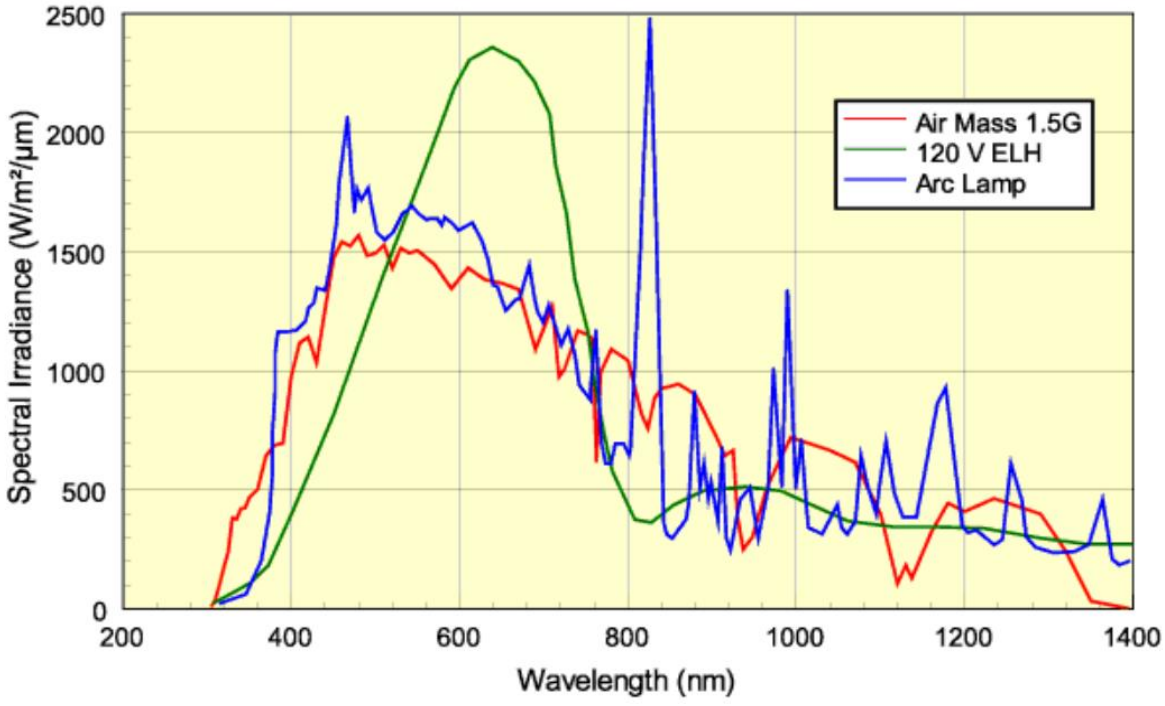

Fig. 4.4. Comparison of the Sun spectrum AM 1.5 at the Earth's surface (red line), spectrum of an ELH halogen lamp with a dichroic reflector (green line), and spectrum of a xenon arc lamp (blue line) [97].

4.3 Quantum Efficiency

A quantum efficiency measurement describes how effectively energy of incident photons is transformed into energy of excited charge carriers in a solar cell with respect to particular light wavelengths. Two types of quantum efficiency are commonly distinguished:

a) external quantum efficiency (EQE) – the ratio of number of photogenerated electron-hole pairs P_{eh} per second contributing to the energy produced by the cell to *number of photons N_{ph} per second illuminating the cell*,
b) internal quantum efficiency (IQE) – the ratio of number of photogenerated electron-hole pairs P_{eh} per second contributing to the energy produced by the cell to *number of photons N_{aph} per second absorbed in the cell*, i.e. without reflection on the solar cell's front surface and transmission through the cell.

IQE is always larger than EQE, because external quantum efficiency takes into account also losses caused by reflection and transmission, while IQE deals only with the light absorbed in the solar cell. IQE of a solar cell is calculated from the measured EQE, reflection and transmission.

EQE can give valuable information about a quality of an antireflection coating on the front solar cell's surface. IQE offers even more important insight because it describes what happens with photons absorbed in the solar cell with respect to particular wavelengths. While a reduction of IQE at short wavelengths (blue) is connected with recombination processes at the solar cell's emitter, the middle part of IQE refers to the bulk material and long wavelengths describe recombination at the back contact. Quantum efficiency measurements can help revealing undesirable recombination processes and to identify the most critical interfaces and regions in a cell.

EQE and IQE of a crystalline silicon solar cell are presented in Fig. 4.5. There is also a measurement of the solar cell's reflection together with transmission. Ideal quantum efficiency without any reflection, transmission and recombination achieves 100 % throughout the whole measured wavelength range, but it is just a theoretical case.

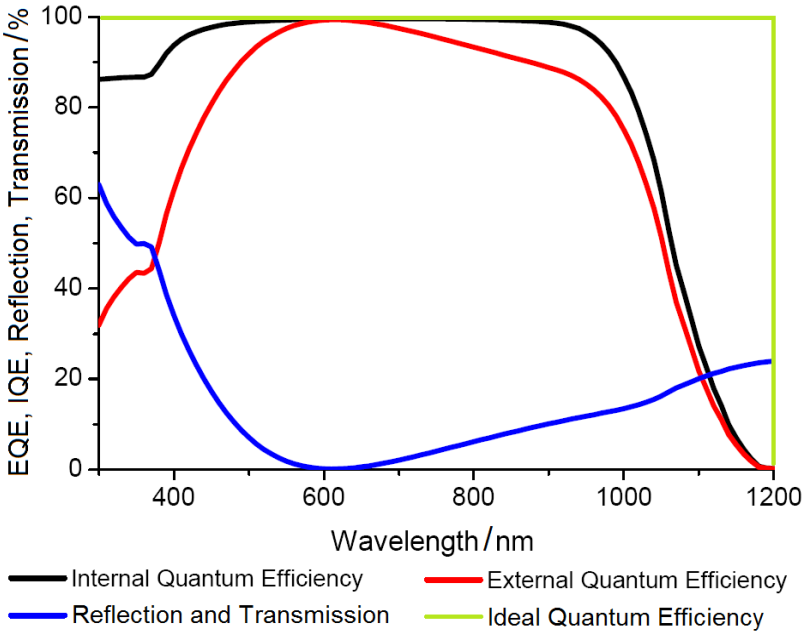

Fig. 4.5. External (red), internal (black) quantum efficiency, reflection together with transmission (blue) of a crystalline silicon solar cell and ideal quantum efficiency (green) as a function of wavelengths. With modifications from [98].

5 State-of-the-Art: Thin Film Poly-Si Solar Cells

Thin film polycrystalline silicon (poly-Si) solar cells are in the centre of interest because of a very attractive combination of their relatively low manufacturing costs, i.e. material and energy demands and high efficiency potential. However, there are two main drawbacks of these solar cells that need to be solved:

a) a low Si electrical quality resulting in the low open-circuit voltage V_{OC} and
b) a small thickness of a solar cell and a low absorption coefficient of light in crystalline silicon resulting in a small photocurrent I_{ph}.

Low silicon electrical quality can be improved either during the crystallization process or as an additional manufacturing step for instance by plasma hydrogenation. There are several approaches to crystallize an amorphous silicon layer deposited on a glass substrate, e.g. solid phase crystallization (SPC) at around 600°C for 20 hours or liquid phase crystallization (LPC) by laser or electron beam. The LPC brings significantly better results, see Chapter 5.2.

Solution of the second drawback can be found in an appropriate surface texture of the solar cell substrate to reduce light reflection from the front surface and a back reflector to prolong the path of light in the silicon layer and to increase probability of photon absorption this way.

5.1 Solid Phase Crystallized (SPC) Si Solar Cells

Passivation effect of water vapour and hydrogen plasma was investigated in the frame of this research work with use of solid phase crystallized silicon (SPC Si) solar cells. Description of the solar cell structure and manufacturing process are presented in the following subchapters.

5.1.1 Structure and Preparation Sequence of the SPC Si Solar Cells

Polycrystalline silicon (poly-Si) thin film solar cells were prepared on borosilicate glass by the company Crystalline Silicon on Glass (CSG Solar AG) in Germany [16], [40]. The solar cell manufacturing procedure shown in Fig. 5.1 involved a deposition of amorphous silicon layer (thickness of around 1.5 μm) with the structure $n^+/p^-/p^+$ by plasma enhanced chemical vapour deposition (PECVD) on a borosilicate glass substrate (thickness of 3.3 mm) coated with an antireflection SiN thin film (thickness of 65 nm) acting also as a diffusion barrier against impurities from glass. Amorphous silicon was subsequently crystallized at 600°C for 20 hours by a solid phase crystallization process to prepare polycrystalline silicon with an average grain size of μm. Tensile stress introduced into the silicon layer by the crystallization was removed by a rapid thermal annealing (RTA) with a short plateau phase at around 1,000°C for a few seconds. Incomplete structure of the poly-Si thin film solar cells is shown in Fig. 5.2. Open-circuit voltage of the solar cell after RTA measured by Suns-V_{OC} method was around 220 at the light intensity of 1,000 W/m^2. In the frame of this work, the solar cells of this structure were passivated in hydrogen plasma or in water vapour. Further manufacturing procedures including also a preparation of metal electrodes followed usually in the mass production, see Fig. 5.3. Nevertheless, these steps were omitted in our case to enable the investigation of interaction between the silicon layer and the water vapour or the hydrogen plasma. While a current-voltage characteristic cannot be measured without metallization (too high series resistance impacts current), a pseudo-I-V curve is available due to the Suns-V_{OC} method.

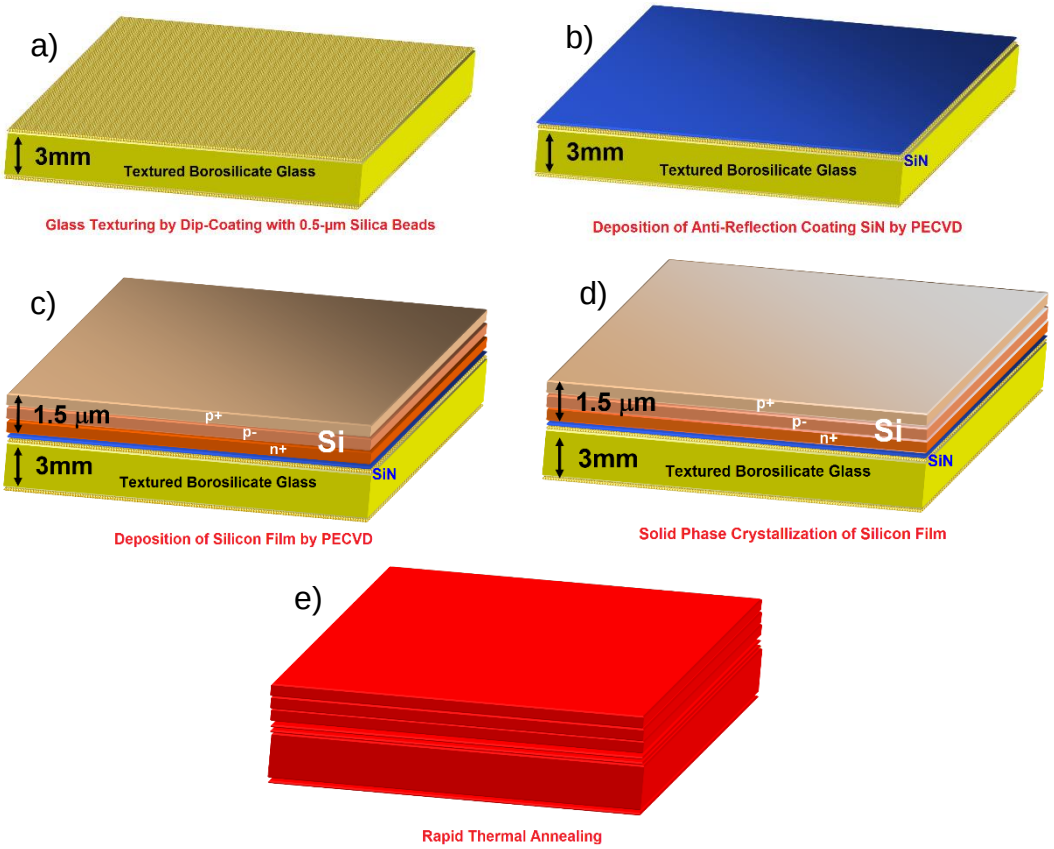

Fig. 5.1. Manufacturing sequence of the passivated thin film SPC polycrystalline silicon solar cells with an incomplete structure involving: a) preparation of a textured borosilicate glass substrate by dipping in a bath with glass pellets, b) deposition of an antireflection coating SiN by plasma enhanced chemical vapour deposition (PECVD), c) deposition of amorphous silicon $n^+/p^-/p^+$ structure by PECVD, d) crystallization of the silicon layer to prepare polycrystalline silicon, e) rapid thermal annealing to remove tensile stress from the crystallized Si layer. With modifications taken from [99].

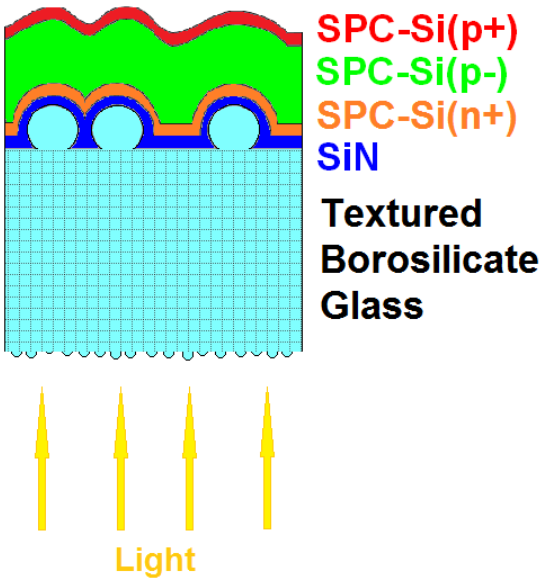

Fig. 5.2. Structure of a solid phase crystallized (SPC) thin film poly-Si solar cell without metallization – borosilicate glass (3.3 mm), antireflection coating SiN (65 nm, $\varepsilon_r \approx 2.1$), SPC-Si($n^+$) (50 nm, $P \approx 10^{20}$ cm^{-3}), SPC-Si(p^-) (1.4 µm, $B \approx 5 \times 10^{16}$ cm^{-3}), SPC-Si(p^+) (100 nm, $B \approx 2 \times 10^{19}$ cm^{-3}).

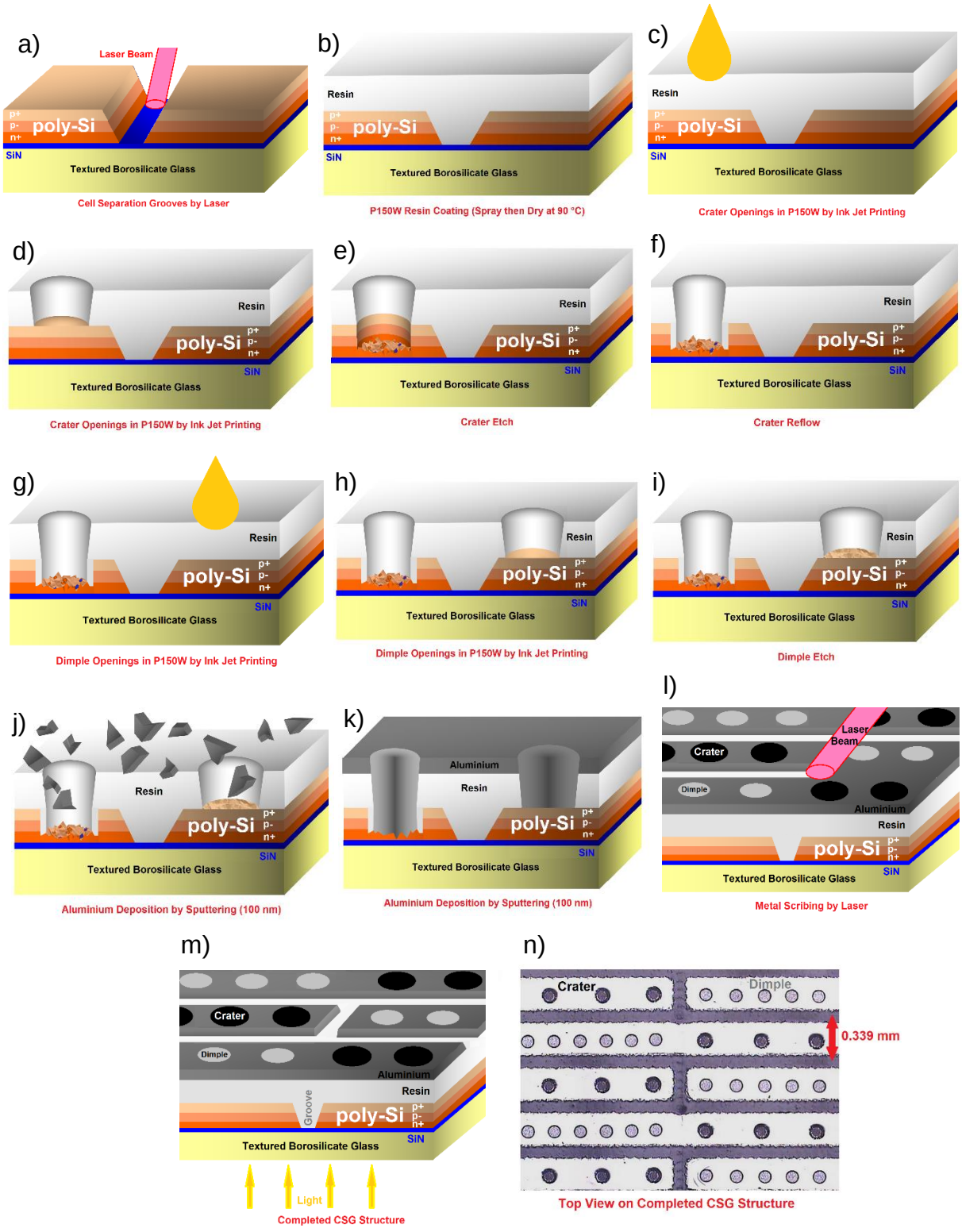

Fig. 5.3. Manufacturing sequence of the solid phase crystallized (SPC) polycrystalline silicon thin film solar cells after RTA and the plasma hydrogenation: a) cell separation grooves to define individual cells performed by laser, b) resin coating, c) and d) crater openings by ink jet printing, e) crater etch to make available n^+ silicon layer, f) crater reflow to avoid short-circuit between p^- or p^+ and n^+ layers of the junction, g) and h) dimple openings by ink jet printing, i) dimple etch to make available p^+ silicon layer, j) and k) metallization – aluminium deposition by sputtering to contact n^+ and p^+ parts of the junction, l) metal scribing by laser to separate individual solar cells and to connect them in series, m) completed structure of the SPC polycrystalline thin film silicon solar cells, and n) top view on the metallization of the solar cells. With modifications taken from [99].

5.1.2 Achieved Results and Potential of the SPC Si Solar Cells

Concept of the crystalline silicon on glass (CSG) was designed in the late 1980s by a research group at the University of New South Wales in Sydney and it is closely connected with the teams of prof. M. Green and P. Basore. Pacific Solar was formed in 1995 to develop and commercialize thin film CSG technology. Further expansion step was establishment of the company CSG Solar GmbH in Germany in 2004 [100], [101].

Efficiency of the CSG Solar's modules (aperture-masked to area of 90 cm^2) increased from around 2.3 % in 1998 to 8.1 % in 2002 measured independently at Sandia National Laboratories [101]. This outstanding improvement indicated very promising achievable results. Despite hard research work and huge investment, the maximum efficiency of 10.4 % was achieved and confirmed independently by Fraunhofer ISE in 2007 for a 20-cell minimodule aperture-masked to area of 94 cm^2 [16], Fig. 5.4.

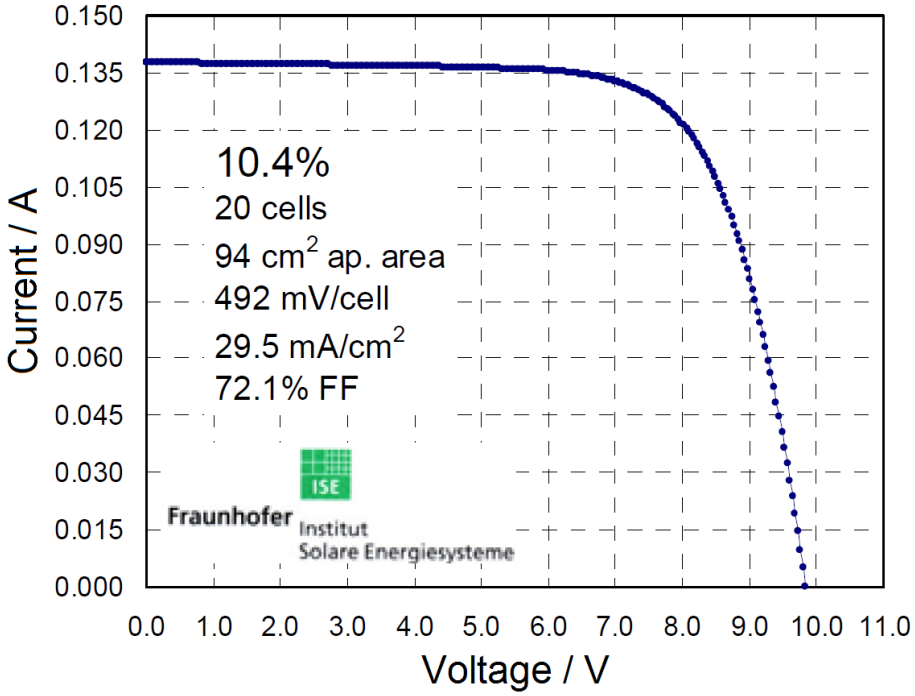

Fig. 5.4. CSG 20-cell minimodule tested at the Fraunhofer Institut in 2007 achieved efficiency of 10.4 %, aperture-masked to area of 94 cm^2 [16].

Further improvement was limited mainly by low open-circuit voltage V_{OC} connected with a low electrical quality of polycrystalline silicon prepared by solid phase crystallization. Hydrogen plasma passivation brought a significant improvement, but V_{OC} higher than 500 mV/cell has not been achieved in the mass production [51]. Electrical quality of poly-Si thin films was significantly influenced by too high defect concentration, e.g. grain boundaries, intra-grain dislocations, and impurities whose electrical activity has not been effectively suppressed by the hydrogen plasma passivation. Production costs were too high in comparison with achieved solar cell efficiency. One possible solution was to reduce the manufacturing costs by finding an alternative to the plasma hydrogenation, which was the second most expensive step of the CSG Solar technology. Another option was change the CSG technology at the very beginning, the crystallization step, to prepare silicon of a higher quality, e.g. crystallization from liquid phase (LPC) by laser or electron beam, see the next chapter for more details.

This work is focused mainly on silicon passivation in the water vapour as a low cost alternative to hydrogen plasma passivation. For comparison, we also explored possible improvement by modification of some hydrogen plasma passivation parameters.

5.2 Liquid Phase Crystallized (LPC) Si Solar Cells

Solid phase crystallized silicon suffers from too high concentration of electrically active structural imperfection. Crystallization of silicon from liquid phase was invented to prepare polycrystalline silicon (poly-Si) of a higher quality. This approach connects a cheaper thin film technology (lower material, energy and manufacturing costs) with a high silicon electrical quality comparable with wafer-based multicrystalline silicon.

5.2.1 Structure and Preparation Sequence of the LPC Si Solar Cells

Research of thin film crystalline silicon solar cells on glass is nowadays focused mainly on silicon crystallized from liquid phase by laser or electron beam. The achievable grain size of centimetres in the direction of the beam and of millimetres in the orthogonal direction makes this material comparable with multicrystalline Si of wafer-based solar cells.

There are many possible concepts of liquid phase crystallized (LPC) silicon thin film solar cells. The UNSW group in Australia led by prof. M. Green achieved a very promising results: open-circuit voltage V_{OC} of 585 mV/cell and efficiency of 10.7 %, see Fig. 5.5 [46]. This solar cell concept is a new version of a solid phase crystallized (SPC) solar cell (see the previous chapter) based also on superstrate configuration with a few significant modifications. Manufacturing procedure of the Green's LPCSG solar cells includes sputtering of a ONO triple stack (100 nm SiO_x, 50 nm SiN_x and 10 nm SiO_x) acting as a diffusion barrier and also as an antireflection coating on a planar borosilicate glass substrate (3.3 mm). Then a 10-μm-thick boron-doped silicon layer used as a solar cell absorber (2-3 x 10^{16} cm^{-3}, sheet resistance ≈ 2 kΩ/□) is prepared by high rate electron beam evaporation. Liquid phase crystallization with a laser beam at temperature above 1400 °C is applied to crystallize the absorber and to activate dopants in the layer. The next step is a preparation of the solar cell's emitter by thermal diffusion of phosphorus into the rear surface of the LPCSG film from a spin-on dopant glass (SOD glass) at around 900 °C (sheet resistance ≈ 200 Ω/□). Hydrogen plasma passivation is applied to electrically deactivate dangling bonds at grain boundaries of silicon and at the Si/SiO_2 interface. A rear silicon surface texture is prepared by etching to enhance light trapping of the structure. Similar metallization as in the case of the SPC Si solar cells (see Chapter 5.1) is used with a few differences: a) deep contact (called crater) terminates in the middle of the low P-doped absorber b) shallow contact (called dimple) terminates in the emitter c) LPCSG cells have PN-junction instead of PIN-junction used for SPC cells.

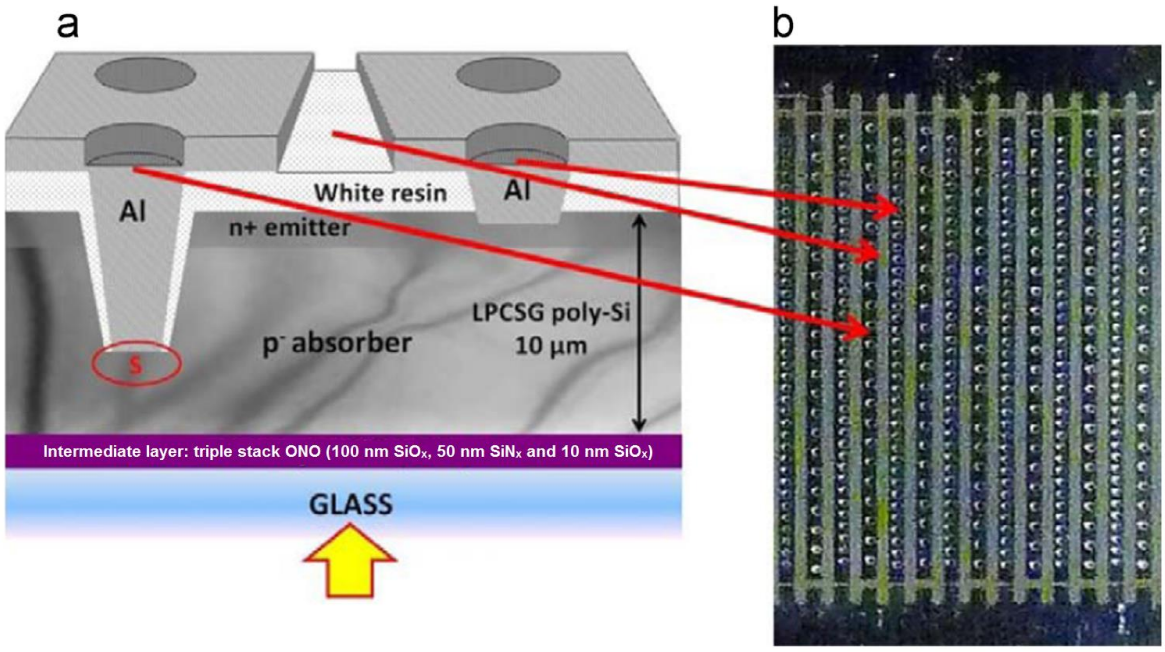

Fig. 5.5. Structure of a liquid phase crystallized silicon on glass (LPCSG) solar cell manufactured by Green's group in Australia: a) cross section of the solar cell b) top view on solar cell metallization. With modifications taken from [46].

While only a single thin film SiN (65 nm) was used in the case of SPC thin film solar cells as a diffusion barrier and as an antireflection coating (see Chapter 5.1), a relatively complicated triple stack ONO ($SiO_x/SiN_x/SiO_x$) was prepared for LPCSG solar cells [46]. The reason is that this structure is needed to fulfil several simultaneous conditions, e.g. to be stable at the silicon melting point to enable good adhesion of molten silicon to the substrate, to prevent diffusion of impurities from the glass (diffusion barrier), to serve as a dopant source for the cell absorber during the LPC Si process, to passivate the buried front silicon-glass interface, to provide the antireflection effect (AR) for the cells used in superstrate configuration. Three most promising thin films SiO_x, SiN_x, SiC_x were tested, but none of them alone had all the required properties. Solar cells with SiO_x had the best open-circuit voltages due to low concentration of defects, but there was almost no AR effect. SiN_x or SiC_x provided very good AR properties, but allowed diffusion of impurities from the glass substrate and only poorly passivated front interface. Only their combination was able to fulfil all the requirements.

Another concept of the LPC solar cells on glass was designed and realized at the Helmholtz-Zentrum Berlin, see Fig. 5.6. Liquid phase crystallized a-Si:H/c-Si heterojunction solar cells were prepared by the following sequence of steps: SiO_2 diffusion barrier (200 nm) was deposited on a Corning Eagle XG glass substrate (1.1 mm). Two different deposition techniques were used to deposit SiO_2, either PVD or PECVD. Boron-doped ($4x10^{16}$ cm^{-3}) microcrystalline silicon layer (11 µm) used as an absorber was prepared by electron-beam evaporation at 600°C. SiO_2 capping layer (200 nm) was deposited by PVD at 450°C to prevent de-wetting of silicon during the crystallization of amorphous silicon performed by either laser (LC) or e-beam (EBC) [102]. Rapid thermal annealing (RTA) with the plateau time of 60 s at 960°C was applied to remove tensile stress from glass. The capping layer was subsequently removed by 5% hydrofluoric acid.

Plasma hydrogenation, the last high temperature step, was performed at the temperature of 600°C and hydrogen pressure of 100 Pa. The other parameters were: plasma exposure time of 15 min, plasma power of 50 W at radio frequency of 13.56 MHz, distance between electrodes of 20 mm. Intrinsic amorphous silicon interlayer (5 nm) and phosphorus-doped a-Si layer (10 nm) used as an emitter were prepared by PECVD. Aluminium contacts (1 μm) were deposited through a mask by PVD. Planar indium tin oxide (ITO) with the thickness of 80 nm was used as an antireflection coating and for better charge collection, it was prepared by PVD. Complete structure of the liquid phase crystallized silicon samples is shown in Fig. 5.6. Each sample contained 8 solar cells.

Success of the plasma hydrogen passivation was determined by comparing the passivated cells with two non-passivated reference LPC silicon solar cells, one for the samples crystallized by laser beam (LC) and the other one for the electron beam (EBC) crystallized samples. SiO_2 diffusion barrier was prepared by PECVD for both reference cells.

The completed LPC Si solar cells were measured by a sun simulator and external quantum efficiency (EQE) with negative bias voltage (-1V). A white paper back reflector was used at EQE and Suns-V_{OC} measurements. While the above described concept of LPC Si solar cells was not optimised for an effective light trapping, it provided first and fast way to check electrical quality of laser beam and electron beam liquid phase crystallized polycrystalline silicon solar cells. Samples of this structure were used to investigate a passivation effect of the hydrogen plasma at different processing conditions. Efficiency of almost 10 % was achieved regardless of the crystallization technique (LC or EBC) and the varied plasma hydrogenation parameters (temperature of 550, 600, 650 °C and hydrogen pressure of 100, 200, 300 Pa), see Chapter 7.4.

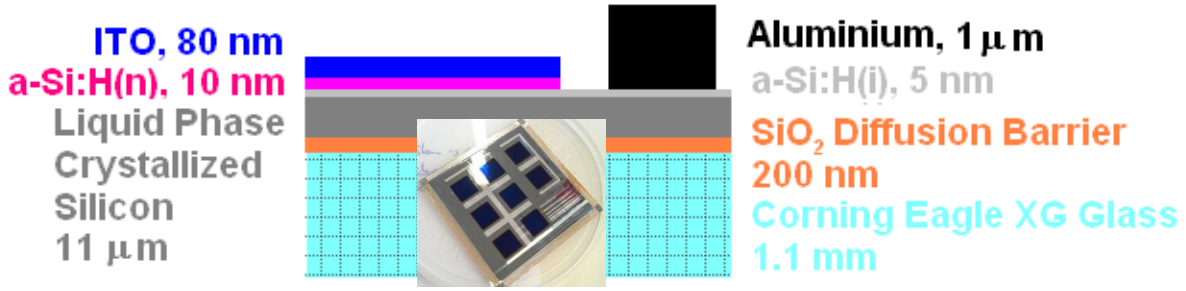

Fig. 5.6. Complete structure of liquid phase crystallized thin film Si solar cells on glass made at the Helmholtz-Zentrum Berlin.

The above described LPC Si solar cell concept was further optimized and it resulted in the new solar cell structure presented in Fig. 5.7 [103]. This concept achieved a stable efficiency of 11.5 % and open-circuit voltage V_{OC} of 629 mV/cell. Corning Eagle XG glass with thickness of 1 mm was used as a substrate of the LPC solar cells. The glass was coated with an ONO triple stack (250 nm SiO_x, 80 nm SiN_x and 20 nm SiO_x) by reactive RF-magnetron sputtering. The nominally intrinsic-silicon absorber (thickness of 11 μm) was deposited by electron beam evaporation (EBE) with deposition rate of 500-600 $nm.min^{-1}$ at substrate temperature of 600 °C. As a source of phosphorus was used a thin layer N-doped hydrogenated amorphous silicon (a-Si:H(n)) deposited by plasma enhanced chemical vapour deposition (PECVD). The structure was subsequently annealed for one hour at 600 °C to drive out the hydrogen that could cause cracks during the following high temperature steps. SiO_2 capping layer (200 nm) was sputtered to stabilize liquid phase crystallization performed by electron or laser beam. High temperature of silicon (1400 °C) achieved during the crystallization was important for both silicon melting and diffusion of phosphorus from

a-Si:H(n) layer into the poly-Si absorber. N-doped silicon as an absorber was preferred because of a lower concentration of metallurgical impurities compared to P-doped Si, no light induced degradation due to Boron-Oxygen complexes, and lower surface recombination velocities [104]–[107]. Rapid thermal annealing (RTA at 950 °C for 60 seconds) was the subsequent step to reduce stress in the glass substrate induced by the crystallization. The capping layer was removed in 5% hydrofluoric acid. The superficial layer of poly-Si (300-500 nm) was removed in an acid mixture $HF/HNO_3/H_3PO_4$ (60 s) to eliminate surface defects induced by the LPC crystallization.

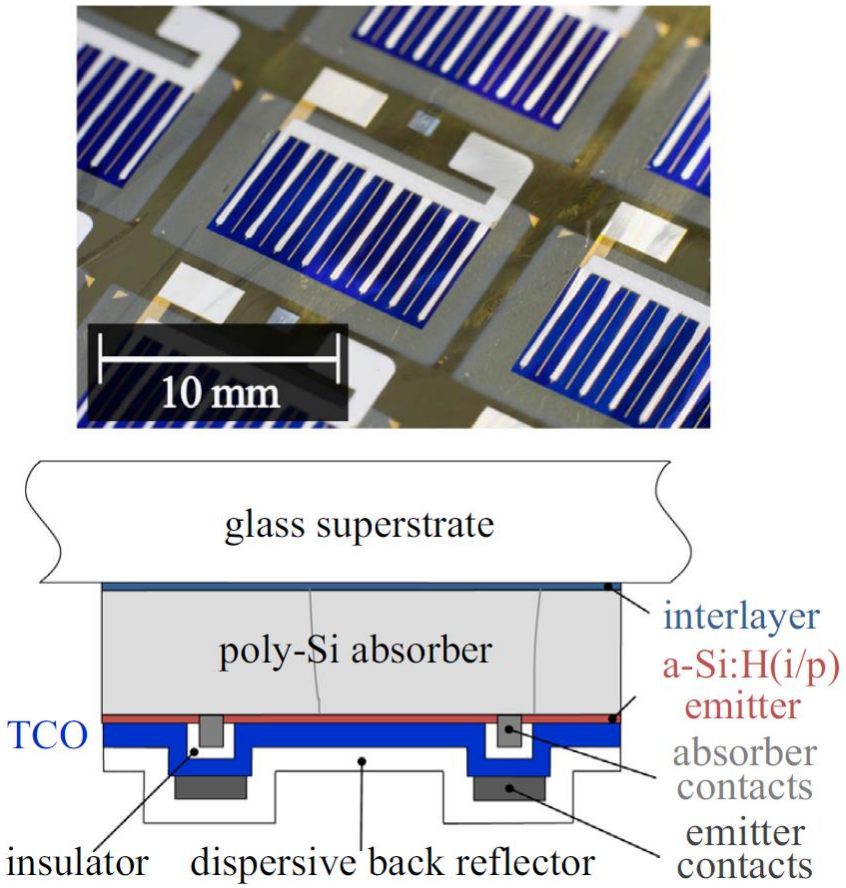

Fig. 5.7. Liquid phase crystallized (LPC) polycrystalline silicon thin film solar cells on glass: a) photograph of the solar cells prepared at the Helmholtz-Zentrum Berlin without a back reflector and b) cross section of the cell. With modifications from [103].

Hydrogen plasma passivation for 15 minutes at 600 °C and hydrogen pressure of 100 Pa was performed to passivate silicon dangling bonds at intra-grain defects, grain boundaries and at the Si/SiO_2 interface. Surface defects caused by the plasma were removed by etching of the samples in the above mentioned acid mixture for 60 s. The standard RCA cleaning step was subsequently applied to ensure a good quality of a-Si:H/c-Si interface. A stack of 5 nm a-Si:H(i) and 10 nm a-Si:H(p) acting as an emitter was deposited by PECVD to prepare a PN-heterojunction poly-Si(n)/a-Si:H(p) of a suitable electrical quality. A short additional treatment in the hydrogen plasma was performed after the deposition of a-Si:H(i) to enhance chemical saturation of dangling bonds at the silicon surface. A lift-off mask was used to remove the a-Si:H(p) emitter at desired positions before the deposition of the Ti/Pd/Ag (50 nm/50 nm/1 µm) absorber contact grid. ITO (80 nm) was sputtered with usage of a mask and then the emitter contact grid Ti/Pd/Ag was prepared through another mask. A white dispersive back reflector (TippEx® ECOLUTIONS – Aqua) was deposited on the grid and transparent conductive oxide (TCO).

5.2.2 Achieved Results and Potential of the LPC Si Solar Cells

Thin film polycrystalline silicon solar cells based on liquid phase crystallized silicon on glass (LPCSG) achieved up to now better results than solid phase crystallized (SPC) thin film silicon solar cells. Quality of LPC polycrystalline silicon starts to become comparable with quality of wafer-based silicon solar cells as demonstrated by the first promising results of Green's Australian group and the group of D. Amkreutz in Germany.

Both used solar cell concepts are totally different with specific drawbacks that need to be solved before a further improvement can be reached. In the case of prof. M. Green's LPCSG concept, there are still some problems with crystalline quality at the regions of buried electrodes that negatively impact V_{OC} and also I_{SC}. Nevertheless, this concept has a larger active illuminated area because both electrodes are realized from the rear side. LPCSG solar cells seem to be very promising, the efficiency above 13 % is expected after improving light-coupling and contacting [103]. The team of D. Amkreutz used an n-type doped absorber, which is not usual and achieved better solar cell parameters. The approach of metallization from both sides seems to benefit from a higher silicon electrical quality exceeding also the shadowing effect of the front electrode. In this case, the interface of interlayer and silicon absorber plays the most challenging region of this concept.

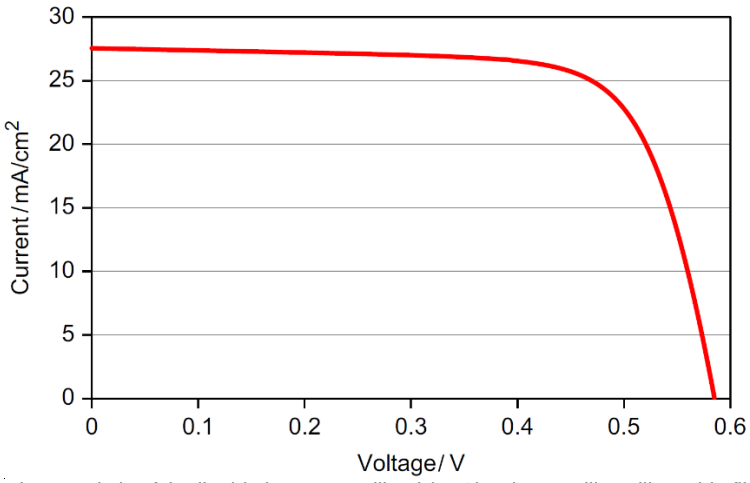

Fig. 5.8. Current-voltage characteristic of the liquid phase crystallized (LPC) polycrystalline silicon thin film solar cell on glass with efficiency of 10.7 % and open-circuit voltage of 585 mV/cell [46]. The solar cell was manufactured by the group of prof. M. Green in Australia.

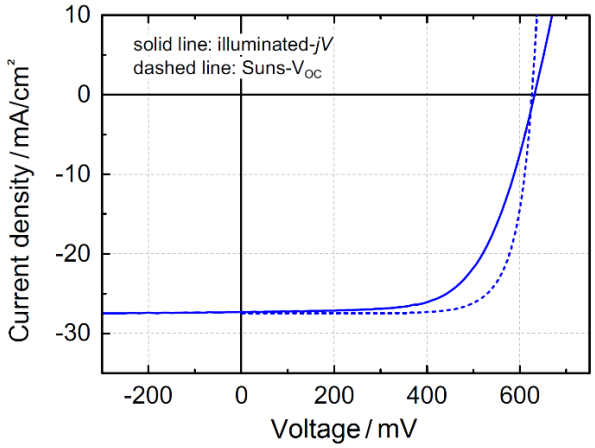

Fig. 5.9. Current-voltage characteristic of the liquid phase crystallized (LPC) polycrystalline silicon thin film solar cell on glass with the efficiency of 11.5 % and open-circuit voltage of 629 mV/cell. With modifications taken from [103]. The solar cell was fabricated by the group of D. Amkreutz in Germany.

6 Water Vapour Passivation of the SPC Si Solar Cells

Effect of varied water vapour passivation parameters on the SPC polycrystalline silicon thin film solar cells were investigated in this work, e.g. silicon temperature, water vapour pressure, treatment duration, and different passivation media. It should be underlined that the treatment in water vapour changes only electrical quality of silicon and all other sample properties (e.g. optical, structural) remain unchanged. This enables evaluation of a passivation effect of water vapour on polycrystalline silicon.

6.1 Preparation of the SPC Silicon Solar Cells

The tested SPC poly-Si solar cells were prepared as described in paragraph 5.1.1. Rapid thermal annealing was the last manufacturing step followed by etching in 5% hydrofluoric acid for 30 s to remove native SiO_2. The delay between the etching in HF and the passivation process was around 15 minutes. Subsequently, passivation in water vapour was realized at particular processing conditions. Deionized water prepared by reverse osmosis was used for all annealing processes in water vapour.

6.2 In-Situ Investigation of the Water Vapour Passivation

To determine optimum water vapour passivation conditions, there are 4 main passivation parameters that should be tested – temperature of the SPC poly-Si, pressure of the water vapour, duration of the treatment, and ratio of hydrogen and oxygen in the applied passivation atmosphere. Treatment duration as the passivation parameter could be eliminated by an *in-situ* investigation (V_{OC} of the solar cell measured during the passivation process). This approach could significantly reduce research time needed for determination optimum passivation conditions and for understanding the processes taking place during the treatment. In-situ Suns-V_{OC} measuring system has been designed and built for this purpose, see Fig. 6.1.

However, two basic physical principles stand against each other and significantly complicate the in-situ investigation: a) solar cell open-circuit voltage decreases with increasing temperature and b) the passivation process needs high enough temperature to give an observable improvement.

Open-circuit voltage of a non-passivated SPC solar cell is around 220 mV at light intensity of 1,000 W/m^2 at room temperature. While elevated temperature enhances the passivation effect of the water vapour, V_{OC} at these temperatures becomes unmeasurably small. Moreover, this signal needs to be separated from thermoelectric voltage generated due to temperature gradients inside the pressure chamber. To solve these complications a lock-in detector can be used to generate alternating signal with appropriate frequency (70 Hz in our case) supplying a light source used for the solar cell illumination. V_{OC} generated with the same frequency by the solar cell is selectively detected by the lock-in detector. Even small signals can be detected this way, because only signals with specific frequency are measured. Design of the pressure chamber and the contacting system were invented and realized in the frame of this work.

Comparison of a direct DC voltage measurement of V_{OC} (green circles) including also thermoelectric voltage V_{th}, an alternate AC voltage signal transferred into DC (red

triangles) and thermoelectric voltage V_{th} (blue squares) at different temperatures are shown in Fig. 6.2.

Temperature coefficient of open-circuit voltage of around -3 mV/°C, -0.14 %/°C was calculated for polycrystalline thin film silicon from the linear part of the curve corresponding to AC voltage transferred into DC voltage, see Fig. 6.2. This value is in a reasonable agreement with the coefficients presented by A. Shah [3], i.e. -0.15 %/°C for a-Si:H, -0.4%/°C for c-Si.

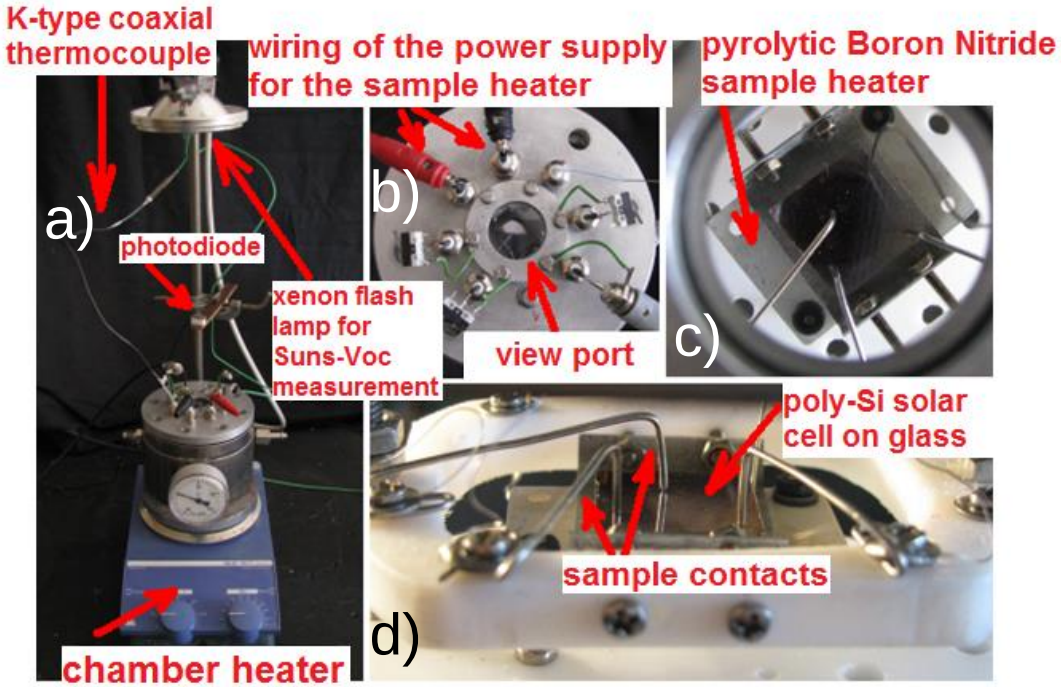

Fig. 6.1. In-situ Suns-V_{OC} measuring system: a) a stainless steel pressure chamber, a xenon flash lamp with a photodiode for Suns-V_{OC} measurement, K-type coaxial thermocouple, heater b) a flange of the chamber with a view port to enable illumination of the sample during Suns-V_{OC} measurement, wiring of a power supply for a sample heater, green cables to measure open-circuit voltage response of the solar cell to the light intensity c) the SPC solar cell with contacts placed on the pyrolytic Boron Nitride sample heater d) the polycrystalline Si thin film solar cell on glass contacted by stainless steel wires.

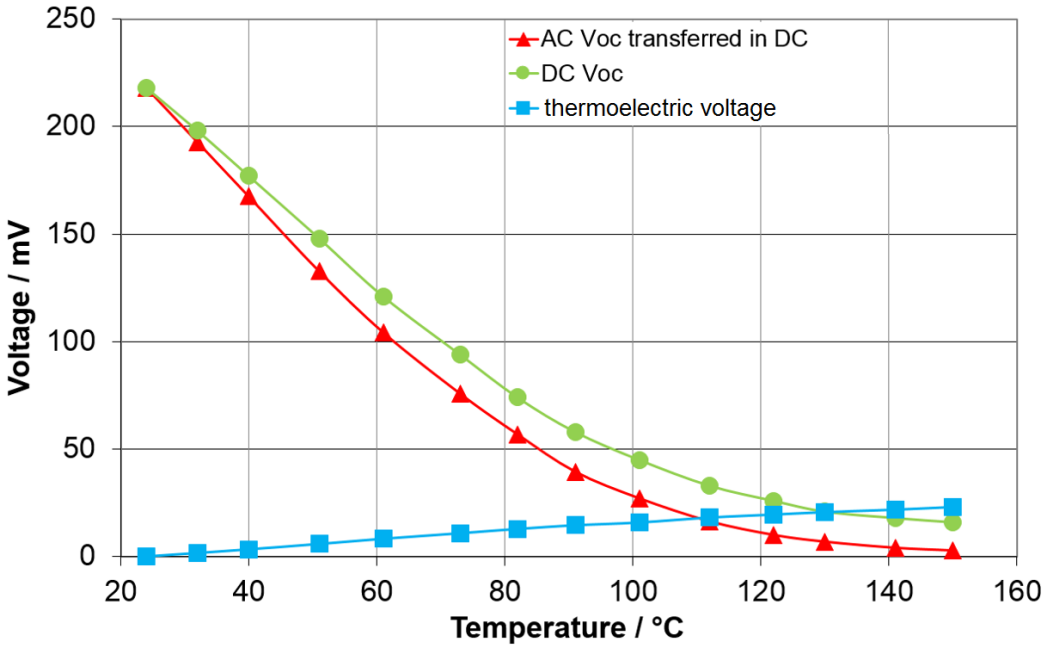

Fig. 6.2. Temperature dependences of open-circuit voltage V_{OC} for a SPC polycrystalline silicon thin film solar cell: a) alternate AC signal measured by a lock-in amplifier subsequently transferred in DC (red triangles) b) direct DC voltage measurement by the in-situ integrated Suns-V_{OC} system (green circles) c) thermoelectric voltage V_{th} (blue squares). Data were measured at light intensity of 1,000 W/m^2 of a xenon flash lamp.

However, the in-situ investigation of the passivation process could not be successfully applied because: a) AC V_{OC} signal is too small to be detected even by the lock-in detector at the temperature of around 400 °C suitable for the passivation in the water vapour, b) stainless steel wire contacts are unstable during the passivation process, and c) value of thermoelectric voltage is changing during the treatment. Finally, it was concluded there is no appropriate parameter that could be measured in-situ at such high passivation temperatures.

6.3 Conventional Investigation of the Water Vapour Passivation

Conventional approach to the investigation of the water vapour passivation effect was taken to uncover a role of particular passivation parameters (temperature of the poly-Si thin film, steam pressure, treatment duration, and redox character of a passivation medium). In this case, *conventional* means that success of the passivation treatment was determined by the solar cell's open-circuit voltage V_{OC} measured before and after the passivation treatment, not during the passivation process as it was intended for the in-situ investigation. Impacts of the particular passivation parameters are presented and discussed in the following paragraphs. The tested passivation conditions and their ranges are presented in Tab. 6.1.

Tab. 6.1. Tested parameters of the water vapour passivation process to determine optimum passivation conditions for the SPC poly-Si thin film solar cells.

Tested water vapour passivation parameter	**Range / Unit**
Temperature of the poly-Si thin film	145-650 °C
Additional pressure due to the water vapour	0*-1.0 MPa
Duration of the treatment	5-225 minutes
Redox character of the passivating medium	H_2 (g), H_2O (g) in H_2 (g), H_2O (g), boiling H_2O_2 (30%)

*…0 MPa corresponds to ambient atmospheric pressure

6.3.1 Apparatus for the Water Vapour Passivation

The same stainless steel pressure chamber as intended for the in-situ investigation (see Chapter 6.2) was used for the conventional investigation of the passivation process. Nevertheless, there are several modifications connected mainly with the heating of the solar cell. Since no contacting system (including also Teflon material) for the cell is needed anymore, significantly higher temperatures can be applied, see Fig. 6.3.

Deionized water prepared by reverse osmosis was used for these experiments.

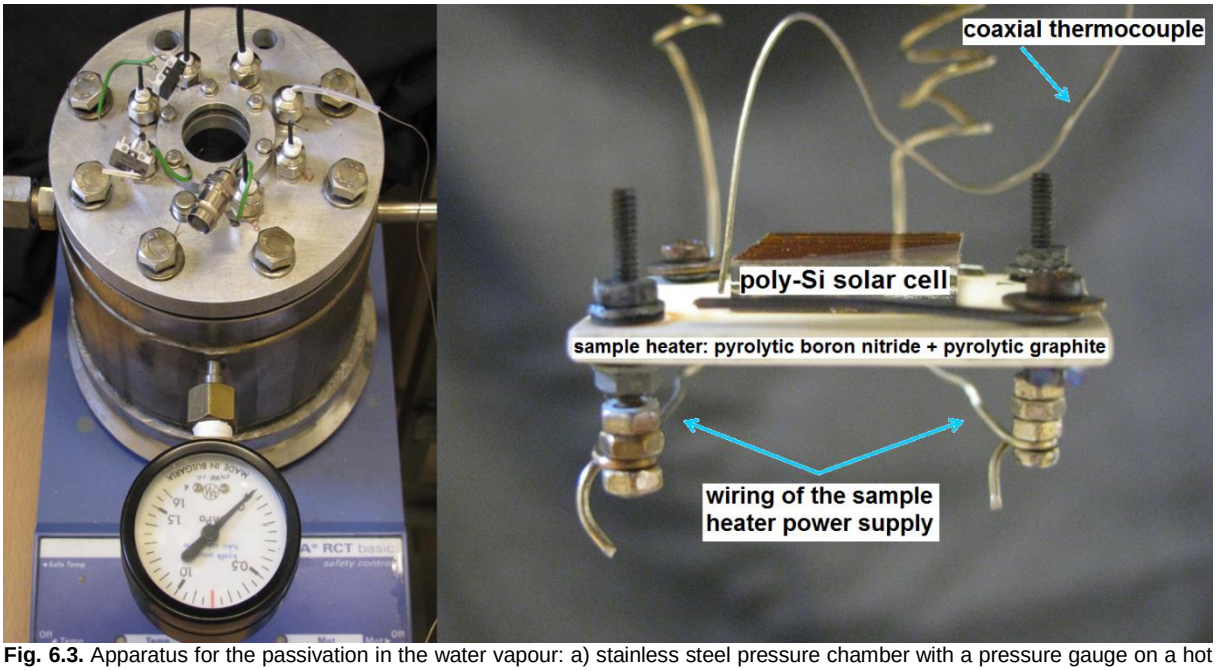

Fig. 6.3. Apparatus for the passivation in the water vapour: a) stainless steel pressure chamber with a pressure gauge on a hot plate used as a chamber heater b) SPC poly-Si thin film solar cell on glass placed on a pyrolytic boron nitride sample heater, wiring of the sample heater power supply, K-type coaxial thermocouple in touch with the sample heater.

6.3.2 Temperature of the Water Vapour Passivation Process

Polycrystalline silicon thin film solar cells were treated in the water vapour at different temperatures under atmospheric pressure. Temperature of the sample and of the steam was controlled independently by a pyrolytic boron nitride sample heater and a hot plate, respectively, see Fig. 6.3. The range of the tested temperatures was 145-650 °C. The passivation effect of the water vapour became observable at temperatures above around 200 °C. Treatments of SPC solar cells in air at particular temperatures were used as references to distinguish impact of the steam and of elevated temperature.

Samples annealed in the water vapour and in air at the temperatures of 350-650°C are presented in Fig. 6.4. There is a similar trend of data points for the samples treated in air (empty symbols) as for those annealed in steam (solid symbols) with the maximum at 450°C. According to the results, the temperature of 450°C corresponded to the strongest passivation impact of the steam on poly-Si with V_{OC} of 335 mV. Moreover, it seems air can also have a passivation effect on silicon (270 mV) at appropriate temperature. Air humidity in the testing room was around 50 %. The treatment duration for these samples was around 100 minutes.

In Fig. 6.5, there is a time progress of V_{OC} for the samples passivated at 450°C in steam and air. While the first 15 minutes of the treatment resulted in similar passivation effect for both steam and air, longer treatments brought different V_{OC} improvements. Finally, the samples reached similar V_{OC} after the treatment duration of 225 minutes due to the further V_{OC} increase in the case of the annealing in air and a significant deterioration for the annealing in steam.

It seems 450°C is the optimum temperature at least for the passivation process realized under atmospheric pressure for 100 minutes. This temperature was used for other experiments.

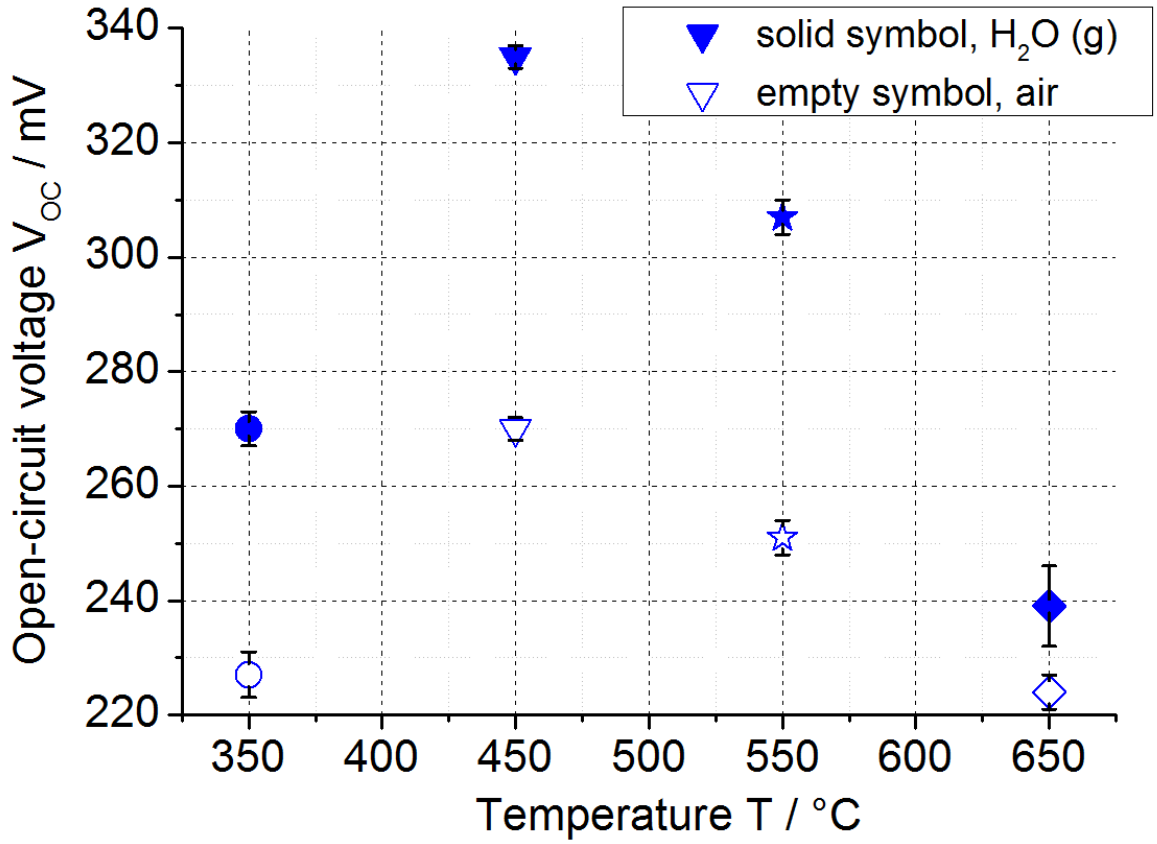

Fig. 6.4. Temperature dependence of open-circuit voltage V_{OC} for the thin film polycrystalline silicon solar cells treated in the water vapour (a solid symbol) under atmospheric pressure for around 100 minutes. The annealing in air at particular temperatures (an empty symbol) were used as references. Air humidity in the testing room was around 50 % [108].

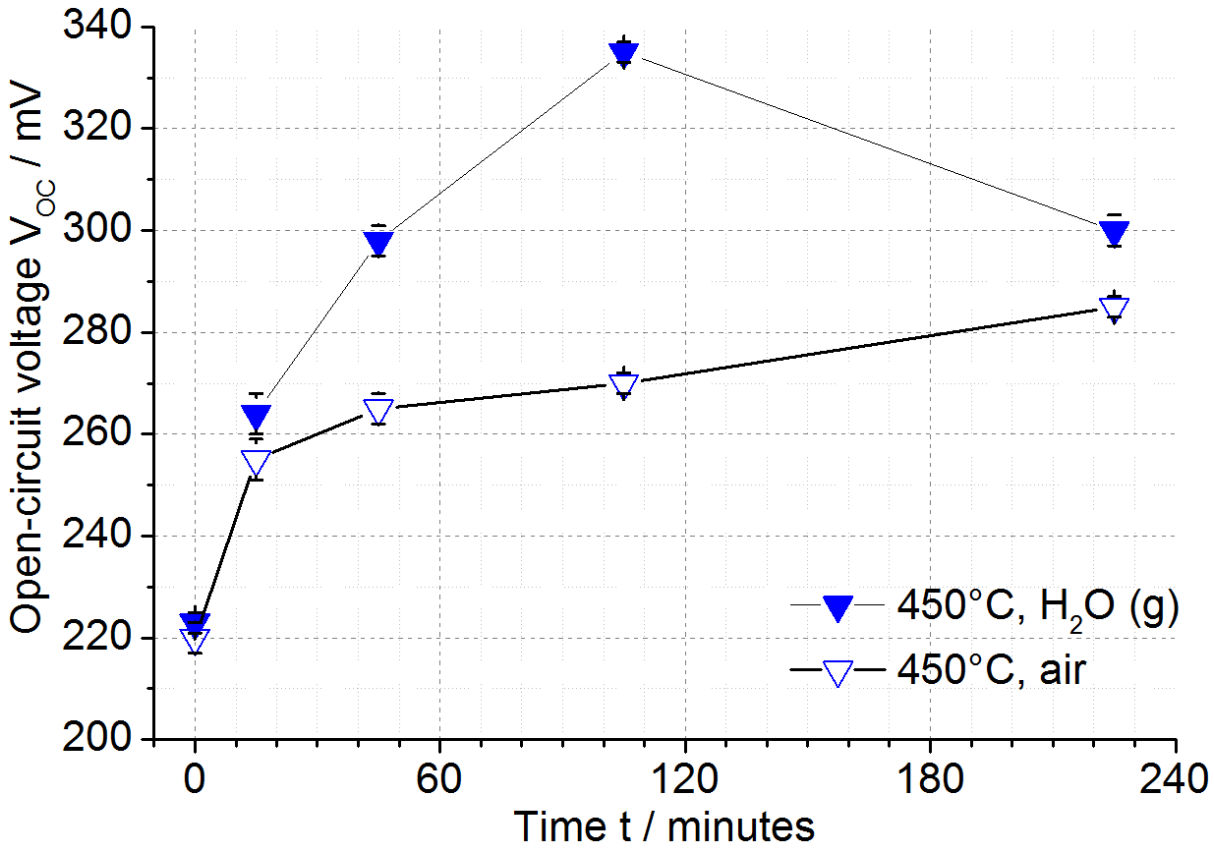

Fig. 6.5. Time progress of open-circuit voltage V_{OC} for the thin film polycrystalline silicon solar cell treated in the water vapour under atmospheric pressure at 450 °C. The annealing in air was used as a reference [108].

6.3.3 Steam Pressure of the Water Vapour Passivation Process

After the temperature variation, an impact of the steam pressure was investigated in the range from the atmospheric pressure up to 10 MPa. In Fig. 6.6, there is the pressure variation for the samples treated at 450°C for 100 minutes. The annealing in the steam under atmospheric pressure gave an unexpectedly strong passivation improvement in the context of other data points. Except the treatment under atmospheric pressure, there is a trend of increasing V_{OC} with elevated steam pressure of up to 0.75 MPa, where a maximum occurred and a further pressure increase brought a degradation. The treatment in air (empty triangle) was used as a reference.

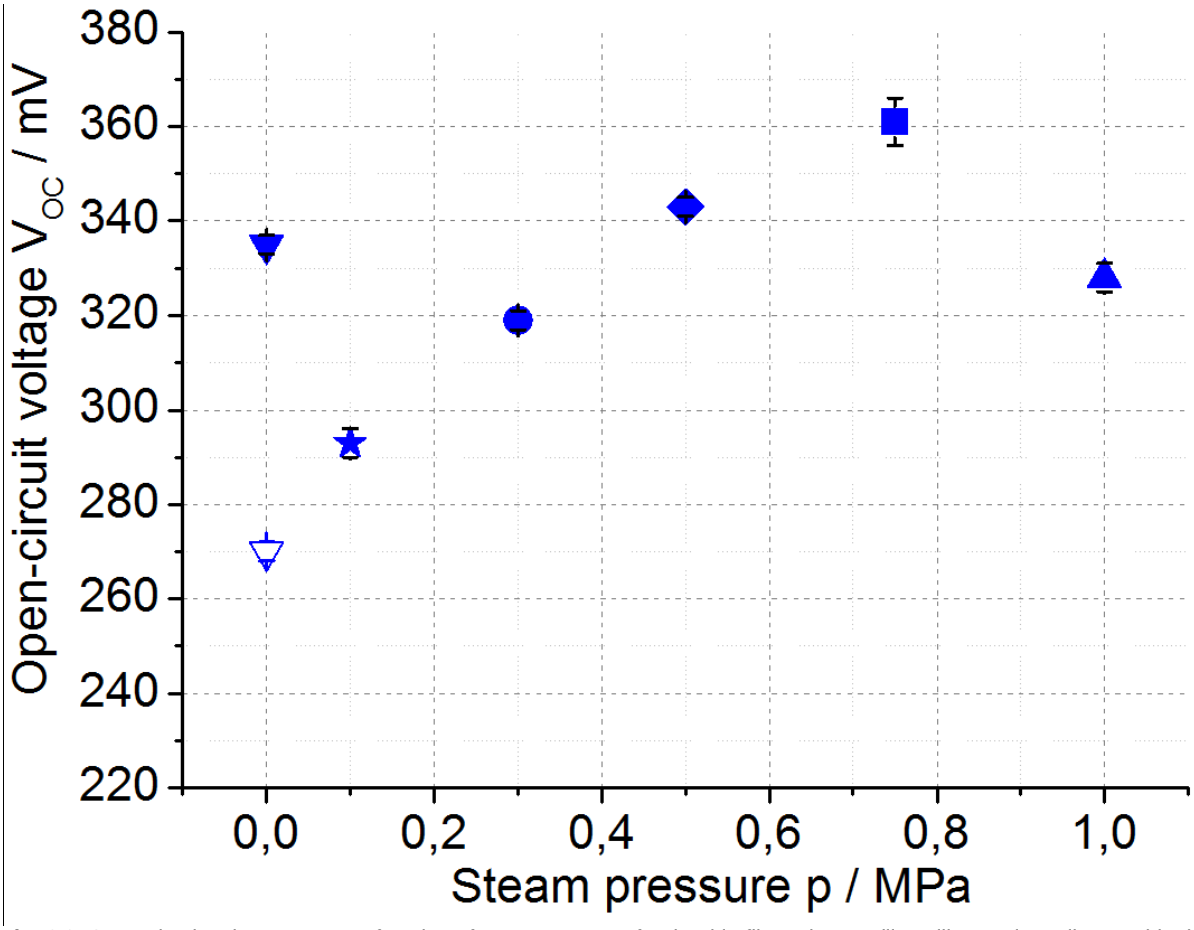

Fig. 6.6. Open-circuit voltage V_{OC} as a function of steam pressure for the thin film polycrystalline silicon solar cell treated in the water vapour at different steam pressures and constant sample temperature of 450 °C for around 100 minutes. The annealing at 450 °C in air (an empty triangle) was used as a reference [108].

The whole passivation process as a function of time for the sample that achieved the best V_{OC} of 360 mV at the pressure of 0.75 MPa after 100 minutes is presented in Fig. 6.7. There is a gradual V_{OC} increase with the passivation duration except the last data point of 225 minutes. Nevertheless, there is a clear passivation impact of the water vapour on poly-Si.

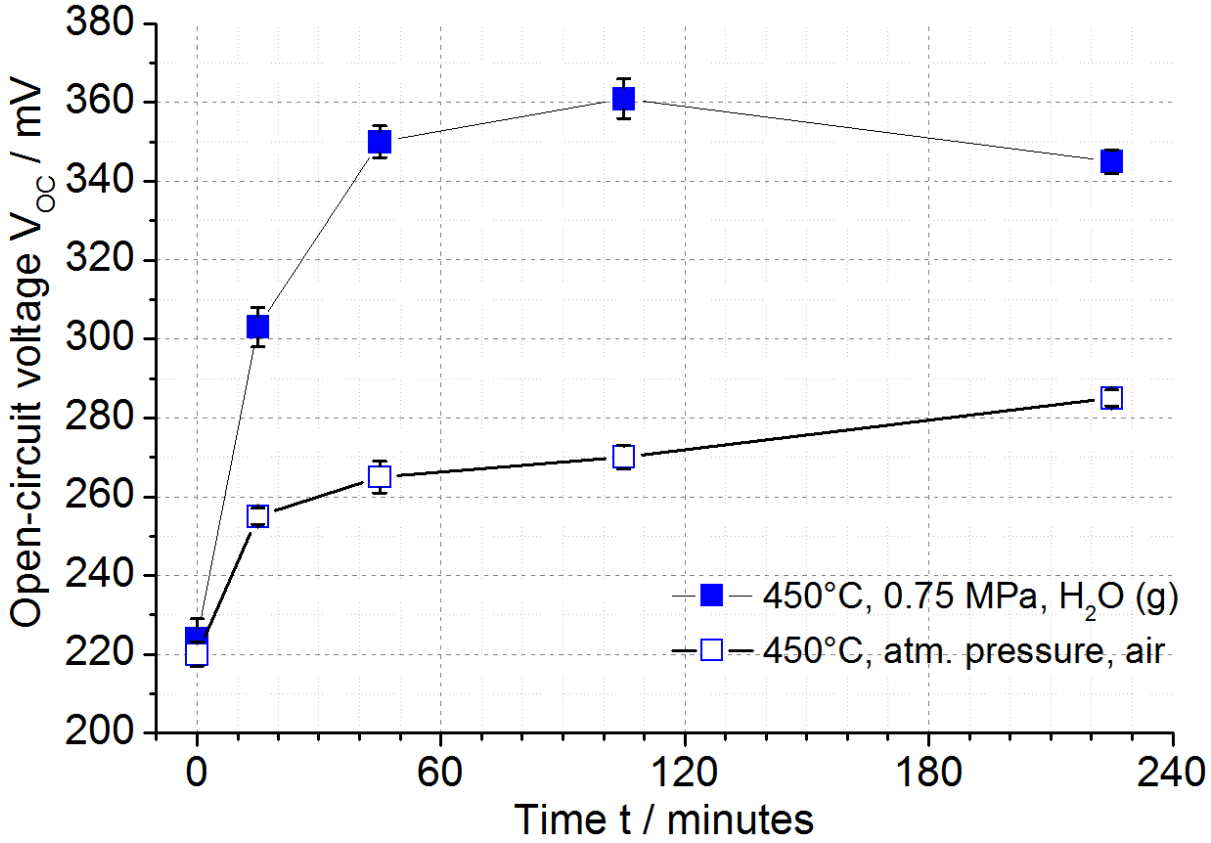

Fig. 6.7. Time progress of open-circuit voltage V_{OC} for the thin film polycrystalline silicon solar cell annealed under the steam pressure of 0.75 MPa and the temperature of 450 °C. The annealing at 450 °C in air was used as a reference [108].

6.3.4 Temperature-Pressure Interaction

In the previous experiments, only one parameter (temperature or steam pressure) was changed to investigate its influence while others were fixed. However, this very commonly used approach omits the possibility of a parameter interaction, in this case the interaction between temperature and pressure. To explore this phenomenon, additional experiments were realized and the results are presented in Tab. 6.2. Two steam pressures of 0.75 MPa and 1.0 MPa were applied for the temperatures of 350°C and 450°C. The results indicate that the same passivation effect (360 mV) of the water vapour on poly-Si can be achieved under different treatment conditions. Therefore an optimum value of a particular passivation parameter, e.g. temperature, should be always completed with other parameters (steam pressure, duration).

Our investigations confirm in most cases that the treatment duration of around 100 minutes brings the strongest passivation effect. This period was therefore used for other experiments.

Tab. 6.2. Interaction of steam pressure and sample temperature for the passivation duration of around 100 minutes.

		Steam pressure / MPa	
		0.75	1.0
Temperature / °C	350	270 mV	360 mV
	450	360 mV	328 mV

6.3.5 Hydrogen and Oxygen Content in Silicon

The polycrystalline Si thin film solar cells were annealed under atmosphere of different media (H_2 (g), H_2O (g) + H_2 (g), 30% boiling H_2O_2) to determine what chemical element(s) or functional group(s) saturate silicon dangling bonds at defects. Treatments were performed under the atmospheric pressure at the sample temperature of 450 °C for around 100 minutes, see Fig. 6.8. Similar passivation effect was achieved for both hydrogen gas H_2 (g) and also for a mixture of steam and hydrogen gas H_2O (g) + H_2 (g) (1:4). The mixture was prepared by bubbling hydrogen gas through deionized water (70 °C) before flowing into the passivation chamber. The experiment carried out under air in the atmosphere of H_2O (g) + O_2 (g) (6:1) resulted in V_{OC} even lower than the annealing in air used as a reference. The best result (335 mV) was achieved for the treatment in water vapour. The time progress for this sample is shown in Fig. 6.5.

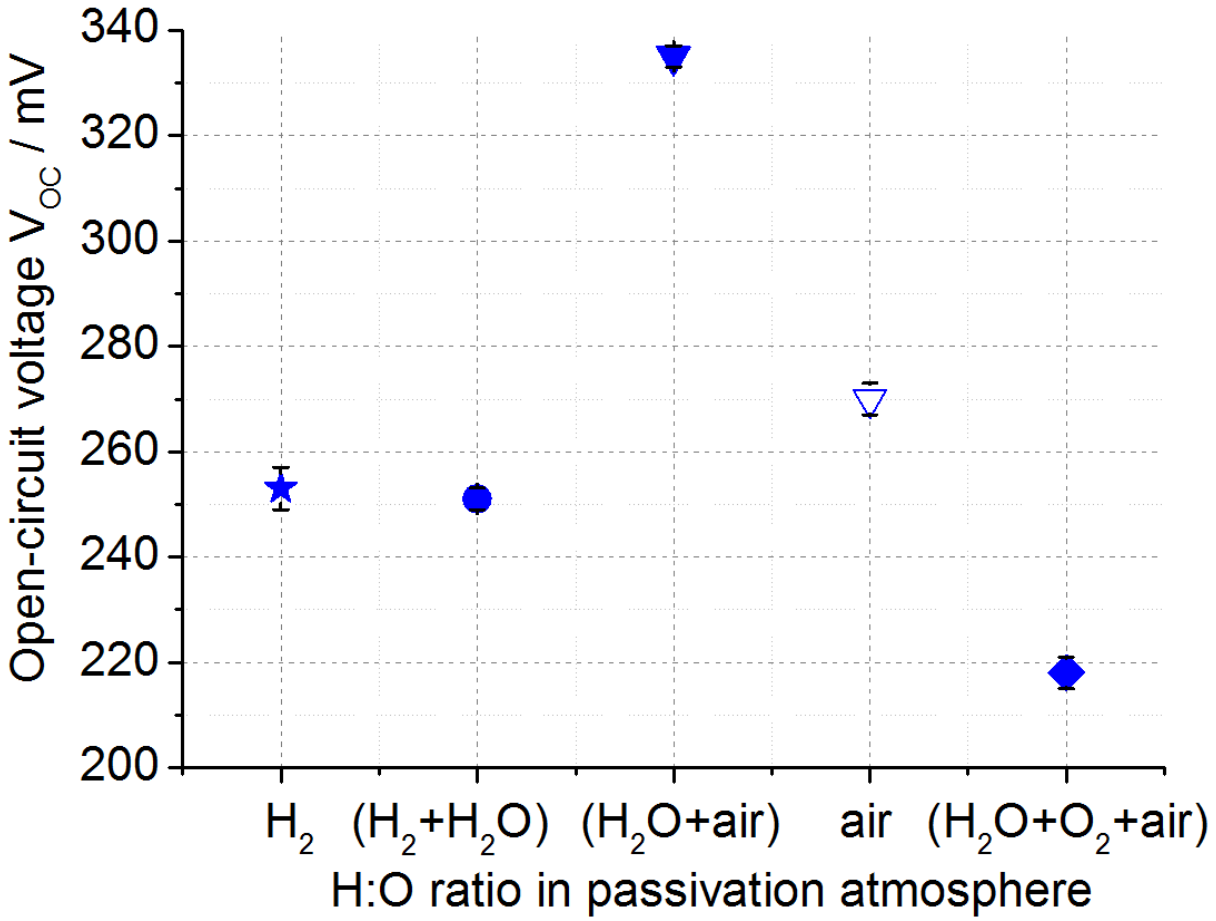

Fig. 6.8. Open-circuit voltage V_{OC} as a function of used passivation atmospheres for thin film polycrystalline silicon solar cells treated at 450 °C under atmospheric pressure for around 100 minutes. The tested reagents: H_2 = hydrogen gas flow, (H_2+H_2O) = hydrogen gas flow enriched with the steam produced outside the chamber, (H_2O+air) = water vapour and air, (H_2O+O_2+air) = boiling 30% hydrogen peroxide producing oxygen gas and steam in air [108].

According to these results, it seems that neither a predominant hydrogen nor oxygen concentration is desirable for a successful passivation process, rather an appropriate ratio of them. The annealing of poly-Si in the steam with the best V_{OC} improvement indicates that the H:O ratio of 2:1 in H_2O molecule is optimum or at least closer to it than other used media.

To determine whether the passivation process is hydrogenation of silicon or rather oxidation, three series of samples were prepared to investigate changes of

hydrogen and oxygen contents in silicon. Thin silicon layers of a-Si:H (600 nm) or µc-Si:H (400 nm) were prepared on monocrystalline silicon wafers by PECVD. They were treated either only in air or only in steam or in air and subsequently in steam to distinguish the effect of the water vapour and of elevated temperature itself, see Tab. 6.3. The annealing temperature of 450°C and the treatment duration of 100 minutes were same for each applied atmosphere. As the borosilicate glass substrate of poly-Si thin film solar cells is not transparent for infrared wavelengths, these samples could not be measured this way.

Tab. 6.3. Hydrogen and oxygen content in µc-Si:H and a-Si:H before and after the treatment.

		As-deposited	Treatment		
			Air (450°C, 100 min.)	**Steam** (450°C, 100 min.)	**Air-steam** (450°C, 100 min. + 100 min.)
[H] / %	µc-Si:H	6.6	Undetectably low concentration		
	a-Si:H	23.5			
[O] / %	µc-Si:H	0.4	5.7	9.7	13.1
	a-Si:H	0.6	2.7	7.4	11.3

A significantly different content of H (640 cm^{-1} and 2010 cm^{-1} for Si-H) in a-Si:H and µc-Si:H before any treatment ("as-deposited") was expected and it can be explained by a different silicon structure. In contrast to this, there was a similar low oxygen content (1090 cm^{-1} for Si-O) in both cases. While hydrogen concentration was undetectably low after the treatment in air and/or steam, oxygen content (1090 cm^{-1} for Si-O) was significantly increased for both a-Si:H and µc-Si:H after each type of annealing. Moreover, the oxygen content was in all cases higher for µc-Si:H. Since oxygen content was for both silicon types higher for the annealing in steam than in air, it seems that oxygen content depends on the applied atmosphere.

Hydrogen and oxygen contents in the silicon thin films were measured by Fourier transform infrared spectroscopy (Nicolet Nexus 870 FTIR) with use of the coefficients from [109].

6.3.6 Summary – Optimum Water Vapour Passivation Parameters

Temperature of the polycrystalline silicon thin film is the key parameter of a successful water vapour passivation. The temperature needs to be high enough, higher than around 200 °C, to observe an unambiguous V_{OC} improvement. Optimum range is relatively broad, from 350 °C to 450 °C, and it depends on other treatment parameters, mainly on steam pressure. It seems there is a temperature-pressure interaction and their appropriate adjustment can lead to similarly satisfying results.

Steam pressure can have a supporting passivation effect if the temperature is chosen appropriately. The best result of 360 mV (from starting 220 mV) was achieved for the pressure of around 0.75 MPa at the temperature of 450°C for 100 minutes. The same improvement was observed also for 1.0 MPa, 350°C, and the same duration.

Optimum treatment duration is around 100 minutes that resulted in the best V_{OC} in most cases.

Experiments under atmospheres with different hydrogen and oxygen content showed that the annealing in deionized water vapour has the strongest passivation effect.

6.3.7 Model of Steam Passivation

On the basis of the realized experiments, a model describing the passivation as a two-step process is presented in Fig. 6.9. Initially, this model expects a thermal decomposition of water molecule to prepare hydrogen cations and hydroxyl anions, Fig. 6.9.a). Subsequently, saturation of silicon dangling bonds is assumed rather by hydroxyl anions than by hydrogen cations due to a high probability of hydrogen out-diffusion from silicon at elevated temperatures as it was demonstrated in the case of a-Si:H and μc-Si:H samples, Fig. 6.9.b). Finally, a creation of Si-O-Si bond is considered and H_2O with H_2 molecules are released, Fig. 6.9.c).

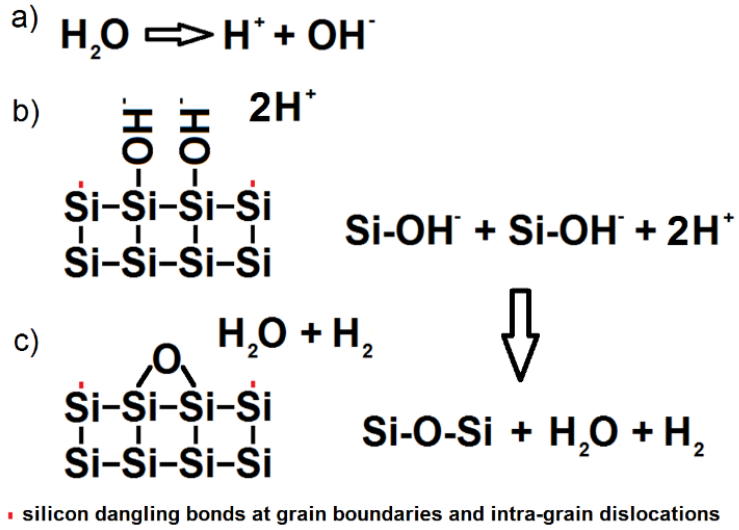

Fig. 6.9. A passivation model for silicon annealed in the water vapour assuming a) decomposition of water molecules, b) saturation of Si dangling bonds by hydroxyl anions, and c) creation of Si-O-Si passivation chains and release of H_2O and H_2 molecules [108].

This model is based on the above presented experimental results and was inspired by passivation of SiO_2 thin films in water vapour, see Chapter 3.4. The model presented in this thesis is in agreement with results of other research works that investigated various types of silicon thin films, transistors or solar cells. However, most of researchers present only assumptions that water vapour passivation of silicon is a formation of Si-OH, Si-O or Si-O_2, without any experimental confirmation and suggest further investigation. According to my best knowledge, there is no other work presenting a model of water vapour passivation for silicon thin film solar cells in such detail supported with both analysis of silicon electrical quality and of hydrogen, oxygen content.

6.3.8 Discussion – Water Vapour Passivation

The temperature variation of the passivation process in the water vapour revealed the need of high enough temperature to observe an unambiguous passivation effect of the steam on polycrystalline silicon. Neither an elevated steam pressure nor a prolonged duration could replace the effect of temperature. Explanation of this observation could be that a sufficient thermal energy is needed to initiate a decomposition process of H_2O molecules needed for passivation. This energy is required for both production of passivating particles from H_2O molecules as well as for their effective diffusion in silicon. These particles could be, e.g. -OH, -H, -OOH [33], [61], [64], [72], [76], [80], [110], [111]. The annealing at 450 °C in the presence of different reagents uncovered that the pure water vapour had the strongest passivation effect on silicon. The ambient air also had a surprisingly strong passivation impact.

Nevertheless, neither more reducing (H_2 (g), H_2O (g) in H_2 (g)) nor more oxidizing (boiling H_2O_2) conditions brought better or even comparable improvement than the steam. On the base of these experiments, it is assumed that the appropriate ratio of hydrogen and oxygen 2:1 is needed for a successful passivation. A negative effect of the oxidizing mixture (O_2 + H_2O) on silicon electrical quality is probably due to a dominant creation of new defects.

The elevated steam pressure brought the additional passivation benefit in the case of the treatment temperature of 350 °C, see Tab. 6.2. Increased pressure can be understood as an increased concentration of H_2O molecules that are present in gaseous phase surrounding the treated silicon surface. Higher amount of the available passivating particles is the most probable explanation of the enhanced passivation impact of the water vapour pressure. However, higher pressure did not always result in higher V_{OC}. There is an optimum concentration of the passivating particles needed for a successful passivation around the steam pressure of 0.75 MPa at 450°C for 100 minutes. Lower or higher pressure means a lack or an excess of the passivating particles, respectively.

In the most cases, the treatment duration of around 100 minutes resulted in the best improvement of silicon electrical quality characterized by open-circuit voltage V_{OC}. The passivation process should be seen as a complex process consisting of at least two sub-processes running against. The first one: deactivation of defects at the SiO_2/Si interface, silicon structural defects and impurities by a creation of bonds between the passivating particles and silicon dangling bonds of the mentioned imperfections acting as recombination centres. The second sub-process taking place simultaneously with the first one is the creation of new defects as a consequence of the elevated temperature allowing relatively easy diffusion of vacancies and activation of up to now non-active defects and impurities. According to the measured results, total effect of the treatment in the water vapour depends on the process duration and other conditions. While annihilation of the defects dominates during around the first 100 minutes of the process, creation of new defects becomes predominant with the prolonged treatment duration. Final effect of the water vapour on a passivated polycrystalline silicon thin film solar cell results in a macroscopically measurable change of V_{OC}.

While the annealing of the sample at 350 °C in air showed only a slight V_{OC} increase in relation to a non-passivated sample (220 mV), the temperature of 450°C had a stronger effect, see Fig. 6.4. The V_{OC} improvement can be partly explained by a relaxation of a tensile stress in the silicon layer [34]. According to the experiments with a-Si:H and µc-Si:H, it seems that oxygen coming from air is to a certain extent able to saturate the silicon dangling bonds. The experiments in air used as references were realized to prove that the achieved V_{OC} improvements were caused by the water vapour and not by elevated temperature.

All the above presented results and their comparison with scientific literature brings us to the final conclusion that the passivation of silicon in the water vapour is at least a two-step process. In the first step hydration of silicon dangling bonds takes place and the passivating particles (–OH) saturate silicon dangling bonds. In the second step, dehydrogenation is realized, where more stable Si-O-Si bonds are formed and hydrogen is released. It seems that hydrogen plays a significant role in the process, but finally oxygen saturates silicon dangling bonds, therefore the water vapour passivation is silicon oxidation.

The results related to the SPC Si solar cells passivated in the water vapour were presented at the 26th ICANS Conference in Aachen, Germany, 2015 and published in the Physica Status Solidi A [108] and Acta Polytechnica [112].

7 Plasma Hydrogenation of SPC and LPC Si Solar Cells

Thin film solid phase crystallized (SPC) and liquid phase crystallized (LPC) silicon solar cells were annealed in hydrogen plasma to deactivate electrically active defects causing recombination of photogenerated charge carriers.

Impact of various hydrogenation parameters (e.g. sample temperature, hydrogen pressure, treatment duration, electrode distance, temperature of plasma switch off, bias voltage V_{bias}) was investigated to uncover a) whether the limit of up to now achieved 492 mV [16] for SPC Si solar cells can be exceeded and b) what is the passivation limit of LPC Si solar cells.

Description of a vacuum chamber and impact of particular passivation parameters are presented in this chapter.

It should be underlined that the treatment in hydrogen plasma change only silicon electrical quality and all other sample properties remain unchanged. This enables evaluation of the hydrogen plasma passivation effect on polycrystalline silicon in comparison with a non-passivated sample.

7.1 Apparatus for the Plasma Hydrogenation

All hydrogen plasma passivation procedures realized in the frame of this thesis were performed in a vacuum chamber at the Helmholtz-Zentrum Berlin in Germany, see Fig. 7.1. Schematic diagram of the passivation chamber with a power supply, heating and dimensions of a hollow cathode is shown in Fig. 7.2.

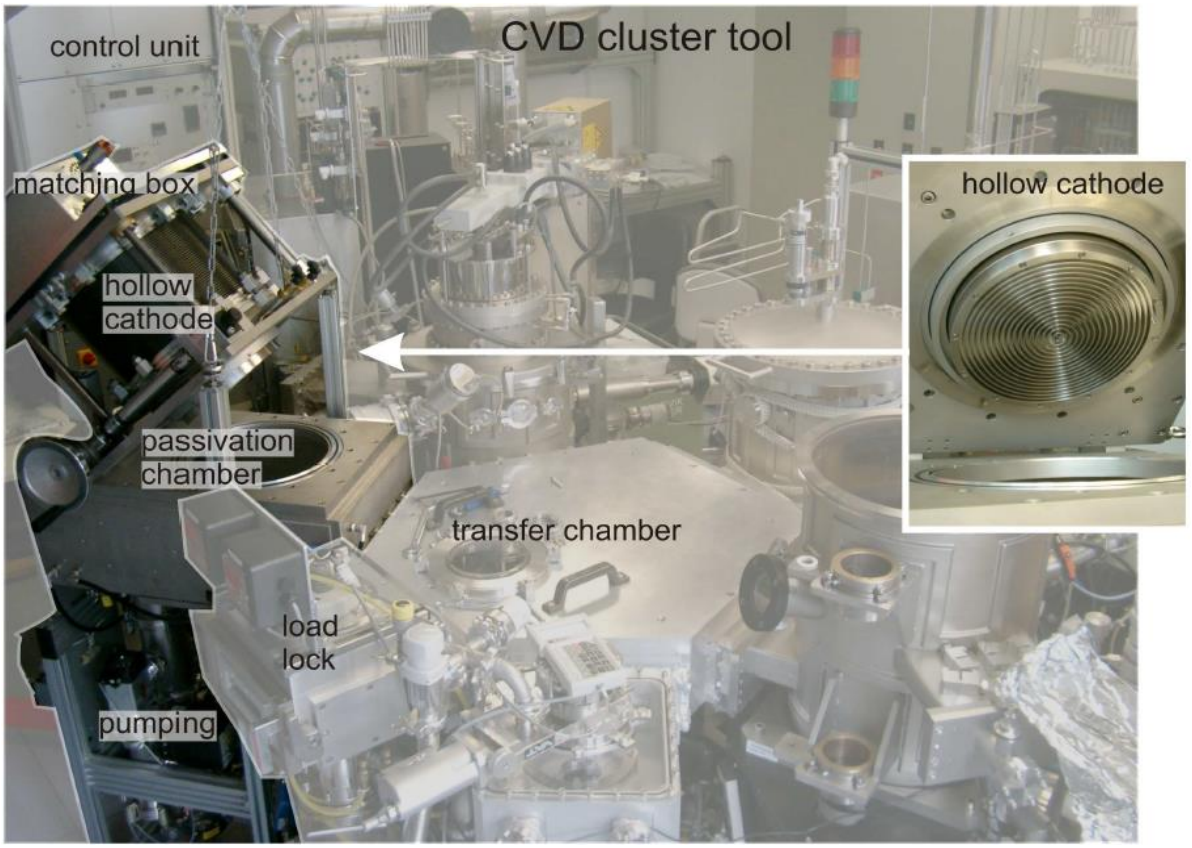

Fig. 7.1. Chemical vapour deposition cluster tool consisting besides other parts of a load lock, transfer chamber, and passivation chamber that was used for the plasma hydrogenation of the polycrystalline thin film silicon solar cells [34].

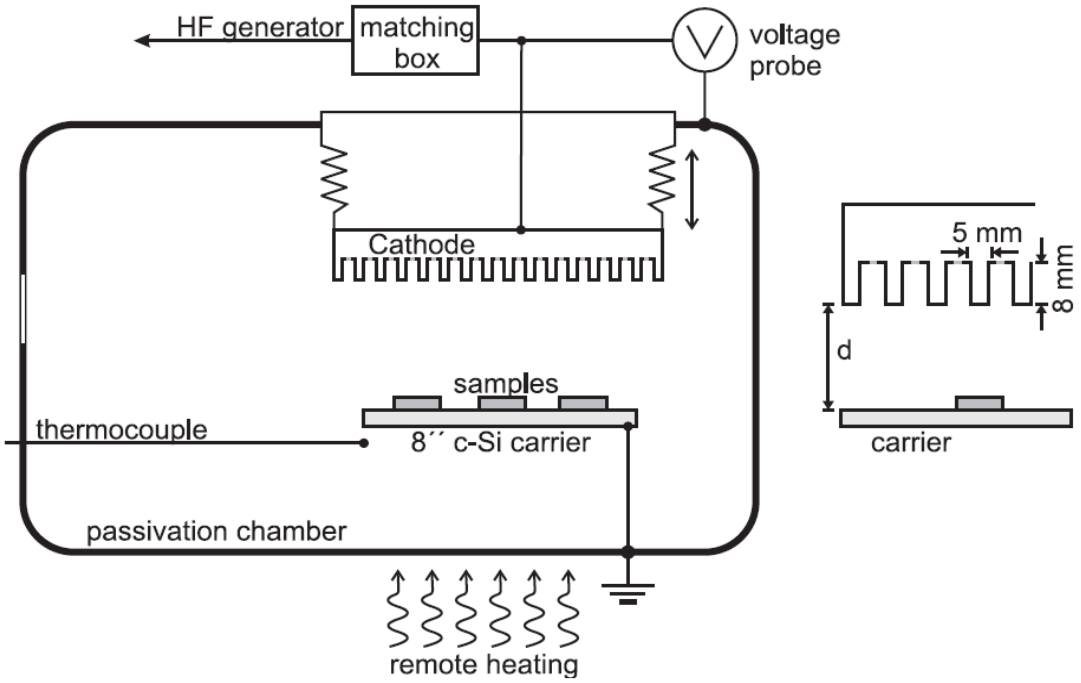

Fig. 7.2. Schematic diagram of the vacuum chamber used for the plasma hydrogenation with a matching box, voltage probe, hollow cathode, c-Si wafer used as a sample carrier, thermocouple, remote heating. Detail for the hollow cathode in [34].

Samples were etched in HF acid (2 %) to remove native SiO_2 and dried by nitrogen gas. They were placed without any delay on an 8-inch c-Si carrying wafer and loaded into the load lock. The samples were transferred into the transfer chamber at the residual pressure of around 10^{-3} Pa and then into the passivation chamber after achieving the pressure of around 10^{-5} Pa. The chamber was filled with hydrogen gas to have a required pressure. Sample heating realized by remote lamps was controlled by a computer according to the standard temperature profile described more in detail in the following chapter.

More detailed description of the used passivation chamber is available in [34].

7.2 Temperature Profile

Temperature profile shown in Fig. 7.3 was used in the case of all plasma hydrogenation procedures. It consisted of three parts – increase, plateau and decrease of temperature. Temperature ramp was rapid at the beginning (200 K/min) and then it became slower to avoid sample destruction due to a temperature gradient in borosilicate glass used as a substrate for the passivated thin film poly-Si solar cells. Plasma was ignited at the beginning of the plateau phase. Last part – sample cooling – was also controlled by the computer and the plasma was turned off at around 350°C (to avoid hydrogen out-diffusion from the silicon at higher temperatures and etching of Si surface by atomic hydrogen bombardment at lower temperatures [32], [34]). Hydrogen was removed from the chamber at the temperature of 280°C.

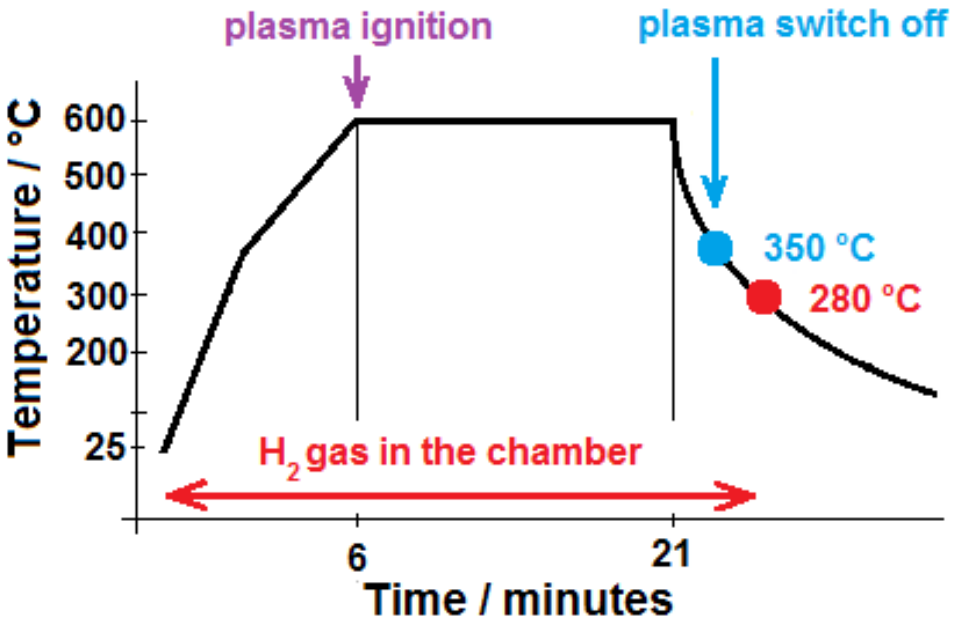

Fig. 7.3. Standard temperature profile of the hydrogen plasma passivation process with the temperature of the plasma switch off at around 350 °C and of hydrogen gas removal from the chamber at around 280 °C.

7.3 Hydrogen Plasma Passivation of SPC Si Thin Film Solar Cells

Impact of plasma termination temperature during the cooling phase of the treatment on the resulting open-circuit voltage V_{OC} was investigated in the first step. Subsequently, effect of the treatment temperature, hydrogen pressure, radio frequency (RF) plasma power, treatment duration, electrode distance, and bias voltage V_{bias} were tested. In spite of our effort for a systematic investigation, there are strong interconnections between some parameters and it was very challenging and in some cases even impossible to separate overlap of their particular impacts. Nevertheless, experiments brought valuable results presented in the following chapters according to the particular investigated treatment parameter.

7.3.1 Temperature of the Plasma Switch off

The temperature of the plasma switch off point was varied to investigate a connection between the resulted open-circuit voltage V_{OC} and hydrogen content in the polycrystalline silicon thin film solar cells. Other plasma hydrogenation conditions (sample temperature of 600 °C, treatment duration of 15 minutes, hydrogen pressure of 100 Pa, plasma power of 50 W, electrode distance of 20 mm) were kept constant. The dependence of the obtained V_{OC} on the switch off temperature is shown in Fig. 7.4. Particular plasma switch off temperatures are displayed also in the temperature profile of the plasma hydrogenation process as numbers 1-7, see the right upper corner of the figure. There is a clear trend with the maximum at the plasma switch off temperature of around 340 °C. Plasma turned off at higher or lower temperatures led to worse results.

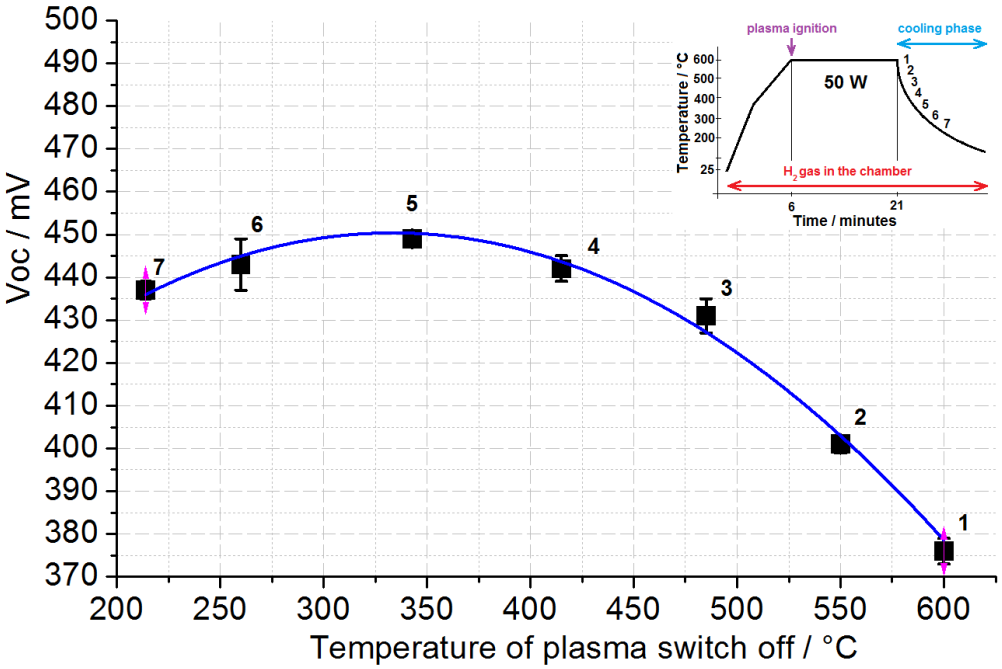

Fig. 7.4. Dependence of the open-circuit voltage V_{OC} on the plasma switch off temperature. Temperature profile of the plasma hydrogenation process with numbers 1-7 is shown in the upper right corner. The numbers correspond to the temperature of the plasma switch off shown in the main graph.

The optimum temperature of the plasma switch off (around 340 °C) was used in the case of all other experiments in this work, if not specified.

7.3.2 Temperature

Influence of the sample temperature was investigated at two different hydrogen pressures of 100 or 300 Pa, see Fig. 7.5. The measured V_{OC} data give an obvious trend with the maximum at around 600 °C in the case of both tested pressures.

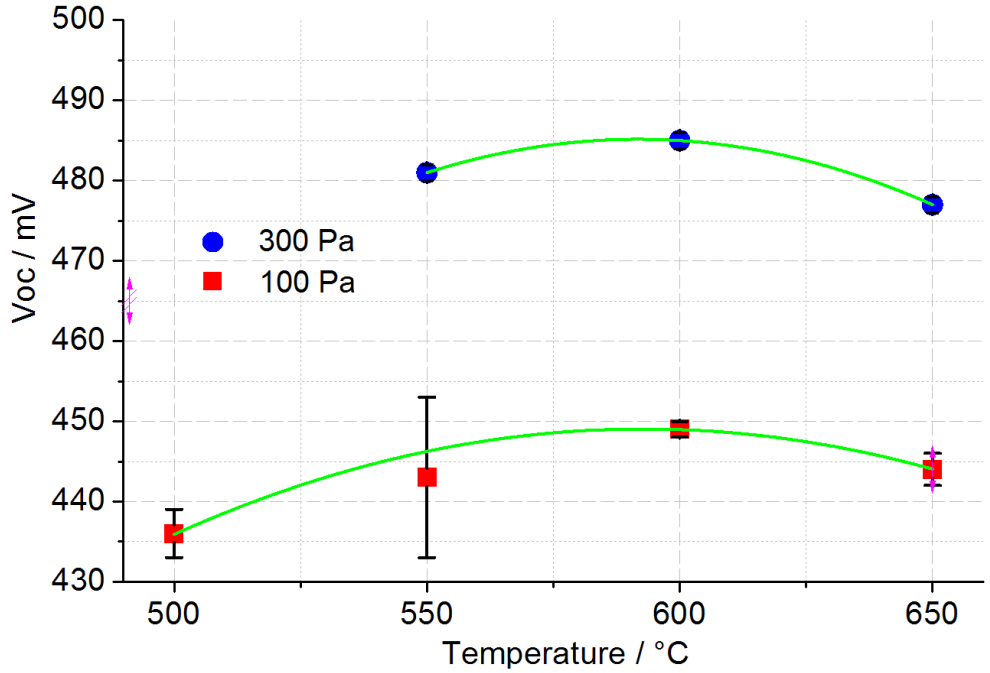

Fig. 7.5. Temperature dependence of the open-circuit voltage V_{OC} for the hydrogen plasma passivation of the solid phase crystallized silicon thin film solar cells. Other treatment parameters were: treatment duration of 15 minutes, plasma power of 50 W, electrode distance of 20 mm.

7.3.3 Treatment Duration

Exposure time of the hydrogen plasma was tested in the range from 5 to 30 minutes, see Fig. 7.6. The SPC poly-Si solar cells were passivated at the hydrogen gas pressure of 100 or 300 Pa. Optimum range of the treatment duration is relatively broad. Nevertheless, the best results were measured for 15 and 20 minutes.

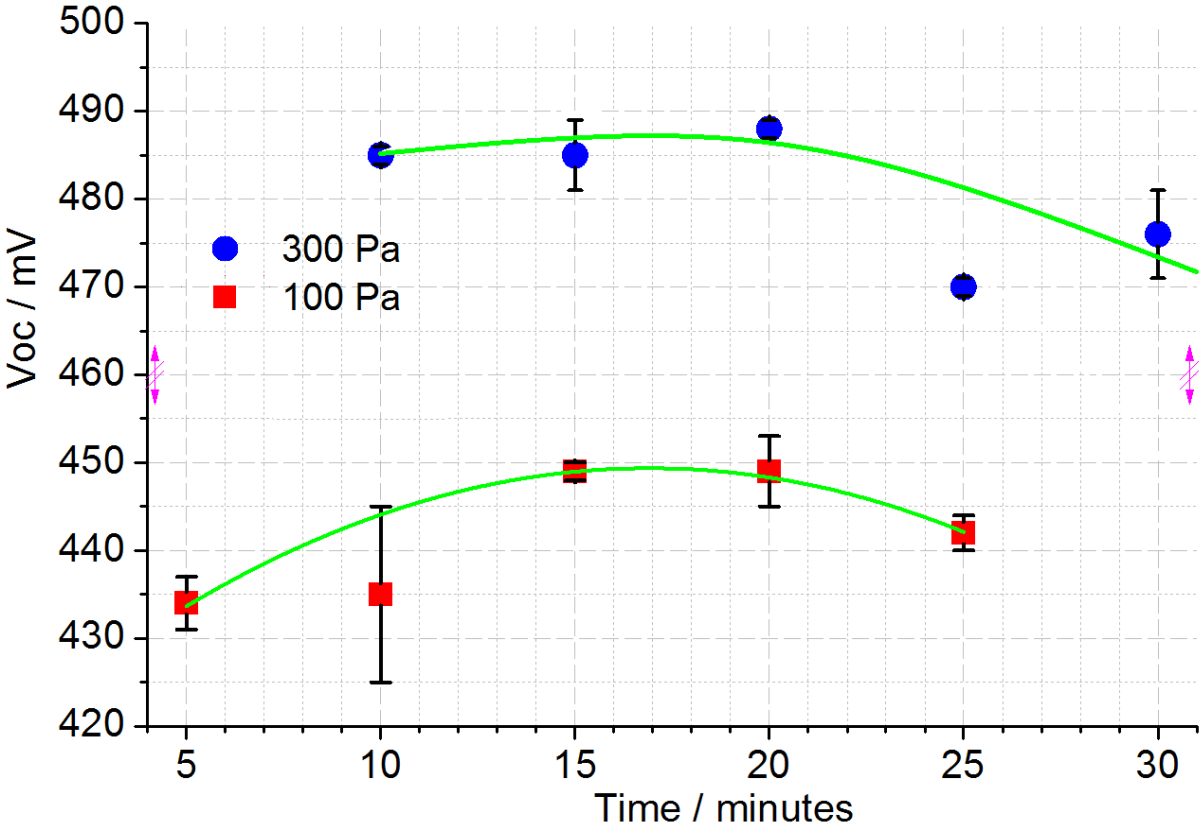

Fig. 7.6. Time dependence of the open-circuit voltage V_{OC} for the hydrogen plasma passivation of the solid phase crystallized silicon thin film solar cells. Other treatment parameters were: sample temperature of 600 °C, plasma power of 50 W, electrode distance of 20 mm.

7.3.4 Hydrogen Pressure

The optimum sample temperature of 600 °C and the treatment duration of 15 minutes were applied in the experiments focused on investigation of hydrogen gas pressure impact, see Fig. 7.7. The hydrogen pressure of 300 Pa brought the best V_{OC} improvement of 485 mV. It should be mentioned that all the plasma hydrogenation processes were performed as a closed system (with the gate valve to vacuum pumps closed). The tested hydrogen pressure was adjusted at the beginning of the process when a plateau temperature was achieved. Then the hydrogen flow into the chamber was closed and the whole process ran in the same atmosphere. Bias voltage V_{bias} shown in the graph is commented more in detail in the following subchapter. For this moment, let's make a note that the best result corresponded to V_{bias} = 10 V.

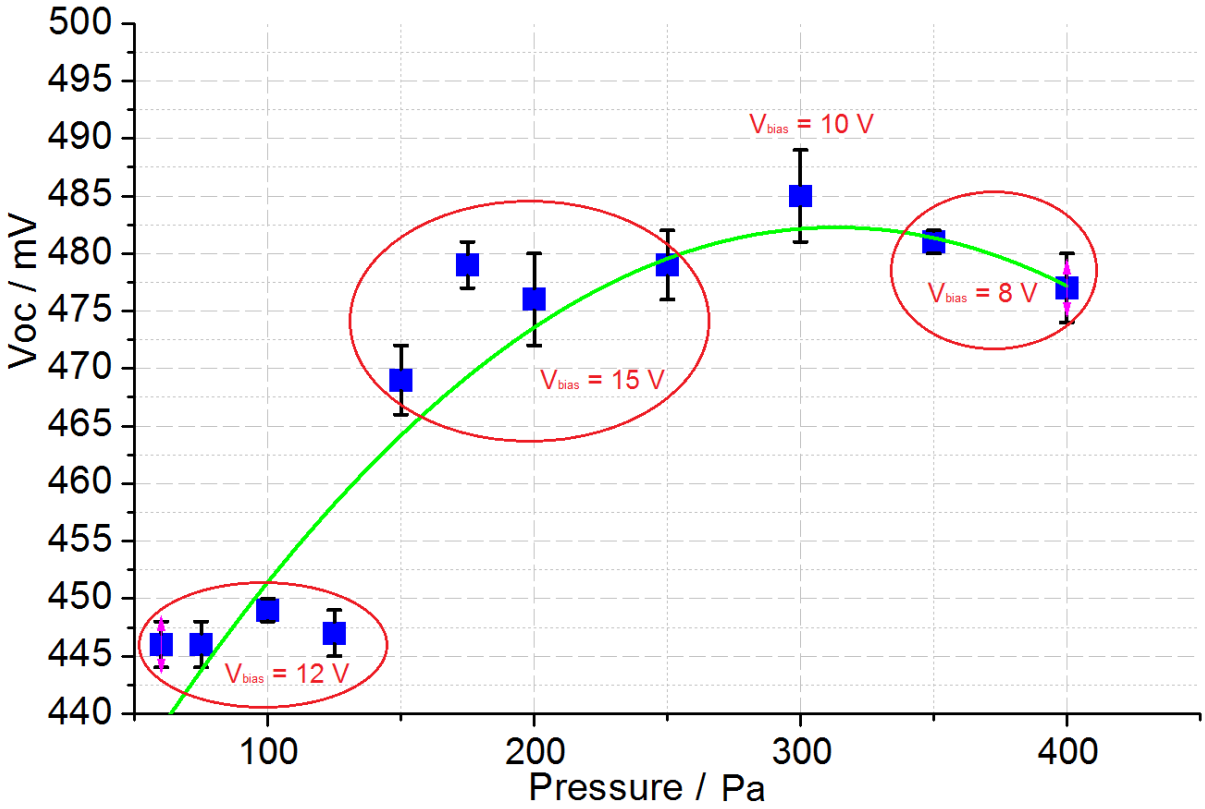

Fig. 7.7. Dependence of the open-circuit voltage V_{OC} on hydrogen gas pressure for the hydrogen plasma passivation of the solid phase crystallized silicon thin film solar cells. Other treatment parameters were: sample temperature of 600 °C, treatment duration of 15 minutes, plasma power of 50 W, electrode distance of 20 mm, different bias voltage shown in the graph.

7.3.5 Bias Voltage

Accelerating voltage V_{acc} is present between the hollow cathode and the grounded c-Si wafer carrying the samples treated in the passivation chamber, see Fig. 7.2. This voltage can be measured directly by a probe, but a special equipment is needed. In contrast to this, value of bias voltage V_{bias} is easily available, but it cannot be adjusted and controlled directly, e.g., it decreases spontaneously during the cooling phase of the passivation process. Value of V_{bias} depends on many other parameters, e.g. hydrogen pressure, temperature, electrode distance, and it is a result of their collective influence. Nevertheless, it can be easily measured. Since there is a correlation between accelerating voltage and bias voltage, impact of V_{bias} is discussed in this work instead of V_{acc}.

Experiments dealing with an impact of hydrogen pressure on the resulting silicon electrical quality represented by V_{OC} uncovered a possible connection between improvement due to the passivation and bias voltage V_{bias}, see Fig. 7.7. The best result was achieved at the hydrogen pressure of 300 Pa corresponding to V_{bias} of 10 V during the constant temperature phase of the hydrogenation process. Although the hydrogenation parameters, e.g. hydrogen pressure, plasma power are kept constant, bias voltage decreases spontaneously during the cooling phase. The experiment at 300 Pa was repeated at the same processing conditions as in Fig. 7.7 just V_{bias} was kept constant during the cooling phase by increasing plasma power. Fig. 7.8 shows a slight additional V_{OC} improvement from 485 mV to 491 mV.

To investigate the effect of constant V_{bias} during the cooling hydrogenation phase, series of the SPC Si solar cells was passivated at different hydrogen pressures and corresponding plasma power to keep V_{bias} = 10 V. This voltage was kept constant also

during the cooling phase. The resulted V_{OC} achieved similar values throughout the whole investigated pressure range, except the experiment carried out at 500 Pa that brought even better V_{OC}.

There are two similar experiments achieving similar results realized at the hydrogen pressure of 500 Pa in Fig. 7.8 that are different only in the treatment duration of 15 minutes (red square) or 8 minutes (blue star).

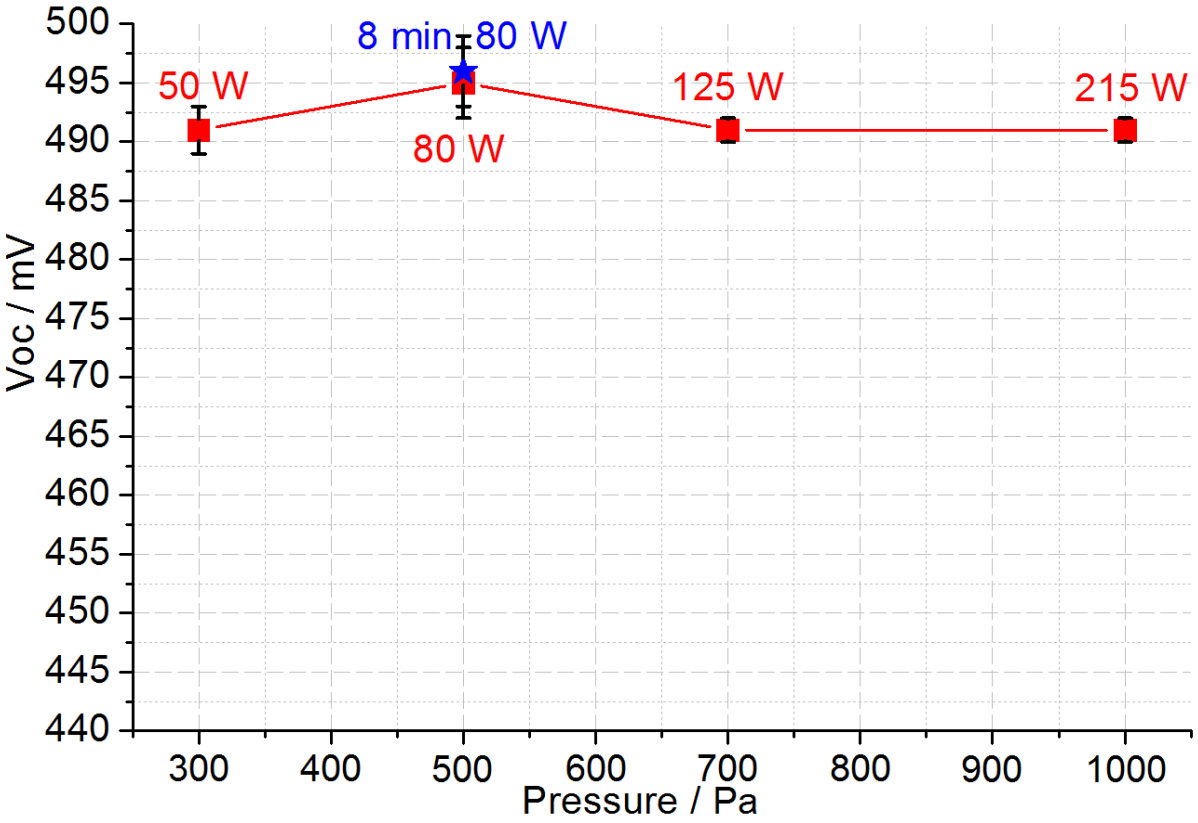

Fig. 7.8. Pressure dependence of the open-circuit voltage V_{OC} for the hydrogen plasma passivation of the solid phase crystallized silicon thin film solar cells treated at the temperature of 600 °C, duration of 15 minutes (if not written in the graph), electrode distance of 20 mm, bias voltage of 10 V kept constant during the cooling phase of the hydrogenation process.

Another pressure series of the poly-Si thin film solar cells was treated in the hydrogen plasma at different RF plasma powers suitably adjusted to keep bias voltage 10 V, see Fig. 7.9. Electrode distance of 50 mm was used to find a connection between the hydrogen plasma passivation effect and geometry of the chamber. There is a clear trend with the maximum at around 300 and 400 Pa. Nevertheless, better results were achieved with the electrode gap of 20 mm.

Further experiments focused on the impact of V_{bias} on the resulted V_{OC}. Series of 3 SPC samples were passivated at the hydrogen pressure of 500 Pa and particular RF plasma powers corresponding to the tested bias voltages of 8, 10, and 13 V, see Fig. 7.10. All the results exceeded the value of 490 mV and the best one 497 mV was achieved at V_{bias} of 13 V.

According to these results, it seems that a particular value of V_{bias} is not important for a successful hydrogenation. The key point is keeping a value of V_{bias} constant during the whole cooling phase (by e.g. increasing plasma power or decreasing hydrogen pressure).

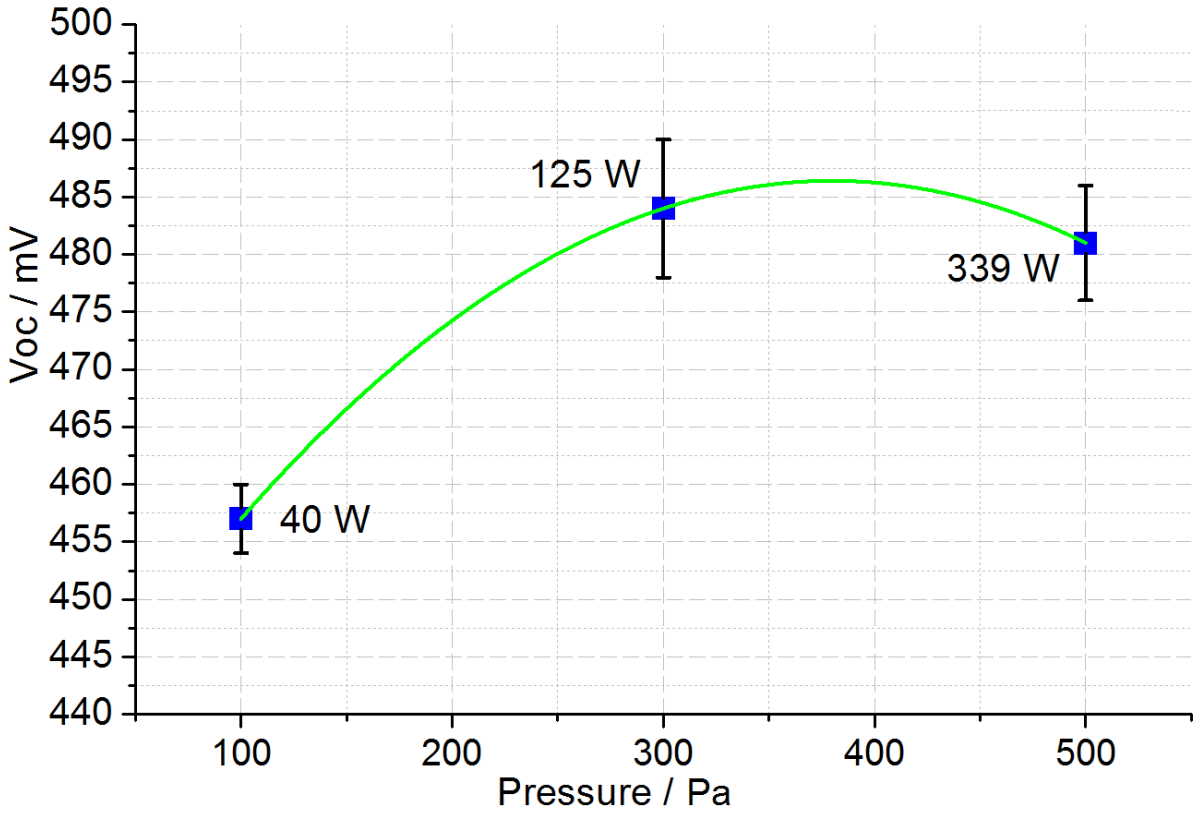

Fig. 7.9. Hydrogen pressure dependence of the open-circuit voltage V_{OC} for the hydrogen plasma passivation of the solid phase crystallized silicon thin film solar cells, treatment parameters were: sample temperature of 600 °C, treatment duration of 15 minutes, electrode distance of 50 mm, plasma power adjusted according to the hydrogen pressure to have bias voltage of 10 V, this voltage was kept constant also during the cooling phase.

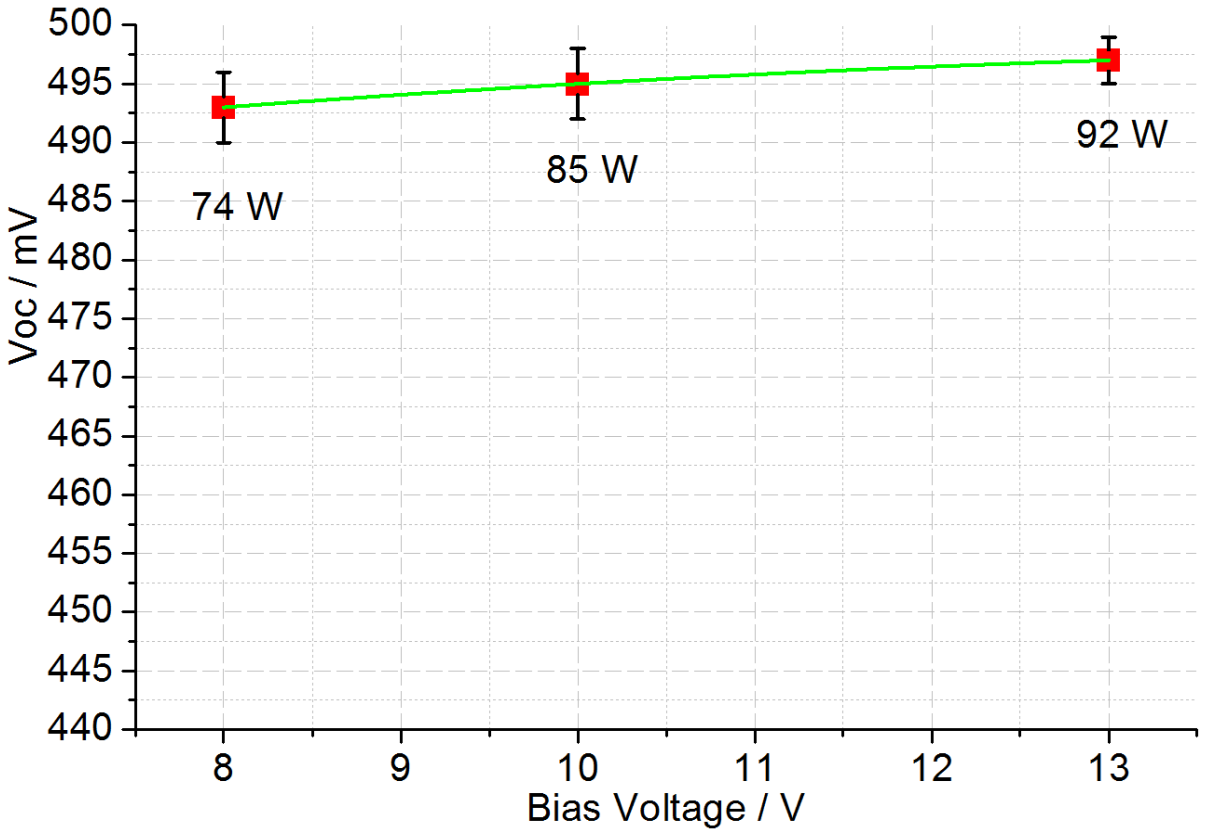

Fig. 7.10. Bias voltage dependence of the open-circuit voltage V_{OC} for the hydrogen plasma passivation of the solid phase crystallized silicon thin film solar cells treated at the temperature of 600 °C, duration of 15 minutes, hydrogen pressure of 500 Pa, electrode distance of 20 mm, bias voltage kept constant during the cooling phase of the hydrogenation process.

7.3.6 Electrode Distance

The same electrode distance of 20 mm was used for all realized hydrogen plasma passivation treatments, if not specified. However, it should be noticed that this distance is not a real distance of electrodes, it is just a position of a pointer on the corresponding meter. Nevertheless, this pointer position can be determined with a relatively high level of accuracy and it is always meant when electrode distance or gap is mentioned in this work, if not specified. Around 30 mm have to be added to the position of the pointer to obtain a real electrode gap.

There is a clear dependence of V_{OC} results on the applied electrode distance shown in Fig. 7.11. Distance of 20 mm brought the best result at the used processing conditions.

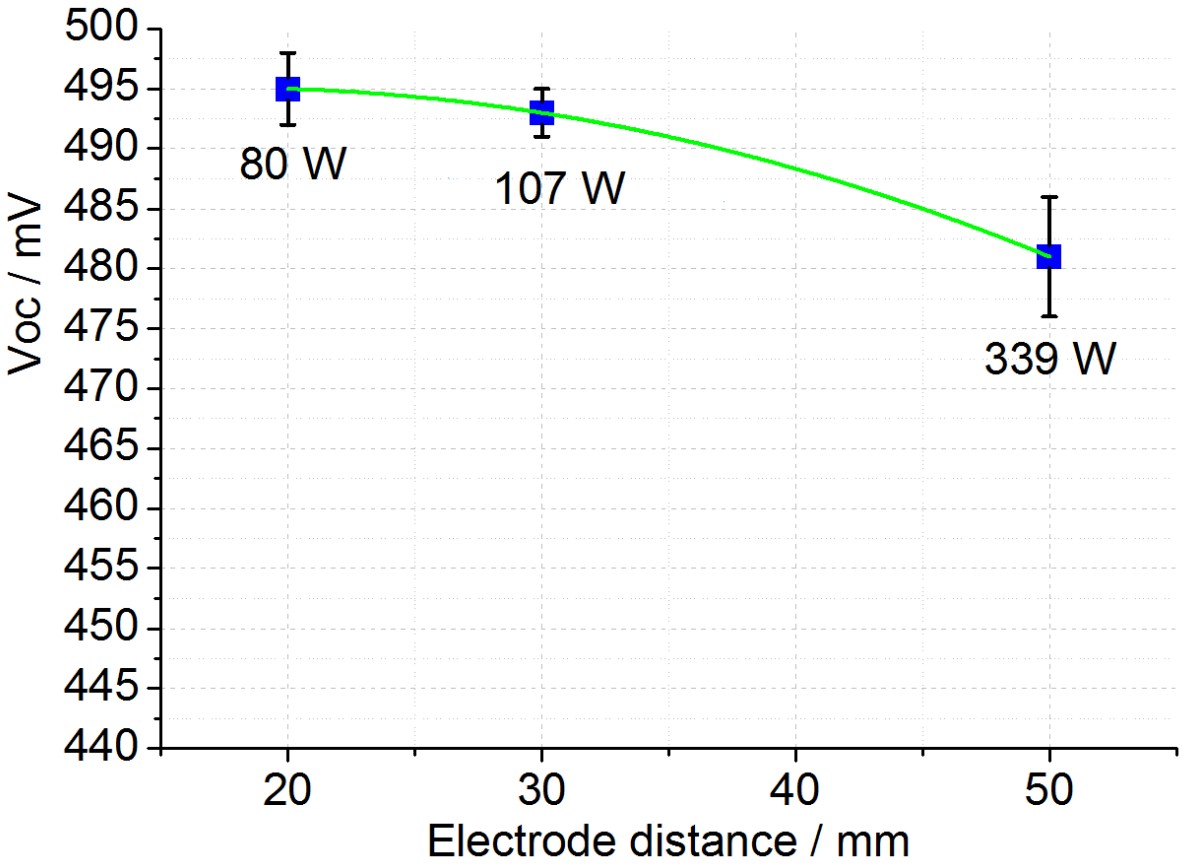

Fig. 7.11. Electrode distance dependence of the open-circuit voltage V_{OC} for the hydrogen plasma passivation of the solid phase crystallized silicon thin film solar cells treated at the temperature of 600 °C, duration of 15 minutes, hydrogen pressure of 500 Pa, bias voltage of 10 V kept constant also during the cooling phase of the hydrogenation process.

7.3.7 Summary – Optimum Hydrogenation Parameters for SPC Poly-Si

Optimum plasma hydrogenation parameters can be determined on the base of the performed investigation presented in the previous subchapters. The appropriate plasma switch off temperature of around 340 °C was confirmed as also the treatment temperature of around 600 °C, duration of 15-20 minutes, and the electrode distance of 20 mm.

Nevertheless, experiments dealing with hydrogen pressure revealed that better results can be achieved at pressures higher than the commonly used 100 Pa. The hydrogen pressures of 300, 500 or even 1,000 Pa seem to be more suitable. Moreover, role of a commonly omitted parameter bias voltage V_{bias} was explored and it was

revealed that keeping this parameter constant not only during the phase of a constant sample temperature but also during the cooling phase brings the best passivation improvements in broad hydrogen pressure and power ranges. Exact value of V_{bias} is not so important at least in the tested voltage range from 8 to 13 V.

7.3.8 Discussion – Plasma Hydrogenation of SPC Solar Cells

According to the above presented results, plasma hydrogenation significantly improves electrical quality of solid phase crystallized polycrystalline silicon. The temperature high enough is one of the key passivation parameters. This temperature is necessary mainly to diffuse hydrogen throughout the whole silicon layer. Hydrogen pressure represents amount of hydrogen molecules in the chamber available for generation of hydrogen radicals. Nevertheless, this parameter is closely connected with the plasma power and the gap between the electrodes. All of them significantly impact plasma ignition and control the transport of hydrogen to the silicon surface where a hydrogen reservoir is created. Hydrogen radicals saturate silicon dangling bonds on the silicon surface or diffuse into the silicon bulk to saturate electrically active dangling bonds of silicon or impurities at the grain boundaries and dislocations inside the grains.

The plasma hydrogenation process seems to be quite clear, but there are still some details that need to be explained. One of them is a connection between the passivation effect of hydrogen and plasma chemistry. Nevertheless, this task requires good knowledge of both semiconductor physics and also plasma chemistry.

Another challenging task is a role of commonly omitted hydrogenation parameter, accelerating voltage V_{acc} or bias voltage V_{bias}. Our results suggest a considerable importance of keeping the voltage constant not only at the temperature plateau phase but also at the cooling phase. While the limit of open-circuit voltage of 500 mV for SPC solar cells was not exceeded, the best results were achieved just by keeping V_{bias} constant. This finding could be valuable information for passivation of other materials. Possible explanation of this phenomenon is that keeping V_{bias} constant even during the cooling phase ensures a constant flow of hydrogen ions to the silicon surface. It is well known that the plasma must ignite up to around 350°C to avoid hydrogen out-diffusion from silicon [34], [46] and I would like to add the suggestion to keep V_{bias} constant during the cooling phase by increasing plasma power to keep the reservoir of hydrogen at the silicon surface full.

The plasma hydrogenation was in the frame of this work always performed as a closed system, there was no exchange of hydrogen in the chamber (no hydrogen input or output) during the process. Although it is rather unique arrangement and flow systems are more common to keep the treatment conditions constant during the whole process, our results are very close to the generally accepted passivation limit of 500 mV for the SPC solar cells. While the best published V_{OC} of 492 mV officially measured at the Fraunhofer Institute was achieved in a flow hydrogenation system [16], our best result of 497 mV measured at the Helmholtz-Zentrum Berlin comes from the treatment carried out as a closed system. It seems that the hydrogenation process can give good results in both configurations as a flow and also a closed system. The explanation could be based on the assumption that the used pressure in the magnitude of 100 Pa represents sufficient source of hydrogen needed for the passivation and no further input is necessary.

7.4 Hydrogen Plasma Passivation of LPC Si Thin Film Solar Cells

Parameters optimal for plasma hydrogenation of the SPC Si solar cells were applied to liquid phase crystallized (LPC) silicon. It is questionable whether these two materials can be meaningfully compared. Nevertheless, the tested hydrogenation parameters connected with the best achieved V_{OC} results for the SPC Si solar cells could be useful at least as a starting point at searching for optimum plasma hydrogenation parameters for LPC Si.

The LPC Si solar cells of the concept described in Fig. 5.6 invented at the Helmholtz-Zentrum Berlin was used for optimization of the plasma hydrogenation process for LPC silicon. The temperatures of 550, 600, 650°C at 300 Pa and hydrogen pressures of 100, 200, 300 Pa at 600°C were tested. Other parameters of the process were the plasma exposure time of 15 minutes, plasma power of 50 W with radio frequency of 13.56 MHz, and the gap between electrodes of 20 mm.

Success of the passivation process was determined on the basis of Suns-V_{OC} method, sun simulator and EQE measurements. Since electrical quality of the interface SiO_2/LPC Si represents a delicate region for the LPC Si thin film solar cells, the samples were analysed from both sides: from the substrate side to measure the solar cell parameters without reflection of the glass substrate and from the superstrate side to determine how the used preparation procedures (PECVD/PVD for silicon deposition, EBC/LC for silicon crystallization) impact solar cell parameters, e.g. recombination at the delicate interface.

Plasma hydrogenation resulted in a valuable increase of all solar cell parameters, e.g. V_{OC}, I_{SC}, and FF. Nevertheless, neither sample temperature variation nor the variation of hydrogen pressure brought any significant difference between the used manufacturing procedures for silicon deposition (PECVD or PVD) and silicon liquid phase crystallization (EBC or LC). Achieved open-circuit voltage V_{OC} and short-circuit current I_{SC} of the LPC Si solar cells passivated at 3 different temperatures compared with a non-passivated sample are presented in Fig. 7.15 and Fig. 7.16, respectively. Similar results were achieved also in the case of the hydrogen pressure variation.

Average increase of V_{OC} for LPC Si solar cells measured from the substrate side was from starting 535 mV to 570 mV, what means a relative increase of around 7 %. In the case of I_{SC}, the increase was from starting 21 mA/cm^2 to 22 mA/cm^2, i.e. a relative increase of around 5 %. Solar cell efficiency increased from around 7 % of the non-passivated sample to 10 %.

The relative improvement is not as high as in the case of SPC Si cells, but an average non-passivated LPC solar cell gives better results than an average passivated SPC cell. Moreover, there is a huge potential of further improvement for the LPC Si solar cells by an effective light trapping, optimization of the crystallization process and passivation of silicon/glass interface [102].

The LPC Si solar cells were measured by EQE from the substrate and superstrate side, see Fig. 7.17 and 7.18, respectively. A relevant improvement was achieved at the silicon/glass interface by the plasma hydrogen passivation. This region is assumed to be critical for the LPC Si solar cells due to a high concentration of defects and impurities. EQE measurements from the superstrate side uncovered a significant improvement of light absorption in a broad wavelength range, see Fig. 7.18. Higher absorption of short light wavelengths corresponds to an effective defect passivation at the silicon/glass interface and better absorption around the peak is attributed to a higher electrical quality of silicon bulk.

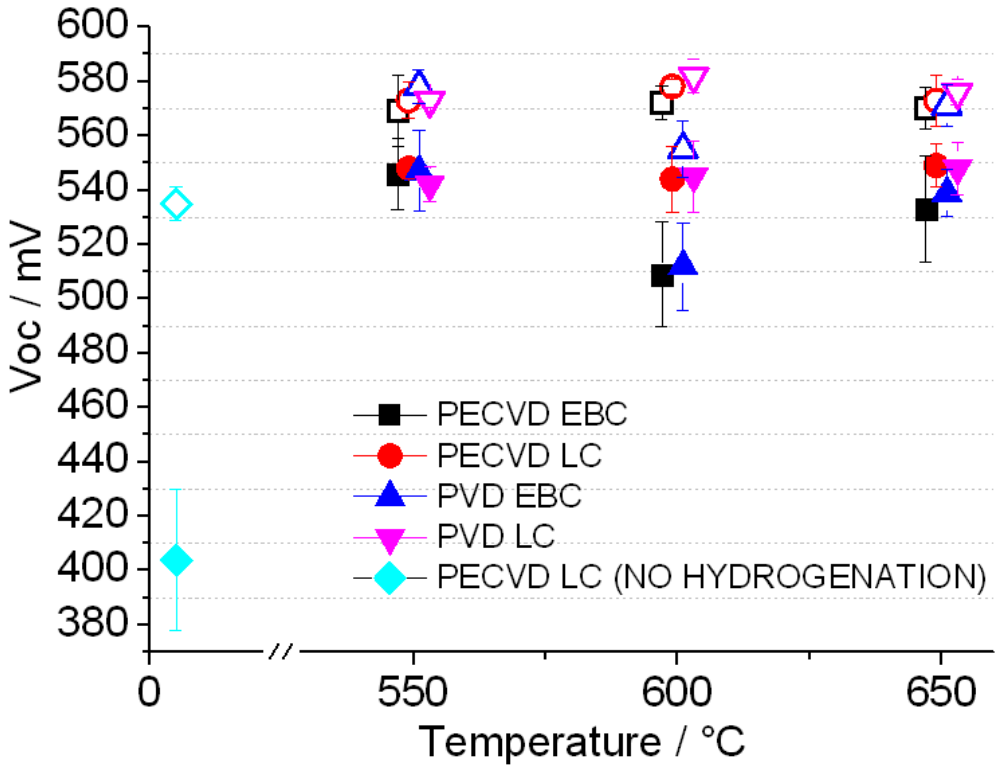

Fig. 7.15. Open-circuit voltage V_{OC} of the LPC Si solar cells measured from the substrate (empty symbols) and superstrate (solid symbols) sides after the hydrogen plasma passivation at the sample temperatures of 550, 600 and 650°C, plasma power of 50 W, duration of 15 minutes and the electrode gap of 20 mm. The SiO_x diffusion barrier was prepared either by plasma enhanced chemical vapour deposition (PECVD) or by physical vapour deposition (PVD), silicon absorber of the solar cells was crystallized either by laser beam (LC) or electron beam (EBC). The non-passivated solar cell (empty diamond for substrate side, solid diamond for superstrate side) prepared by PECVD and LC was used as a reference.

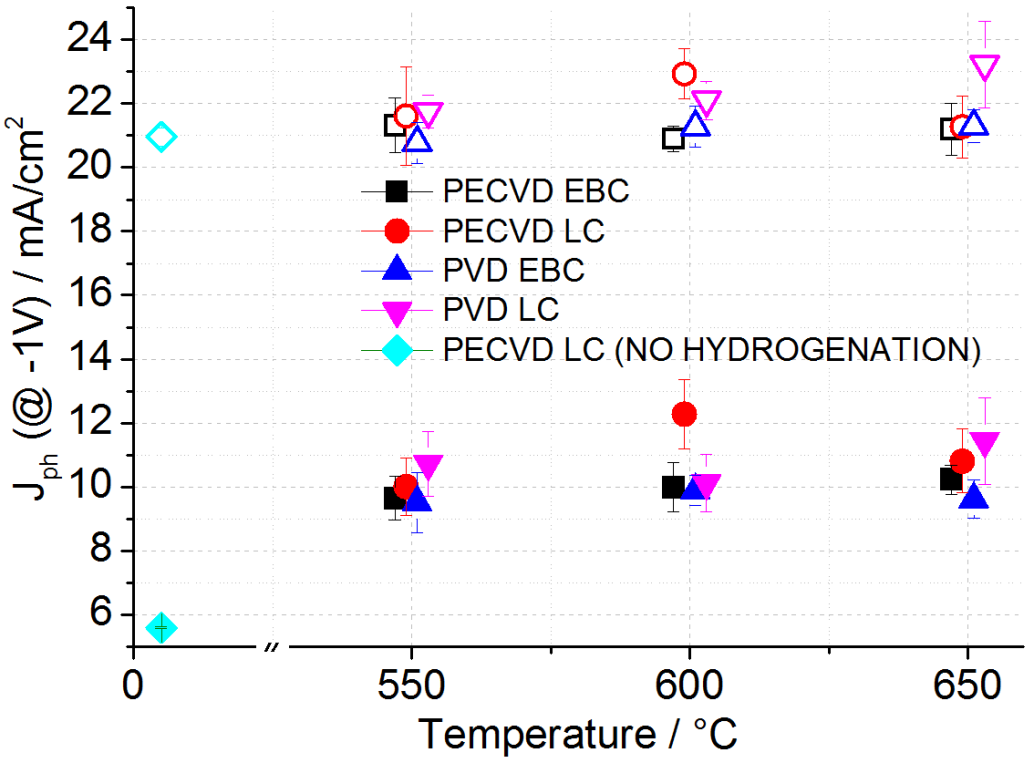

Fig. 7.16. Photogenerated current density J_{ph} at -1V of the LPC Si solar cells measured from the substrate (empty symbols) and superstrate (solid symbols) sides after the hydrogen plasma passivation at the sample temperatures of 550, 600 and 650°C, plasma power of 50 W, duration of 15 minutes and the electrode gap of 20 mm. The SiO_x diffusion barrier was prepared either by plasma enhanced chemical vapour deposition (PECVD) or by physical vapour deposition (PVD), absorber of the solar cells was crystallized either by laser beam (LC) or electron beam (EBC). The non-passivated solar cell (empty diamonds for substrate side, solid diamonds for superstrate side) prepared by PECVD and LC was used as a reference.

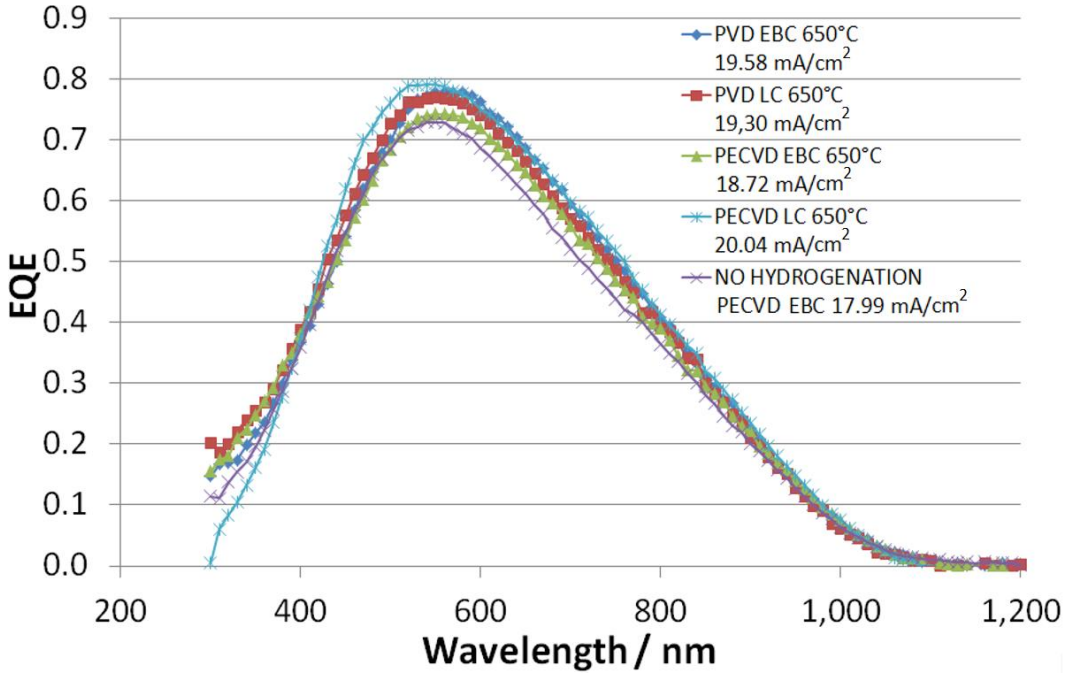

Fig. 7.17. Substrate side EQE measurements of the LPC Si solar cells passivated in the hydrogen plasma at the temperature of 650°C and hydrogen pressure of 300 Pa. The cells were manufactured in different ways - SiO_x diffusion barrier was prepared either by plasma enhanced chemical vapour deposition (PECVD) or by physical vapour deposition (PVD) and absorber of the solar cells was crystallized either by laser beam (LC) or electron beam (EBC).

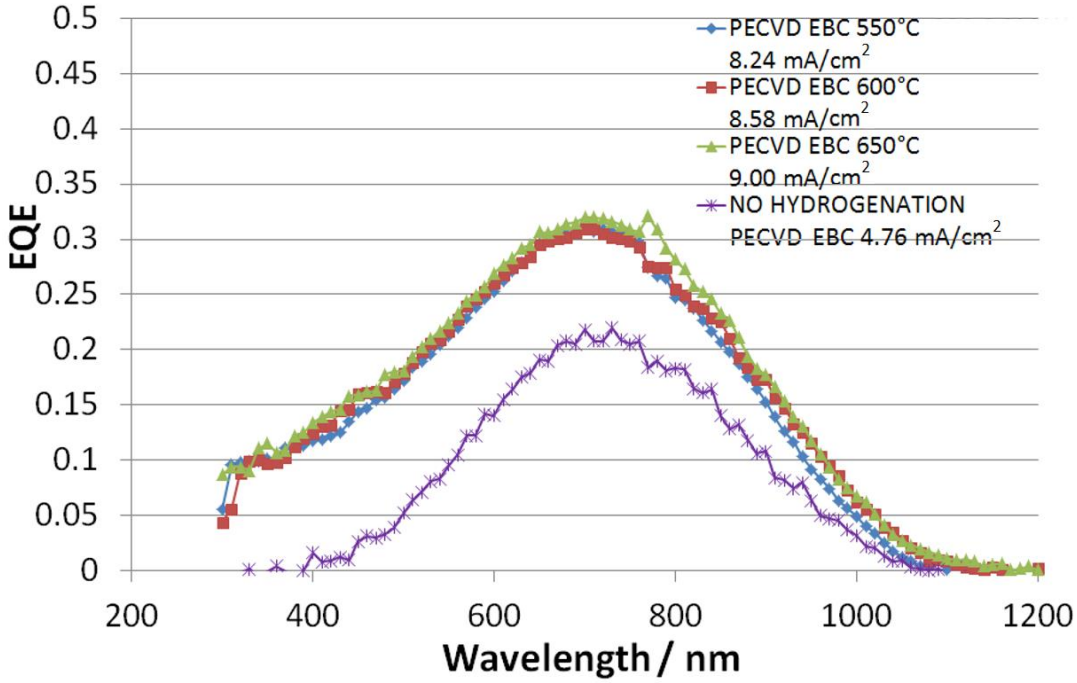

Fig. 7.18. Superstrate side EQE measurements of the LPC Si solar cells passivated in the hydrogen plasma at the temperature of 650°C and hydrogen pressure of 300 Pa. The cells were manufactured in different ways - SiO_x diffusion barrier was prepared either by plasma enhanced chemical vapour deposition (PECVD) or by physical vapour deposition (PVD) and absorber of the solar cells was crystallized either by laser beam (LC) or electron beam (EBC).

The plasma hydrogenation has definitely a positive effect on the LPC Si solar cells. Although the relative improvement of the solar cell parameters is not as significant as for the SPC Si solar cells, it is still reasonable to perform this manufacturing step to suppress recombination activity of silicon defects and impurities. They are not as abundant in LPC Si as in SPC Si, but they are still present and can significantly impact solar cell parameters.

7.5 Plasma Hydrogenation – Comparison of SPC and LPC Silicon

Various plasma hydrogenation parameters were tested to achieve the best passivation effect for both solid phase crystallized (SPC) and liquid phase crystallized (LPC) polycrystalline silicon thin film solar cells. While SPC silicon contains before passivation a significantly higher concentration of electrically active defects, e.g. dangling bonds at grain boundaries and dislocations inside grains, LPC silicon is material of higher electrical quality already after the crystallization procedure [18]. This observation can be demonstrated on the parameter commonly used to determine silicon electrical quality – open-circuit voltage V_{OC} of solar cells. It is typically around 220 mV in the case of the SPC Si solar cells [40] and around 535 mV for the LPC Si cells before passivation. These data express in other words the fact that before hydrogenation the SPC silicon contains significantly more defects than LPC Si. Optimization of the passivation process brought a relative improvement in V_{OC} of more than 120 % for SPC Si (from 220 mV to 497 mV), but only around 7 % for LPC Si (from 535 mV to 570 mV). Although the passivation effect of the plasma hydrogenation is more evident in the case of SPC Si, the problem is not in the passivation procedure. The experiments presented above confirmed the passivation limit for the hydrogenation of SPC Si to be around 500 mV, see also [40], corresponding to the density of dangling bonds at grain boundaries of 1×10^{16} cm^{-3} and dislocations inside grains of 1×10^{10} cm^{-2} [18]. Our investigation uncovered a high electrical quality of LPC Si that cannot be as significantly improved as in the case of SPC Si. The reason does not arise from a non-optimized passivation process, but from a low content of defects in LPC Si whose recombination activity can be suppressed and therefore silicon electrical quality (V_{OC}) can be further improved this way. Nevertheless, it is very encouraging that LPC silicon has such a high electrical quality even without plasma hydrogenation, much higher (535 mV) than SPC Si can ever achieve (500 mV). Experimental data and numerical simulations revealed that if density of Si dangling bonds at grain boundaries is larger than 4×10^{16} cm^{-3}, the maximum achievable V_{OC} is given by density of dislocations. The main difference between the maximum available SPC and LPC silicon electrical quality arises from the density of dislocations inside the grains and not from the density of grain boundaries (in other words size of the grains) [18]. LPC Si solar cells are able to achieve V_{OC} of 656 mV and efficiency of 11.5 % nowadays [103].

Further improvement of LPC Si solar cells is expected by optimization of a cell design, structure and preparation procedures, e.g. a light trapping system, N-type silicon absorber instead of P-type, crystallization process [51], [102], [103].

8 Synergetic Effect of Steam and Hydrogen Plasma on SPC Si

The passivation processes in water vapour or hydrogen plasma for SPC polycrystalline silicon solar cells brought significant improvements of crystalline silicon quality, but the passivation limit of around 500 mV [51] was not broken. A few SPC poly-Si samples were subsequently passivated in both steam and hydrogen plasma to investigate a possibility of synergetic effect of both media.

8.1 Water Vapour Followed by Hydrogen Plasma

A poly-Si thin film solar cell passivated in water vapour (350°C, 1 MPa, 2 hours) achieved V_{OC} = 345 mV (from the starting 214 mV). This sample was subsequently treated by hydrogen plasma at the Helmholtz-Zentrum Berlin at the temperature of 600°C and the hydrogen pressure of 250 Pa for 15 minutes. Final V_{OC} achieved the value of 455 mV. Same passivation conditions were used for another SPC Si sample passivated only in hydrogen plasma and its V_{OC} reached the value of around 480 mV, see Fig. 7.7.

The expectation that some defects are passivated in water vapour and a subsequent treatment in the hydrogen plasma can provide further independent improvement was not right. It seems that oxygen bonded to silicon dangling bonds after the water vapour passivation was out-diffused during the plasma hydrogenation and these defects together with others were deactivated by hydrogen.

It can be assumed that only some defects in SPC poly-Si can be passivated [113]. While a smaller part of these defects can be saturated by oxygen in the water vapour (the best V_{OC} = 360 mV), a significantly bigger part can be passivated in hydrogen plasma (the best V_{OC} = 497 mV). The question still remains whether the defects passivated by oxygen (annealing in water vapour) are the same as those saturated by hydrogen (annealing in hydrogen plasma) or these defect groups are totally independent.

8.2 Hydrogen Plasma Followed by Water Vapour

Some SPC Si samples were passivated in hydrogen plasma and subsequently in water vapour. While the annealing in hydrogen plasma (600°C, hydrogen pressure of 500 Pa, 5 minutes) brought a significant improvement, V_{OC} = 497 mV, the subsequent annealing in water vapour (450°C, steam pressure of 0.75 MPa) resulted in V_{OC} of 454 mV after 15 minutes, 428 mV after further 30 minutes, and 300 mV after further 60 minutes (totally 105 minutes of annealing).

The hydrogen out-diffusion during the treatment in water vapour seems to be the most probable explanation. Nevertheless, the reason why oxygen did not replace hydrogen on the positions of silicon dangling bonds and other defects is unknown. To explain this observation the previous passivation experiments realized in the mixture of hydrogen and water vapour can be helpful. According these investigations, the water vapour enriched with hydrogen gas did not bring better results than around 250 mV and the best H:O ratio in the passivation atmosphere is 2:1 like in H_2O. Hydrogen emitted from the poly-Si thin film could negatively impact the passivation atmosphere and prevent saturation of defects by oxygen.

9 SPC Silicon Thin Film Solar Cells – Plasma Hydrogenation vs. Water Vapour Passivation

In this chapter, comparison of two passivation processes, plasma hydrogenation and water vapour passivation, are presented. This comparison is based on the results coming from the experiments performed in the frame of this research work as well as from scientific publications. Solid phase crystallized (SPC) polycrystalline silicon solar cells were used as testing samples to understand principles and to find limits of both passivation approaches.

While the plasma hydrogenation process is relatively well known, annealing of silicon in the water vapour at temperatures below 500 °C is rather rare. The aim of the annealing is a suppression of the recombination centres at the surface and also in the silicon bulk by incorporation of passivating particles. Oxidation of the silicon surface and preparation of SiO_2 layer is very probable during the treatment, but it is not the aim of the water vapour passivation process as it was realized and investigated in this work.

From the point of view of processes taking place in silicon during the passivation, the plasma hydrogenation needs to take into account only hydrogen. Some details about the passivation mechanisms in hydrogen plasma are still not completely clear, but there is only hydrogen that can stick to the silicon dangling bonds creating deep levels in silicon band gap and deactivate their recombination activity by shifting these levels out the band gap.

In the case of water vapour, more possible passivation mechanisms need to be considered. Two elements, hydrogen and oxygen in H_2O molecules, are present in the passivation chamber. There are many ways how the passivation process can run, what particles can saturate silicon dangling bonds and what way.

Some processing conditions of the plasma hydrogenation and water vapour passivation are similar and others are completely different. Let's go through the particular key parameters of both processes and compare them:

a) temperature

Both passivation processes, the plasma hydrogenation (PH) and water vapour passivation (WVP), require an elevated temperature. While it is around 600 °C in the case of PH, optimum WVP temperature is lower in the range from 350 °C to 450 °C depending on other treatment conditions. Passivation processes run also at lower temperatures, but a lower treatment temperature means a longer exposure time to achieve same passivation effect. The last statement is restricted to the investigated passivation temperature range. At too low temperatures, passivation is not activated (either due to diffusion or reactions activation energy), at too high temperatures new defects are generated while no more defects can be passivated. Effect of the temperature is relatively clear in the case of both passivation approaches. Appropriate temperature is needed to enable in-diffusion of passivating particles into silicon, their movement in the silicon bulk throughout whole silicon layer at both passivation processes. The elevated temperature is additionally necessary also for decomposition of H_2O molecules at WVP. Moreover, it is well known that diffusivity of hydrogen and oxygen can be significantly affected by doping level and also concentration of defects [35]–[38], [114].

b) pressure

PH and WVP are completely different processes from the pressure point of view. While optimum hydrogen pressure for PH is in the order of several 100s Pa, the best passivation effect was achieved in the case of WVP at the steam pressure of around 1 MPa. Steam pressure can be interpreted as a density of particles available for the passivation process. PH is a more complicate process due to presence of the plasma because in this case plasma chemistry has to be taken into account and the final passivation effect depends on several other parameters that are closely connected, e.g. electrode gap, plasma power, accelerating voltage. Consequently, the connection between hydrogen pressure and amount of hydrogen that is really available for incorporation into silicon does not have to be as straightforward as in the case of the treatment in water vapour.

c) exposure time

While the optimum treatment duration is around 100 minutes for WVP, it is around 15 minutes for PH, or even about 4 minutes in some cases [40], [52]. Possible explanation of such a long exposure time is that while PH is just a one step process and hydrogen radicals are extremely movable and reactive particles, WVP is assumed to be at least a two-step process. Initially, hydration of Si dangling bonds by –OH takes place and subsequently more stable Si-O-Si bonds are formed while hydrogen is released. This explanation is based on analogy with the interaction of water vapour with SiO_2 [30], [66], [67], [84].

10 Optical Pump Transient Terahertz Probe Spectroscopy to Study SPC Poly-Si Solar Cells

SPC polycrystalline silicon thin film contains grains with a grain size of up to around μm. However, the lifetime of photogenerated carriers is in the range of ns due to a low electrical quality. From this point of view it is a nanostructured material and ultrafast processes are a key issue in this case.

Nevertheless, measurement of ns-long minority carrier lifetime is a challenging task. For poly-Si thin film solar cells it is commonly measured indirectly [14]. Lifetime is extracted from fitting of solar cell's external quantum efficiency simultaneously with optical reflectance.

Microwave decay measurements are also often used for silicon quality characterization [115]. They are sensitive to free electrons, they are contactless and non-destructive. However, microwave measuring is suitable rather for wafer-based solar cells than for thin films, nanoobjects or nanostructured materials. The reasons are: a) lifetime of polycrystalline and nanocrystalline materials of ≈ ns is too short therefore appropriate probing pulses in the range of ≈ ps are desired, b) amplitude of electrons oscillation when interacting with microwaves is too large to investigate ultrafast processes inside grains of nano- and polycrystalline materials with the typical grain size of 100 nm – 1 μm, c) amount of material in nanoobjects and thin films (with less than a few μm thickness) is not enough to observe strong enough signal.

Optical pump transient terahertz probe spectroscopy offers a *direct* measurement of ns-long lifetimes according to our experiments and it is a *contact-free* characterization technique suitable for investigation of ultrafast processes in materials with a complicate structure (e.g. nanowires). Pulses of terahertz waves are short enough (≈ ps) to measure ns-long lifetimes, they are sensitive to free electrons and the amplitude of electron oscillations after interaction with terahertz waves is small enough to analyse ultrafast processes inside grains of a nanostructured material.

SPC poly-Si solar cells of different silicon electrical quality expressed as open-circuit voltage V_{OC} at the light intensity of 1 000 W/m^2 were analysed by optical pump transient terahertz probe spectroscopy.

Two series of SPC poly-Si samples with different electrical quality were prepared by treatment in hydrogen plasma under various processing conditions. In the case of the temperature series, the temperature of plasma switch off was varied, see Fig. 7.4. The pressure series involved 4 samples treated by the hydrogen plasma at hydrogen pressures of 125, 150, 200, 300 Pa, see Fig. 7.7. All other processing parameters were kept constant.

It should be underlined that the treatment in hydrogen plasma changes only electrical quality of silicon and all other sample properties remain unchanged. The samples were measured by Suns-V_{OC} method and subsequently transferred from the borosilicate glass substrate onto a Scotch® Crystal Tape. The reason for this was a low transparency of the glass substrate for terahertz waves. To transfer the sample it was stuck to the tape from the top side (p^+ Si film) and the glass substrate was subsequently removed by etching in 50% hydrofluoric acid (room temperature, 12 hours). The transferring procedure was invented at the Helmholtz-Zentrum Berlin.

Terahertz spectroscopy uses short optical pulses (10-100 fs) to photogenerate free charge carriers in a semiconductor and to analyse the changed photoconductivity by terahertz (THz) waves. Lifetime of charge carriers or decay rate can be evaluated from the changed photoconductivity measured directly after the photogeneration.

Setup for transient THz probe spectroscopy [116] displayed in Fig. 10.1 was used for all measurements presented in this work. The setup consists of 3 lines: a) optical pump delay line, b) line of THz probe and c) THz gating delay line.

The optical pump delay line with a laser beam (Ti:sapphire laser amplifier, Spitfire ACE, 800 nm central wavelength, 40 fs pulse length, 1 mJ pulse energy, 5 kHz repetition rate) was used to photogenerate free charge carriers in the sample. The photogeneration is here way how to characterize electrical quality of an investigated material expressed as a lifetime of charge carriers or in other words a decay rate of photoconductivity measured after an optical pulse. A higher concentration of trapping centres, e.g. defects and impurities, means a shorter lifetime.

The probe line consists of a Ti:sapphire laser amplifier emitting the THz probe beam used for investigation of the sample. A pump-probe delay between the laser beam and THz probe can be applied to study the dynamic conductivity measurements (the maximum pump-probe delay for the presented setup is 650 ps).

The THz gating delay line was used for sampling of the THz probe wave.

The whole THz part of the setup (THz pulse generator 1-mm-thick (110)-oriented ZnTe crystals, THz probing wave, sensor) was located in a hermetic box with appropriate vacuum to avoid absorption of THz radiation by water vapour.

The transient signal can be understood as a photoconductivity or a concentration of photogenerated charge carriers decreasing in time due to trapping processes at defects. Lifetime of charge carriers can be determined by fitting the decay. Electrical quality of silicon can be characterized by its lifetime, therefore the non-passivated sample has a faster decrease of the transient signal than the passivated one, Fig. 10.2.

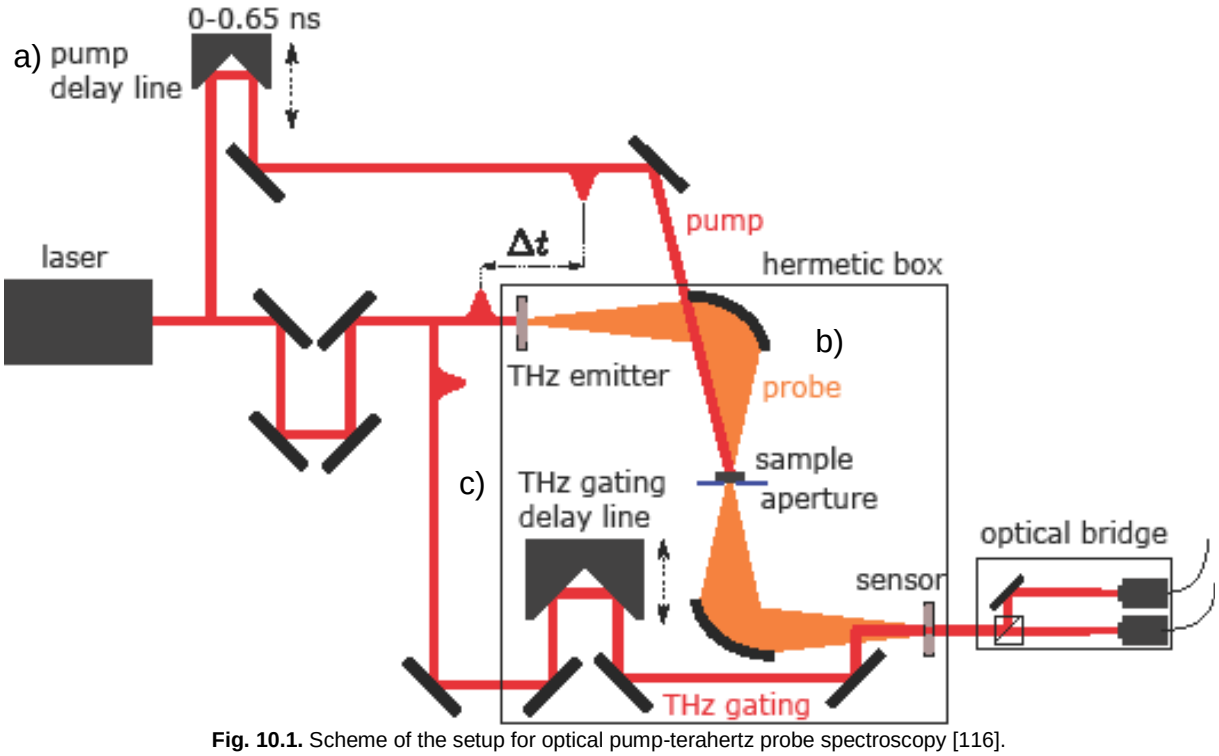

Fig. 10.1. Scheme of the setup for optical pump-terahertz probe spectroscopy [116].

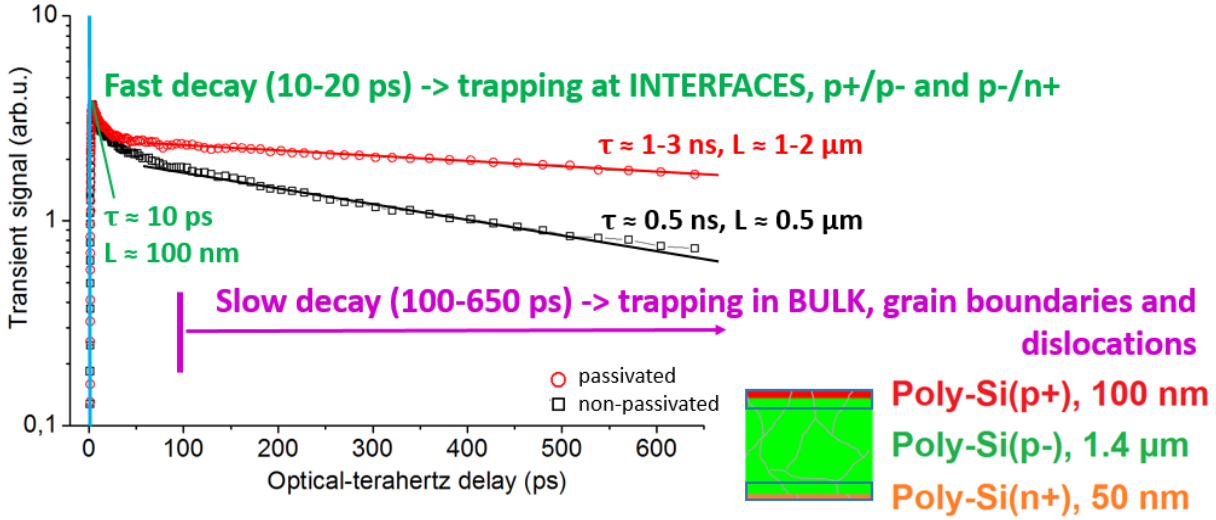

Fig. 10.2. Transient terahertz signal as a function of the optical-terahertz delay for non-passivated (black squares) and passivated (red circles) samples. 40-fs-long optical pulse (blue line) was used for photogeneration.

For both passivated and non-passivated samples, the measured transient exponential decay consisted of two components: a) fast decay and b) slow decay. The fast decay occurring in 10-20 ps range is according to our measurements connected with trapping processes at electrically active defects of p+/p- and p-/n+ interfaces. Lifetime of charge carriers was around 10 ps and diffusion length of around 100 nm (black frames around the interfaces display area participating in the trapping processes connected with the fast decay, see Fig. 10.2). The fast decay was similar for both passivated and non-passivated samples. The second component of the transient, the slow decay, occurred in the range of 100-650 ps and it was assigned to trapping processes in bulk (layer p-), at grain boundaries and dislocation located inside grains. Lifetime and diffusion length of a non-passivated sample was around 0.5 ns and 0.5 µm, respectively. For the best passivated sample, it was 1-3 ns and 1-2 µm.

While the fast decay was assigned to trapping processes at the interfaces, the slow one was connected with trapping in bulk. There are more evidences supporting this assignment: a) the amplitude of the fast decay was larger than of the slow one, b) both fast and slow decay components were observed for two different light intensities corresponding with two initial photogenerated carrier concentrations of 1.3×10^{16} cm^{-3} and 4×10^{16} cm^{-3}. Moreover, the amplitude of the fast decay scaled linearly with the applied light intensity. On the base of above mentioned, we can exclude theory that the fast decay is related to electrons and the slow one to holes. Mobility of holes is in general smaller than of electrons, therefore amplitudes in this case would be vice versa. Presence of both components for different light intensities excludes also the theory of two competing electron trapping channels, because the slower component would occur only after saturation of defects responsible for the fast decay whose amplitude scaled linearly with the applied light intensity. The most probable explanation of the observed results seems to be that these two components correspond to spatially separated parts of the sample, i.e. the bulk and the interfaces. While the smaller amplitude of the fast decay represents a smaller amount of the charge carriers photogenerated at the interfaces, most of electrons are photogenerated in bulk expressed by the larger amplitude of the fast decay.

The fast decay was similar for non-passivated and passivated poly-Si solar cells and it seems that recombination activity of the interfaces is suppressed only slightly by hydrogen plasma passivation. For the slow decay, a significant improvement of lifetime was observed indicating a positive impact of the passivation procedure.

In Fig. 10.3, there is a decay rate of photoconductivity measured by optical pump transient terahertz probe spectroscopy as a function of solar cell's open-circuit voltage V_{OC} that is often used to express silicon electrical quality. Since there is a correlation between the measured terahertz lifetime and V_{OC}, it can be concluded that optical pump transient terahertz probe spectroscopy is a useful tool to characterize silicon electrical quality as V_{OC} does.

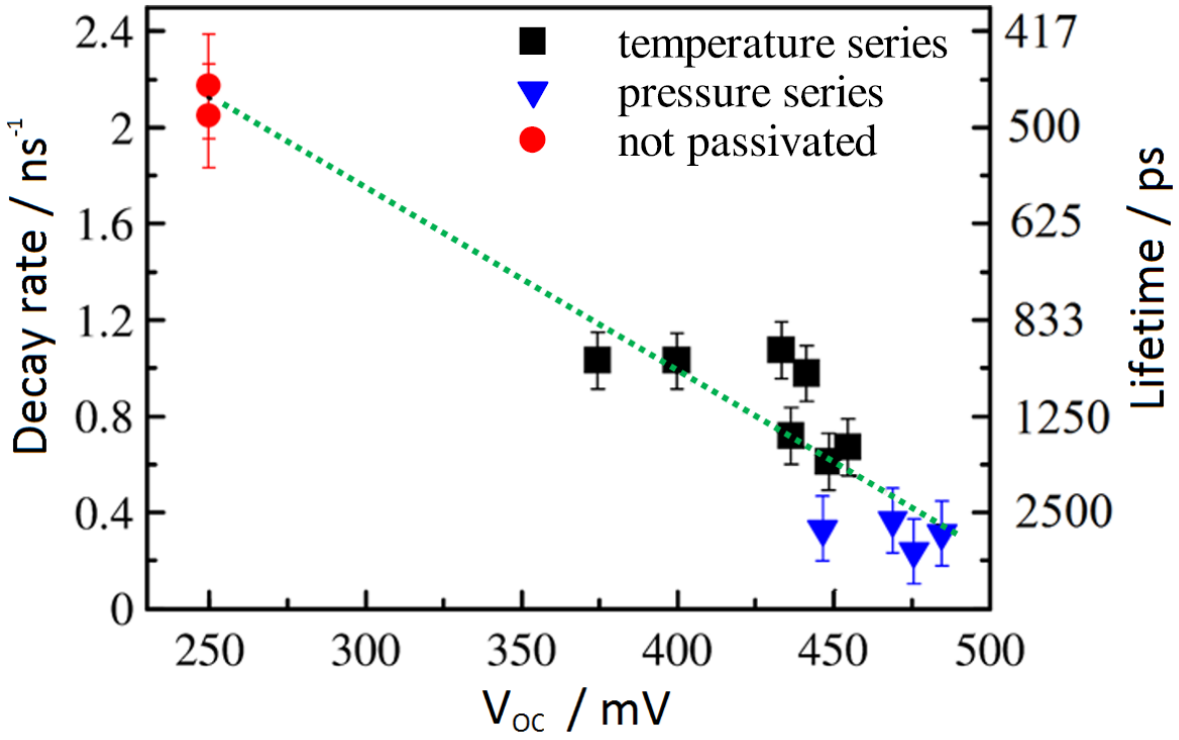

Fig. 10.3. Lifetime of charge carriers in thin film polycrystalline Si solar cells for temperature (black squares) and pressure (blue triangles) series as a function of the open-circuit voltage V_{OC}. Non-passivated samples (red points) were used as references [116].

This correlation deserves attention because each measuring technique characterizes the solar cell at totally different regimes. Optical pump-terahertz probe spectroscopy measures the trapping rate of photogenerated carriers in the p^- absorber layer of the solar cell that is in a highly non-equilibrium regime in the time range of 0-650 ps after photogeneration (with 40-fs-long light pulse). Fermi level is split into two quasi-Fermi levels and there was no time to build V_{OC} yet, see Fig. 10.4 b). In contrast to this, Suns-V_{OC} method analyses V_{OC} of the cell at a quasi-steady state. Since a few ms-long light flash is used, photogeneration and recombination processes are in equilibrium. There is enough time to redistribute photogenerated charge carriers by the space charge region (electrons into n+ layer, holes into p+ layer) and V_{OC} can be measured, see Fig. 10.4 c). Although these two measuring techniques characterize the SPC poly-Si solar cells in totally different states, there is the correlation between the lifetime of charge carriers and V_{OC}.

The lifetime of 1-3 ns for the passivated poly-Si measured by THz spectroscopy is in agreement with the lifetime of ≈ 1 ns presented by Mr. Wong [14].

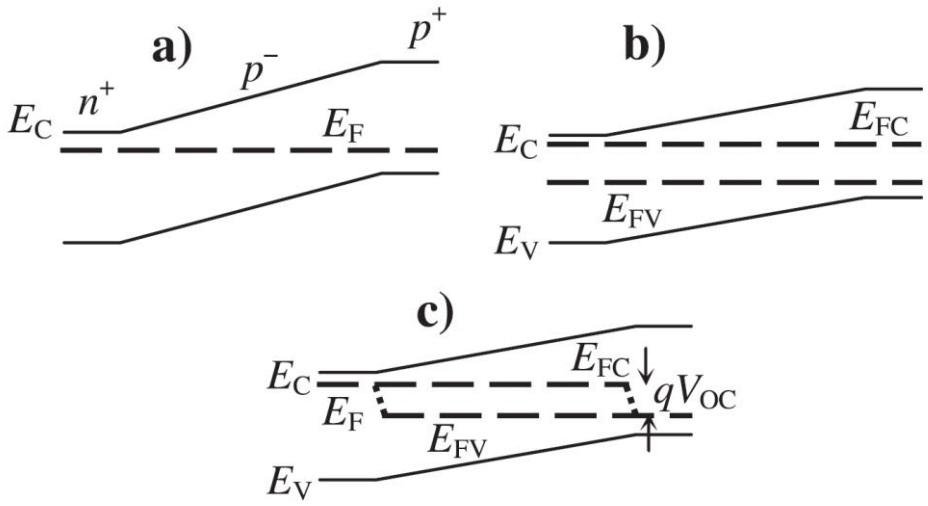

Fig. 10.4. Energy band diagram of a poly-Si solar cell in different regimes: a) equilibrium state without illumination, (b) ultrafast regime immediately after photoexcitation (before the build-up of V_{OC}), (c) in steady-state under continuous illumination [116].

It should be mentioned that all the measured samples showed a Drude-like dynamical terahertz conductivity, in other words the photogenerated charge carriers analysed by terahertz pulses were completely delocalized, mobile in silicon band gap, see Fig. 10.5. The measured mobility was around 360 $cm^2V^{-1}s^{-1}$ and the momentum scattering time reached 60 fs for the passivated sample (600°C, H_2 pressure of 100 Pa, 15 minutes) and 330 $cm^2V^{-1}s^{-1}$ and 57 fs for the non-passivated sample. These values are around 4 times lower than those of monocrystalline Si (1450 $cm^2V^{-1}s^{-1}$).

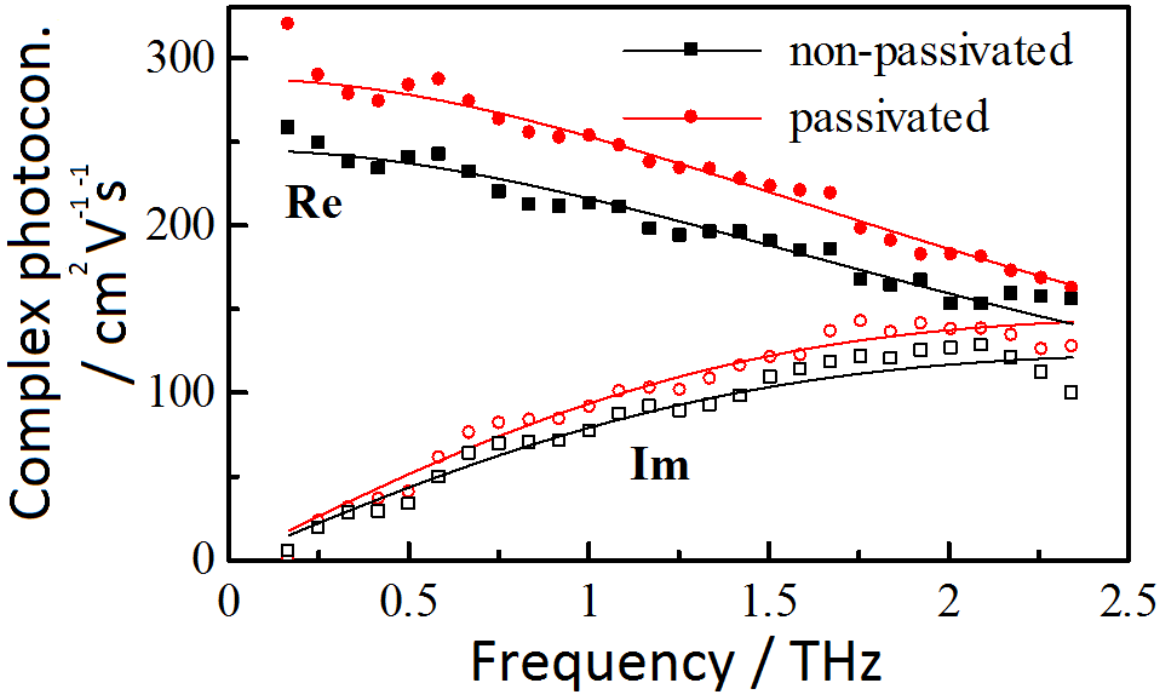

Fig. 10.5. Spectra of normalized complex photoconductivity of a passivated sample (600 °C, H_2 pressure of 100 Pa, 15 minutes) and a non-passivated sample measured at the time delay 10 ps after photoexcitation and at the pump fluence 4×10^{16} photons/cm^2. Symbols: experimental data, lines: fits by the Drude model [116].

The results of SPC Si thin film solar cells characterized by terahertz spectroscopy were presented at the Conference of the European Research Material Society in Lille, France, 2016 and published in the Applied Physics Letters [116].

11 Conclusions

Solid phase crystallized (SPC) silicon thin film solar cells were annealed in hydrogen plasma and in water vapour at various processing conditions, e.g. temperature, pressure, exposure time. Success of the passivation was determined mainly by open-circuit voltage V_{OC} measured by Suns-V_{OC} method. This parameter is commonly used in a photovoltaic industry as a qualitative parameter of silicon. Structure of the liquid phase crystallized (LPC) Si solar cells with metallization allowed us to measure them also by a sun simulator and EQE.

Experiments revealed a significant role of temperature in the case of both used passivation techniques. Optimum passivation conditions for the water vapour passivation were: sample temperature of 350-450 °C, steam pressure of 0.75-1.0 MPa and exposure time of around 100 minutes with the best achieved V_{OC} = 360 mV (from the starting 220 mV). Passivation mechanism was described and discussed. The created model of the passivation in water vapour was based on the experimental data presented in this work and also on review of scientific literature.

During optimization of the plasma hydrogenation for SPC Si, the processing temperature of 600 °C and the distance between electrodes of 20 mm were confirmed to be optimum, but higher hydrogen pressure (300-1,000 Pa) and longer exposure time (15-20 minutes) were suggested in comparison with commonly used conditions. Moreover, a role of usually omitted parameter, bias voltage V_{bias}, was investigated and discussed. The requirement to keep this parameter constant during the whole period of plasma ignition was presented. Since all the plasma hydrogenation experiments were carried out as a closed system and the V_{OC} of 497 mV was achieved (close to limit of SPC Si), the generally accepted necessity to run the hydrogenation process with a hydrogen flux was called into question.

Terahertz spectroscopy appeared to be a useful contactless tool for inspecting the local photoconductivity of solar cells including, in particular, various nanostructured schemes.

12 Contributions of the Thesis

To summarize contributions of this work in the field of plasma hydrogenation and water vapour passivation of polycrystalline thin films and solar cells, I would like to mention the optimized parameters of the plasma hydrogenation process, hydrogen pressure and exposure time, but mainly the necessity to keep V_{bias} constant during the whole process including also the cooling phase. In my opinion, the observation that the plasma hydrogenation process realized as a closed system can bring at least as good results as an open one also deserves an appropriate attention.

Furthermore, a clear correlation between SPC Si solar cell's V_{OC} measured by Suns-V_{OC} method and the charge carrier lifetime detected by optical pump transient terahertz probe spectroscopy was observed. On the basis of these measurements, terahertz spectroscopy has a huge potential as a characterization technique for electronic inspection of ultrafast processes and particularly *direct* lifetime measurements of nanostructured materials and nanoobjects with additional advantage that the technique is contact-free. The results were presented at the Conference of the European Research Material Society in Lille, France, 2016 and published in the Applied Physics Letters [116].

In the case of the water vapour passivation, determination of optimum passivation conditions should be mentioned. The passivation chamber of my own design and construction enables independent regulation of sample temperature and steam pressure. This configuration is relatively rare and it allows experiments that are not possible in common systems operated as a simple closed chamber, where sample temperature and steam pressure are connected according to the liquid-vapour curve of the water phase diagram. There are also experiments with different media (hydrogen gas, boiling 30% hydrogen peroxide) carried out at various conditions which brought results enabling to understand mechanisms of the water vapour passivation more in detail. A model of the water vapour passivation process was created. The results of were presented at several conferences, for instance at the 26th International Conference on Amorphous and Nanocrystalline Semiconductors in Aachen, Germany, 2015 and published in the Physica Status Solidi A [108] and Acta Polytechnica [112].

Finally, I would like to summarize my author's share on this dissertation. Most of the passivation runs in hydrogen plasma (at the Helmholtz-Zentrum Berlin) and in water vapour (at the Institute of Physics in Prague) were realized by myself as well as the plan of the experiments and their evaluation. The model of the water vapour passivation process represents my own interpretation of the measured results and the reviewed scientific literature. The transfer of the SPC Si thin films from the glass substrate onto tape for the terahertz spectroscopy measurements was realized by myself and I participated in the measurements and results interpretation. I designed and constructed the chamber for the water vapour passivation and also the sample contacting system for the Suns-V_{OC} method.

13 Outlook

Material quality improvement and characterization is and most likely will remain a crucial point of semiconductor production (e.g. in microelectronics, photovoltaics) and also of research and application of nanostructures and nanoobjects. In this context effective low cost passivation approaches together with useful contact-free characterization techniques, e.g. optical pump transient terahertz probe spectroscopy, can find here appropriate applications.

Passivation in water vapour still offers undiscovered fields for investigation like more extreme testing conditions (temperature and pressure) or combinations of different chemicals.

Moreover annealing in water vapour offers various ways of utilization. Beside semiconductor passivation there are also metal assisted etching [117] and potentially also growth purposes in nanoscale range.

While hydrogen plasma brings a significant relative improvement of V_{OC} for SPC Si (from 220 mV to around 500 mV), LPC silicon benefits less (from 535 mV to 629 mV [103]) from the passivation procedure. The reason is a high electrical quality of LPC Si already after the crystallization. Nevertheless, the treatment in hydrogen plasma remains an important manufacturing step. To achieve a maximum passivation effect, hydrogenation should be optimized for LPC Si to take into account for instance a different thickness of the glass substrate that is 1 mm for LPC Si and 3 mm for the SPC Si samples and a different thickness of silicon layer (11 µm for LPC Si in comparison with 1.5 µm for SPC Si).

Nomenclature

Symbols

α	absorption coefficient
θ_0	initial light intensity
$\theta(x_L)$	light intensity at absorption depth
μ	charge carrier mobility
τ	charge carrier lifetime
η	solar cell efficiency
D	diffusion coefficient
E_g	band gap
I	electric current
I_0	reverse saturation current of a diode in dark
I_{01}	reverse saturation dark current flowing through the diode 1 in the frame of one or two diode model expecting a predominant recombination in Si bulk and at the surfaces
I_{02}	reverse saturation dark current flowing through the diode 2 in the frame of two diode model expecting a predominant recombination in depletion region of the junction
I_{ph}	photogenerated electric current
I_{MPP}	electric current at maximum power point
I_{SC}	short-circuit current
k	Boltzmann constant
L	diffusion length of a charge carrier
m	ideality factor of a diode
N_A	acceptor concentration
N_{aph}	number of photons absorbed in the solar cell
N_D	donor concentration
N_{ph}	number of photons illuminating the solar cell
n	electron concentration
P_{eh}	number of photogenerated electron-hole pairs
q	elementary charge (1.602×10^{-19} C)

R_s	series resistance
R_L	series resistance at an external circuit, so called load
R_{sh}	shunt resistance
T	thermodynamic temperature
V	electric voltage
V_{acc}	accelerating voltage between two electrodes
V_{bias}	voltage between an electrode and a sample
V_{br}	breakdown voltage
V_{MPP}	electric voltage at maximum power point
V_{OC}	open-circuit voltage
V_t	threshold voltage
V_{th}	thermoelectric voltage
W	width of the cell
x_L	absorption depth
x_N	width of the depletion region in N-doped silicon
x_P	width of the depletion region in P-doped silicon

Abbreviations

AM	atmospheric mass
AR	antireflection coating
a-Si:H	amorphous silicon
EBC	electron beam crystallization
EBE	electron beam evaporation
EQE	external quantum efficiency
FF	fill factor
FWHM	full width at half maximum
IQE	internal quantum efficiency
ITO	indium tin oxide
I-V	current-voltage characteristic
in-situ	measurement realized during a treatment

LC	laser crystallization
LPC	liquid phase crystallization
LPCSG	liquid phase crystallized silicon on glass
MPP	maximum power point
micro-Si	microcrystalline silicon
mono-Si	monocrystalline silicon
multi-Si	multicrystalline silicon
ONO	stack of 3 layers – SiO_x, SiN_x and SiO_x
PECVD	plasma enhanced chemical vapour deposition
PERL	passivated emitter and rear locally diffused solar cell
PH	plasma hydrogenation
PVD	physical vapour deposition
poly-Si	polycrystalline silicon
RCA	standard cleaning process of glass invented by the Radio Corporation of America
RTA	rapid thermal annealing
SPC	solid phase crystallization
SPC Si	solid phase crystallized silicon
Suns-V_{OC}	diagnostic method for solar cells based on detection of light intensity and corresponding solar cell’s open-circuit voltage
WVP	water vapour passivation

Acknowledgement

I would like to thank everyone who supported and encouraged me to create the thesis:

- RNDr. Antonin Fejfar, CSc. for the opportunity to work at the Institute of Physics, Academy of Sciences, CR, to be a part of his team, for his support, guidance throughout my thesis, valuable and inspiring comments and advices,
- Prof. Ing. Vitezslav Benda, CSc. for the opportunity to study, teach and understand photovoltaics more in detail, for his support and guidance throughout my thesis,
- Prof. Dr. Christiane Becker for the opportunity to realize a significant part of this thesis dealing with plasma hydrogenation at the Helmholtz-Zentrum Berlin, for her supportive approach, fruitful and helpful suggestions,
- Doc. RNDr. Petr Kuzel, Ph.D. and Mgr. Volodymyr Skoromets, Ph.D. for the optical pump transient terahertz probe spectroscopy measurements, data interpretation and fruitful discussions,
- Ing. Vlastimil Pic, Ph.D. for his inventiveness, electro-technical support at the building of Suns-V_{OC} method and fruitful discussions,
- Ing. Martin Muller for his kind support, patient help with deposition techniques and also valuable discussions,
- RNDr. Martin Ledinsky, Ph.D. and Ing. Kristina Ganzerova for Raman measurements and valuable suggestions
- Ing. The-ha Stuchlikova, CSc. for the FTIR measurements.

There are many other people who deserve my gratitude for their optimistic, helpful and supportive approach or ''just'' for their kind presence.

Many thanks to all my family and friends for their patient and unshakeable support.

Finally, I would like to acknowledge also the support through several grant projects:

- PolySiMode project, FP7-Energy-2009-1 Grant Agreement No. 240826 funded by European Commission,
- Czech Science Foundation projects 13- 12386S and 14-15357S,
- Laboratory of Nanostructructures and Nanomaterials (project LM2015087 funded by Ministry of Education, Youth and Sports) and
- projects for cooperation with Helmholtz Zentrum Berlin (DAAD-15-27 and M100101216).

List of Publications

Author share of all authors is equal in all publications.

1) Journal papers

P. Pikna, M. Muller, C. Becker, and A. Fejfar, Passivation effect of water vapour on thin film polycrystalline Si solar cells, Physica Status Solidi A, 1-7 (2016).

P. Pikna, V. Skoromets, C. Becker, A. Fejfar, and P. Kuzel, Thin film polycrystalline Si solar cells studied in transient regime by optical pump–terahertz probe spectroscopy, Applied Physics Letters 107, 233901–1-5 (2015).

A. Fejfar, M. Hyvl, A. Vetushka, P. Pikna, Z. Hajkova, M. Ledinsky, J. Kocka, P. Klapetek, A. Marek, A. Maskova, J. Vyskocil, J. Merkel, C. Becker, T. Itoh, S. Misra, M. Foldyna, L. Yu, P. Roca, I. Cabarrocas, Correlative microscopy of radial junction nanowire solar cells using nanoindent position markers, Solar Energy Materials and Solar Cells 135, 106-112 (2015). Citing papers (3).

2) Reviewed papers

P. Pikna, V. Pic, V. Benda, A. Fejfar, Annealing of polycrystalline thin film silicon solar cells in water vapour at sub-atmospheric pressures, Acta Polytechnica, ISSN 1210-2709 (Print) ISSN 1805-2363 (Online) (2014).

3) Conference contributions

P. Pikna, V. Skoromets, C. Becker, A. Fejfar, and P. Kuzel, Ultrafast processes in polycrystalline silicon solar cells, E-MRS spring meeting, Lille, France (2016).

F. Krizek, P. Pikna, A. Fejfar, Silver catalysed nanoscale silicon etching in water vapour, NANOCON, Brno, Czech Republic (2014).

P. Pikna, V. Benda, A. Fejfar, Water vapour passivation of polycrystalline silicon thin film solar cells at elevated steam pressures and temperatures, 11th IUVSTA School: International Summer School on Physics at Nanoscale, Devet Skal, Czech Republic (2014).

P. Pikna, A. Fejfar, V. Pic, M. Muller, M. Ledinsky, J. Kocka, Annealing of polycrystalline thin film silicon solar cells in water vapour at pressures below atmospheric pressure, 8th Czech Photovoltaic Conference, Brno, Czech Republic (2013).

P. Pikna, Suns-V_{OC} measuring system for in-situ observation of thin film poly-Si solar cells annealed in water vapour, 17th International Student Conference on Electrical Engineering POSTER 2013, Czech Technical University in Prague, ISBN: 978-80-01-05242-6 (2013).

P. Pikna, A. Fejfar, V. Pic, M. Muller, M. Ledinsky, A. Vetushka, J. Kocka, Water vapour passivation of poly-Si thin film solar cells, 27th European Photovoltaic Solar Energy Conference and Exhibition, Frankfurt, Germany, ISBN 3-936338-28-0 (2012).
P. Pikna, A. Fejfar, M. Muller, M. Ledinsky, A. Vetushka, J. Stuchlik, J. Kocka, Annealing of thin film polycrystalline silicon solar cells in water vapour, 7th Czech Photovoltaic Conference, Eds., Brno, Czech Republic, ISBN: 978-80-260-2232-9 (2012).

P. Pikna, A. Fejfar, Water vapour passivation (VVVP) vs. plasma passivation procedures, 10th IUVSTA School: International Summer School on Physics at Nanoscale, Devet Skal, Czech Republic, ISBN 978-80-260-0619-0 (2011).

P. Pikna, A. Fejfar, M. Ledinsky, A. Vetushka, J. Kocka, V. Benda, In-situ measuring system designed for improvement of poly-Si thin film solar cells, 4th International Forum on Multidisciplinary Education and Research for Energy Science, Hawaii, USA (2011).

P. Pikna, V. Benda, Advanced course of photovoltaics – Suns-V_{OC} method, 6th International Workshop on Teaching in Photovoltaics, Czech Technical University in Prague, ISBN 978-80-01-05022-4 (2012).

P. Pikna, V. Benda, Basic course of photovoltaics especially for Erasmus students, 6th International Workshop on Teaching in Photovoltaics, Czech Technical University in Prague, ISBN 978-80-01-05022-4 (2012).

P. Pikna, V. Benda, Passivation of thin film poly-Si solar cells in water vapour, 12th Traditional workshop of postgraduate students and young scientists, Technical University of Ostrava, ISBN 978-80-248-2664-6 (2012).

P. Pikna, V. Benda, Water vapor passivation of poly-Si thin film solar cells, 16th International Student Conference on Electrical Engineering POSTER 2012, Czech Technical University in Prague, ISBN 978-80-01-05043-9 (2012).

O. Kurik, P. Pikna, Diagnostic system for measurement of crystalline silicon solar cells, 15th International Student Conference on Electrical Engineering POSTER 2011, Czech Technical University in Prague, ISBN 978-80-01-04806-1 (2011).

Bibliography

[1] P. Gleick, Why don't we get our drinking water from the ocean by taking the salt out of seawater?, www.scientificamerican.com/article/why-dont-we-get-our-drinking-water-from-the-ocean/, accessed 27/05/2016.

[2] V. Quaschning, Regenerative Energiesysteme – Technologie - Berechnung - Simulation, Hanser Verlag, ISBN (Book): 978-3-446-44267-2, ISBN (E-Book): 978-3-446-44333-4 (2015).

[3] A. V. Shah, Editor, Thin-Film Silicon Solar Cells, CRC Press, ISBN 9781420066746 (2010).

[4] K. Mertens, Photovoltaik - Lehrbuch zu Grundlagen, Technologie und Praxis, Hanser Verlag, ISBN (Book): 978-3-446-42172-1, ISBN (E-Book): 978-3-446-42904-8 (2013).

[5] S. M. Sze, Physics of Semiconductor Devices, Wiley, ISBN: 978-0-471-14323-9 (2016).

[6] M. F. Thorpe and L. Tichy, Properties and Applications of Amorphous Materials, Springer Science & Business Media, ISBN: 978-0-7923-6811-3 (2012).

[7] P. P. Altermatt and G. Heiser, Development of a three-dimensional numerical model of grain boundaries in highly doped polycrystalline silicon and applications to solar cells, Journal of Applied Physics **91**, 4271–4274 (2002).

[8] L. Carnel, I. Gordon, K. Van Nieuwenhuysen, D. Van Gestel, G. Beaucarne, and J. Poortmans, Defect passivation in chemical vapour deposited fine-grained polycrystalline silicon by plasma hydrogenation, Thin Solid Films **487**, 147–151 (2005).

[9] L. Carnel, I. Gordon, D. Van Gestel, G. Beaucarne, J. Poortmans, and A. Stesmans, High open-circuit voltage values on fine-grained thin-film polysilicon solar cells, Journal of Applied Physics **100**, 63702 (2006).

[10] A. Abass, B. Maes, D. Van Gestel, K. Van Wichelen, and M. Burgelman, Effects of inhomogeneous grain size distribution in polycrystalline silicon solar cells, Energy Procedia **10**, 55–60 (2011).

[11] D. Van Gestel, M. J. Romero, I. Gordon, L. Carnel, J. D'Haen, G. Beaucarne, M. Al-Jassim, and J. Poortmans, Electrical activity of intragrain defects in polycrystalline silicon layers obtained by aluminum-induced crystallization and epitaxy, Applied Physics Letters **90**, 92103 (2007).

[12] I. Gordon, L. Carnel, D. Van Gestel, G. Beaucarne, and J. Poortmans, Fabrication and characterization of highly efficient thin-film polycrystalline-silicon solar cells based on aluminium-induced crystallization, Thin Solid Films **516**, 6984–6988 (2008).

[13] D. Van Gestel, I. Gordon, H. Bender, D. Saurel, J. Vanacken, G. Beaucarne, and J. Poortmans, Intragrain defects in polycrystalline silicon layers grown by aluminum-induced crystallization and epitaxy for thin-film solar cells, Journal of Applied Physics **105**, 114507 (2009).

[14] J. Wong, J. L. Huang, B. Eggleston, M. A. Green, O. Kunz, R. Evans, M. Keevers, and R. J. Egan, Lifetime limiting recombination pathway in thin-film polycrystalline silicon on glass solar cells, Journal of Applied Physics **107**, 123705 (2010).

[15] R. A. Sinton and A. Cuevas, A Quasi-Steady-State Open-Circuit Voltage Method for Solar Cell Characterization, 16th European Photovoltaic Solar Energy Conference, Glasgow, United Kingdom (2000).

[16] M. J. Keevers, T. L. Young, U. Schubert, and M. A. Green, 10% Efficient CSG Minimodules, 22nd European Photovoltaic Solar Energy Conference and Exhibition, Milan, Italy (2007).
[17] M. A. Green and M. J. Keevers, Optical properties of intrinsic silicon at 300 K, Progress in Photovoltaics: Research and Applications **3**, 189–192 (1995).
[18] S. O. Kasap, Principles of electronic materials and devices, 3rd edition, Mc Graw-Hill, ISBN: 0-07-295791-3 (2006).
[19] D. Ballutaud, A. Riviere, M. Rusu, S. Bourdais, and A. Slaoui, EBIC technique applied to polycrystalline silicon thin films: minority carrier diffusion length improvement by hydrogenation, Thin Solid Films **403–404**, 549–552 (2002).
[20] A. M. Oliver Schultz, Thermal oxidation for crystalline silicon solar cells exceeding 19% efficiency applying industrially feasible process technology, Progress in Photovoltaics: Research and Applications **16**, 317–324 (2008).
[21] F. Clement, M. Neidert, and A. Henning, Processing of highly - efficient MWT silicon solar cells, 25th European Photovoltaic Solar Energy Conference and Exhibition, Valencia, Spain (2010).
[22] J. Benick, Passivation quality of wet oxides grown from purified steam, 24th European Photovoltaic Solar Energy Conference and Exhibition, Hamburg, Germany (2009).
[23] J. Zhao, A. Wang, and M. A. Green, 24.5% efficiency silicon PERT cells on MCZ substrates and 24.7% efficiency PERL cells on FZ substrates, Progress in Photovoltaics: Research and Applications **7**, 471–474 (1999).
[24] D. Biro, S. Mack, and A. Wolf, Thermal oxidation as a key technology for high efficiency screen printed industrial silicon solar cells, 34th IEEE Photovoltaic Specialists Conference, Philadelphia, United States (2009).
[25] A. Wolf and A. Walczak, The SiN TO process: utilizing a SiNx anti-reflection layer for emitter masking during thermal oxidation, 34th IEEE Photovoltaic Specialists Conference, Philadelphia, United States (2009).
[26] S. Mack, A. Wolf, and A. Lemke, Control and optimization of the thermal processes for industrial solar cell fabrication, 34th IEEE Photovoltaic Specialists Conference, Philadelphia, United States (2009).
[27] S. Mack, D. Biro, A. Wolf, A. Walczak, B. Thaidigsmann, E. A. Wotke, J. J. Spiegelman, and R. Preu, Properties of purified direct steam grown silicon thermal oxides, Solar Energy Materials and Solar Cells **95**, 2570–2575 (2011).
[28] O. Schultz, S. W. Glunz, G. P. Willeke, Multicrystalline silicon solar cells exceeding 20% efficiency, Progress in Photovoltaics: Research and Applications **12**, 553–558, (2004).
[29] T. Sameshima and M. Satoh, Improvement of SiO_2 Properties by Heating Treatment in High Pressure H_2O Vapor', Japanese Journal of Applied Physics **36**, L687–L689 (1997).
[30] Company Rasirc, Uses of Water Vapor for Solar Cell Fabrication, Rasirc, Inc., San Diego, United States, www.rasirc.com, accessed 27/05/2016.
[31] B. Gorka, B. Rau, P. Dogan, C. Becker, F. Ruske, S. Gall, and B. Rech, Influence of hydrogen plasma on the defect passivation of polycrystalline Si thin film solar cells, Plasma Processes and Polymers **6**, S36–S40 (2009).
[32] S. Honda, A. Fejfar, J. Kocka, T. Yamazaki, A. Ogane, Y. Uraoka, and T. Fuyuki, Annealing in water vapor as a new method for improvement of silicon thin film properties, Journal of Non-Crystalline Solids **352**, 955–958 (2006).
[33] B. Gorka, Hydrogen passivation of polycrystalline Si thin film solar cells, doctoral thesis, Helmholtz-Zentrum Berlin, Germany (2010).

[34] R. Hull, Editor, Properties of Crystalline Silicon, Institution of Engineering and Technology, ISBN: 978-0-86341-556-2 (1999).
[35] S. A. McQuaid, R. C. Newman, J. H. Tucker, E. C. Lightowlers, R. A. A. Kubiak, and M. Goulding, Concentration of atomic hydrogen diffused into silicon in the temperature range 900–1300 °C, Applied Physics Letters **58**, 2933–2935 (1991).
[36] R. C. Newman, J. H. Tucker, A. R. Brown, and S. A. McQuaid, Hydrogen diffusion and the catalysis of enhanced oxygen diffusion in silicon at temperatures below 500 °C, Journal of Applied Physics **70**, 3061–3070 (1991).
[37] S. J. Pearton, J. W. Corbett, and T. S. Shi, Hydrogen in crystalline semiconductors, Applied Physics A: Materials Science & Processing **43**, 153–195 (1987).
[38] K. Christmann, Interaction of hydrogen with solid surfaces, Surface Science Reports **9**, 1–163 (1988).
[39] M. J. Keevers, A. Turner, U. Schubert, P. A. Basore and M. A. Green, Remarkably effective hydrogenation of crystalline silicon on glass modules, 20th European Photovoltaic Solar Energy Conference and Exhibition, Spain (2005).
[40] N. H. Nickel, Editor, Hydrogen in Semiconductors II, Academic Press, San Diego, United States, ISBN: 0127521704 (1999).
[41] J. Huang, J. Wong, M. Keevers, M. A. Green, Cell performance limitation investigation of polycrystalline silicon thin-film solar cells on glass by transmission electron microscopy, 25th European Photovoltaic Solar Energy Conference and Exhibition, Valencia, Spain (2010).
[42] K. Alberi, H. M. Branz, H. Guthrey, M. J. Romero, I. T. Martin, C. W. Teplin, P. Stradins, and D. L. Young, Dislocation-limited open circuit voltage in film crystal silicon solar cells, Applied Physics Letters **101**, 123510 (2012).
[43] J. Wong, J. Huang, S. Varlamov, M. A. Green, and M. Keevers, The roles of shallow and deep levels in the recombination behavior of polycrystalline silicon on glass solar cells, Progress in Photovoltaics: Research and Applications **20**, 915–922 (2012).
[44] J. Wong, J. L. Huang, S. Varlamov, M. A. Green, R. Evans, M. Keevers, and R. J. Egan, Structural inhomogeneities in polycrystalline silicon on glass solar cells and their effects on device characteristics, Progress in Photovoltaics: Research and Applications **19**, 695–705 (2011).
[45] S. Varlamov, J. Dore, R. Evans, D. Ong, B. Eggleston, O. Kunz, U. Schubert, T. Young, J. Huang, T. Soderstrom, K. Omaki, K. Kim, A. Teal, M. Jung, J. Yun, Z. M. Pakhuruddin, R. Egan, and M. A. Green, Polycrystalline silicon on glass thin-film solar cells: A transition from solid-phase to liquid-phase crystallised silicon, Solar Energy Materials and Solar Cells **119**, 246–255 (2013).
[46] Y. Qiu, O. Kunz, A. Fejfar, M. Ledinsky, B. Teik Chan, I. Gordon, D. Van Gestel, S. Venkatachalm, and R. Egan, On the effects of hydrogenation of thin film polycrystalline silicon: A key factor to improve heterojunction solar cells, Solar Energy Materials and Solar Cells **122**, 31–39 (2014).
[47] D. Madi, P. Prathap, A. Focsa, A. Slaoui, and B. Birouk, Effective hydrogenation and surface damage induced by MW-ECR plasma of fine-grained polycrystalline silicon, Applied Physics A: Materials Science & Processing **99**, 729–734 (2010).
[48] E. P. A. Slaoui, Passivation and etching of fine-grained polycrystalline silicon films by hydrogen treatment, Solar Energy Materials and Solar Cells **90**, 2087–2098 (2006).

[49] N. M. Johnson, F. A. Ponce, R. A. Street, and R. J. Nemanich, Defects in single-crystal silicon induced by hydrogenation, Physical Review B **35**, 4166–4169 (1987).
[50] C. Becker, D. Amkreutz, T. Sontheimer, V. Preidel, D. Lockau, J. Haschke, L. Jogschies, C. Klimm, J. J. Merkel, P. Plocica, S. Steffens, and B. Rech, Polycrystalline silicon thin-film solar cells: Status and perspectives, Solar Energy Materials and Solar Cells **119**, 112–123 (2013).
[51] S. Steffens, C. Becker, J.-H. Zollondz, A. Chowdhury, A. Slaoui, S. Lindekugel, U. Schubert, R. Evans, and B. Rech, Defect annealing processes for polycrystalline silicon thin-film solar cells, Materials Science and Engineering: B **178**, 670–675 (2013).
[52] S. Honda, T. Mates, B. Rezek, A. Fejfar, and J. Kocka, Microscopic study of the H_2O vapor treatment of the silicon grain boundaries, Journal of Non-Crystalline Solids **354**, 2310–2313 (2008).
[53] H. Watakabe, T. Sameshima, T. Strutz, T. Oitome, and A. Kohno, Defect Reduction Treatment for Plasma–Tetraethylorthosilicate–SiO_2 by High-Pressure H_2O Vapor Heat Treatment, Japanese Journal of Applied Physics **44**, 8367–8370 (2005).
[54] N. Sano, M. Sekiya, M. Hara, A. Kohno, and T. Sameshima, Improvement of SiO_2/Si interface by low-temperature annealing in wet atmosphere, Applied Physics Letters **66**, 2107–2109 (1995).
[55] T. S. H. Watakabe, Oxygen plasma and high pressure H_2O vapor heat treatments used to fabricate polycrystalline silicon thin film transistors, Applied Physics A: Materials Science & Processing **77**, 141–144 (2003).
[56] K. S. T. Sameshima, Defect reduction and surface passivation of SiO_2/Si by heat treatment with high-pressure H_2O vapor, Applied Physics A: Materials Science & Processing **69**, 221–224 (1999).
[57] T. Sameshima and M. Kimura, Characterization of polycrystalline silicon thin-film transistors, Japanese Journal of Applied Physics **45**, 1534 (2006).
[58] Y. Urabe, T. Sameshima, K. Motai, and K. Ichimura, Improvement in SiO_2 film properties formed by sputtering method at 150 °C, Japanese Journal of Applied Physics **47**, 8003 (2008).
[59] K. Sakamoto, K. Asada, and T. Sameshima, Field effect surface passivation of SiO_2/Si interfaces by heat treatment with high-pressure H_2O vapor, Solar Energy Materials and Solar Cells **65**, 565–570 (2001).
[60] H. Watakabe and T. Sameshima, High-pressure H_2O vapor heat treatment used to fabricate poly-Si thin film transistors, Japanese Journal of Applied Physics **41**, L974–L977 (2002).
[61] D. A. Mutsumi Kimura, Analysis of plasma treatment and vapor heat treatment for thin-film transistors by extracting trap densities at front and back interfaces, Applied Physics Letters **84**, 4026–4028 (2004).
[62] G. Chun-Lin, W. Lei, Z. Yan-Rong, Z. Hai-Feng, L. Feng, Y. Zhen-Hui, and Y. De-Ren, High-pressure water-vapor annealing for enhancement of a-Si:H film passivation of silicon surface, Chinese Physics Letters **31**, 108501 (2014).
[63] K. Sakamoto and T. Sameshima, Passivation of SiO_2/Si interfaces using high-pressure-H_2O-vapor heating, Japanese Journal of Applied Physics **39**, 2492–2496 (2000).
[64] K. Sakamoto, K. Asada, T. Sameshima, and T. Saitoh, High-pressure H_2O vapor heating used for passivation of SiO_2/Si interfaces, Solar Energy Materials and Solar Cells **65**, 571–576 (2001).

[65] A. Ogane, A. Kitiyanan, Y. Uraoka, and T. Fuyuki, High-pressure water vapor heat treatment for enhancement of SiOx or SiNx passivation layers of silicon solar cells, Japanese Journal of Applied Physics **48**, 66504 (2009).
[66] T. Sameshima, K. Sakamoto, and M. Satoh, Heat treatment in high pressure H_2O vapor used for improvement of Si-O bonding network near SiO_2/Si interface, Thin Solid Films **335**, 138–141 (1998).
[67] T. Sameshima, H. Hayasaka, and T. Haba, Analysis of microwave absorption caused by free carriers in silicon, Japanese Journal of Applied Physics **48**, 21204 (2009).
[68] P. Punchaipetch, M. Miyashita, Y. Uraoka, T. Fuyuki, T. Sameshima, and S. Horii, Improving high-κ gate dielectric properties by high-pressure water vapor annealing, Japanese Journal of Applied Physics **45**, L120 (2006).
[69] K. Asada, K. Sakamoto, T. Watanabe, T. Sameshima, and S. Higashi, Heat treatment with high-pressure H_2O vapor of pulsed laser crystallized silicon films, Japanese Journal of Applied Physics **39**, 3883–3887 (2000).
[70] T. Sameshima, M. Satoh, K. Sakamoto, A. Hisamatsu, K. Ozaki, and K. Saitoh, Heat treatment of amorphous and polycrystalline silicon thin films with H_2O vapor, Japanese Journal of Applied Physics **37**, L112–L114 (1998).
[71] T. Sameshima, M. Satoh, K. Sakamoto, K. Ozaki, and K. Saitoh, Heat treatment of amorphous and polycrystalline silicon thin films with high-pressure H_2O vapor, Japanese Journal of Applied Physics **37**, 4254–4257 (1998).
[72] T. Watanabe, H. Watakabe, T. Sameshima, and M. Miyasaka, Electrical properties of solid-phase crystallized polycrystalline silicon films, Applied Physics A: Materials Science & Processing **77**, 87–92 (2003).
[73] H. Watakabe, Y. Tsunoda, N. Andoh, and T. Sameshima, Characterization and control of defect states of polycrystalline silicon thin film transistor fabricated by laser crystallization, Journal of Non-Crystalline Solids **299–302**, 1321–1325 (2002).
[74] T. Sameshima, K. Sakamoto, K. Asada, M. Kondo, A. Matsuda, and S. Higashi, Reduction of defects of polycrystalline silicon thin films by heat treatment with high-pressure H_2O vapor, Solar Energy Materials and Solar Cells **65**, 577–583 (2001).
[75] T. Sameshima, H. Hayasaka, M. Maki, A. Masuda, T. Matsui, and M. Kondo, Defect reduction in polycrystalline silicon thin films by heat treatment with high-pressure H_2O vapor, Japanese Journal of Applied Physics **46**, 1286–1289 (2007).
[76] J. Takenezawa, M. Hasumi, T. Sameshima, T. Koida, T. Kaneko, M. Karasawa, and M. Kondo, Heat treatment of amorphous silicon p-i-n solar cells with high-pressure H_2O vapor, Journal of Non-Crystalline Solids **358**, 2285–2288, (2012).
[77] T. Kamiya, A. Suemasu, T. Watanabe, T. Sameshima, and I. Shimizu, Improvement of transport properties for polycrystalline silicon prepared by plasma-enhanced chemical vapor deposition, Applied Physics A: Materials Science & Processing **73**, 151–159 (2001).
[78] T. Sameshima, Y. Mizutani, K. Motai, and K. Ichimura, Defect reduction in polycrystalline silicon thin films at 150 °C, Japanese Journal of Applied Physics **49**, 03CA02 (2010).
[79] T. Sameshima, T. Nagao, M. Hasumi, A. Shuku, E. Takahashi, and Y. Andoh, Surface passivation of crystalline silicon by combination of amorphous silicon deposition with high-pressure H_2O vapor heat treatment, Japanese Journal of Applied Physics **51**, 03CA06 (2012).

[80] K. Ohdaira, S. Nishizaki, Y. Endo, T. Fujiwara, N. Usami, K. Nakajima, and H. Matsumura, High-quality polycrystalline silicon films with minority carrier lifetimes over 5 μs formed by flash lamp annealing of precursor amorphous silicon films prepared by catalytic chemical vapor deposition, Japanese Journal of Applied Physics **46**, 7198 (2007).
[81] T. F. Yohei Endo, Thin-film polycrystalline silicon solar cells formed by flash lamp annealing of a-Si films, Thin Solid Films **518**, 5003-5006 (2010).
[82] K. Ohdaira, Y. Abe, M. Fukuda, S. Nishizaki, N. Usami, K. Nakajima, T. Karasawa, T. Torikai, and H. Matsumura, Poly-Si films with long carrier lifetime prepared by rapid thermal annealing of Cat-CVD amorphous silicon thin films, Thin Solid Films **516**, 600-603 (2008).
[83] Y. Uraoka, M. Miyashita, Y. Sugawara, H. Yano, T. Hatayama, T. Fuyuki, and T. Sameshima, Improvement of reliability in low-temperature polycrystalline silicon thin-film transistors by water vapor annealing, Japanese Journal of Applied Physics **45**, 5657 (2006).
[84] U. Kroll, C. Bucher, S. Benagli, I. Schonbachler, J. Meier, A. Shah, J. Ballutaud, A. Howling, C. Hollenstein, A. Buchel, M. Poppeller, and I. Schonbachler, High efficiency p-i-n a-Si:H solar cells with low boron cross-contamination prepared in a large area single-chamber PECVD reactor, Thin Solid Films **451–452**, 525–530 (2004).
[85] T. Sameshima, H. Watakabe, N. Andoh, and S. Higashi, Pulsed laser annealing of thin silicon films, Japanese Journal of Applied Physics **45**, 2437 (2006).
[86] B. G. Masayuki Fujita, Reduction in surface recombination and enhancement of light emission in silicon photonic crystals treated by high-pressure water-vapor annealing, Applied Physics Letters **97**, 121111 (2010).
[87] A. Brewer and K. Haeften, In situ passivation and blue luminescence of silicon clusters using a cluster beam/H_2O codeposition production method, Applied Physics Letters **94**, 261102 (2009).
[88] H. Chen, X. Hou, G. Li, F. Zhang, M. Yu, and X. Wang, Passivation of porous silicon by wet thermal oxidation, Journal of Applied Physics **79**, 3282–3285 (1996).
[89] B. Gelloz and N. Koshida, Stabilization and operation of porous silicon photonic structures from near-ultraviolet to near-infrared using high-pressure water vapor annealing, Thin Solid Films **518**, 3276–3279 (2010).
[90] B. Gelloz and N. Koshida, Mechanism of a remarkable enhancement in the light emission from nanocrystalline porous silicon annealed in high-pressure water vapor, Journal of Applied Physics **98**, 123509 (2005).
[91] B. Gelloz, A. Kojima, and N. Koshida, Highly efficient and stable luminescence of nanocrystalline porous silicon treated by high-pressure water vapor annealing, Applied Physics Letters **87**, 31107 (2005).
[92] B. Gelloz, T. Shibata, and N. Koshida, Stabilization of nano-crystalline porous silicon electroluminescence by high pressure water vapor annealing, Physica Status Solidi C **4**, 2141–2144 (2007).
[93] M. Fehr, P. Simon, T. Sontheimer, C. Leendertz, B. Gorka, A. Schnegg, B. Rech, and K. Lips, Influence of deep defects on device performance of thin-film polycrystalline silicon solar cells, Applied Physics Letters **101**, 123904 (2012).
[94] A. B. Sproul, Dimensionless solution of the equation describing the effect of surface recombination on carrier decay in semiconductors, Journal of Applied Physics **76**, 2851–2854 (1994).

[95] Measurement of Solar Cell Efficiency, www.pveducation.org/pvcdrom, accessed 27/05/2016.
[96] Illumination Sources, www.pveducation.org/pvcdrom, accessed 27/05/2016.
[97] Solarcelliqe.png, Wikipedia, https://en.wikipedia.org/wiki/File:Solarcelliqe.png, accessed 27/05/2016.
[98] Crystalline Silicon on Glass - Silicon Preparation Process, Presentation, Germany (2006).
[99] M. A. Green, P. A. Basore, N. Chang, D. Clugston, R. Egan, R. Evans, D. Hogg, S. Jarnason, M. Keevers, P. Lasswell, J. O'Sullivan, U. Schubert, A. Turner, S. R. Wenham, and T. Young, Crystalline silicon on glass (CSG) thin-film solar cell modules, Solar Energy **77**, 857–863 (2004).
[100] P. A. Basore, Pilot production of thin-film crystalline silicon on glass modules, 29th IEEE Photovoltaic Specialists Conference, New Orleans, United States (2002).
[101] D. Amkreutz, J. Haschke, T. Haring, F. Ruske, and B. Rech, Conversion efficiency and process stability improvement of electron beam crystallized thin film silicon solar cells on glass, Solar Energy Materials and Solar Cells **123**, 13–16 (2014).
[102] J. Haschke, D. Amkreutz, L. Korte, F. Ruske, and B. Rech, Towards wafer quality crystalline silicon thin-film solar cells on glass, Solar Energy Materials and Solar Cells **128**, 190–197 (2014).
[103] J. Schmidt and A. Cuevas, Electronic properties of light-induced recombination centers in boron-doped Czochralski silicon, Journal of Applied Physics **86**, 3175–3180 (1999).
[104] K. Bothe, R. Sinton, and J. Schmidt, Fundamental boron–oxygen-related carrier lifetime limit in mono- and multicrystalline silicon, Progress in Photovoltaics: Research and Applications **13**, 287–296 (2005).
[105] D. Macdonald and L. J. Geerligs, Recombination activity of interstitial iron and other transition metal point defects in p- and n-type crystalline silicon, Applied Physics Letters **85**, 4061–4063 (2004).
[106] H. C. Sio and D. Macdonald, Direct comparison of the electrical properties of multicrystalline silicon materials for solar cells: conventional p-type, n-type and high performance p-type, Solar Energy Materials and Solar Cells **144**, 339–346 (2016).
[107] P. Pikna, M. Muller, C. Becker, and A. Fejfar, Passivation effect of water vapour on thin film polycrystalline Si solar cells, Physica Status Solidi A, 1-7 (2016).
[108] G. Lucovsky, J. Yang, S. S. Chao, J. E. Tyler, and W. Czubatyj, Oxygen-bonding environments in glow-discharge-deposited amorphous silicon-hydrogen alloy films, Physical Review B **28**, 3225–3233 (1983).
[109] S. Rico, Si oxidation mechanisms as studied by oxygen tracer methods, in The physics and chemistry of SiO_2 and the Si-SiO_2 interface, C. R. Helms and B. E. Deal, Editors, Springer, United States, 75–84 (1988).
[110] E. H. Poindexter, P. J. Caplan, and G. J. Gerardi, Chemical and structural features of inherent and process-induced defects in oxidized silicon, in The physics and chemistry of SiO_2 and the Si-SiO_2 interface, C. R. Helms and B. E. Deal, Editors, Springer, United States, 299-308 (1988).
[111] P. Pikna, V. Pic, V. Benda, and A. Fejfar, Annealing of polycrystalline thin film silicon solar cells in water vapour at sub-atmospheric pressures, Acta Polytechnica **54**, 341–347 (2014).

[112] S. Steffens, C. Becker, D. Amkreutz, A. Klossek, M. Kittler, Y.-Y. Chen, A. Schnegg, M. Klingsporn, D. Abou-Ras, K. Lips, and B. Rech, Impact of dislocations and dangling bond defects on the electrical performance of crystalline silicon thin films, Applied Physics Letters **105**, 22108 (2014).
[113] J. Deckers, E. Bourgeois, M. Jivanescu, A. Abass, D. Van Gestel, K. Van Nieuwenhuysen, B. Douhard, J. D'Haen, M. Nesladek, J. Manca, I. Gordon, H. Bender, A. Stesmans, R. Mertens, and J. Poortmans, Comparing n- and p-type polycrystalline silicon absorbers in thin-film solar cells, Thin Solid Films **579**, 144–152 (2015).
[114] C. A. Londos, M. J. Binns, A. R. Brown, S. A. McQuaid, and R. C. Newman, Effect of oxygen concentration on the kinetics of thermal donor formation in silicon at temperatures between 350 and 500 °C, Applied Physics Letters **62**, 1525–1526 (1993).
[115] Standard ASTM F1535 - Standard test method for carrier recombination lifetime in silicon wafers by noncontact measurement of photoconductivity decay by microwave reflectance, standards.globalspec.com/std/643867/astm-f1535, accessed 27/05/2016.
[116] P. Pikna, V. Skoromets, C. Becker, A. Fejfar, and P. Kuzel, Thin film polycrystalline Si solar cells studied in transient regime by optical pump–terahertz probe spectroscopy, Applied Physics Letters **107**, 233901 (2015).
[117] F. Krizek, P. Pikna, and A. Fejfar, Silver catalysed nanoscale silicon etching in water vapour, 6th International Conference on Nanomaterials NANOCON 2014, Brno, Czech Republic (2014).